

ACHIEVABLE RATES AND TRANSCEIVER DESIGN IN ULTRA-WIDEBAND  
COMMUNICATIONS

by

Nazlı Güney

B.S., in Electrical and Electronics Engineering, Boğaziçi University, 2001

M.S., in Electrical and Electronics Engineering, Boğaziçi University, 2003

Submitted to the Institute for Graduate Studies in  
Science and Engineering in partial fulfillment of  
the requirements for the degree of  
Doctor of Philosophy

Graduate Program in Electrical and Electronics Engineering  
Boğaziçi University

2009

ACHIEVABLE RATES AND TRANSCEIVER DESIGN IN ULTRA-WIDEBAND  
COMMUNICATIONS

APPROVED BY:

Prof. Hakan Deliç .....  
(Thesis Supervisor)

Assoc. Prof. Fatih Alagöz .....

Prof. Mehmet Ertuğrul Çelebi .....

Assist. Prof. Mutlu Koca .....

Assoc. Prof. Mehmet Kıvanç Mihçak .....

DATE OF APPROVAL: 4.June.2009

## ACKNOWLEDGEMENTS

I would like to thank Prof. Hakan Deliç for giving me the chance to work on this exciting topic, which has enabled me to explore the world of telecommunication. It would be impossible to complete this thesis without his help and support.

The jury members made interesting and valuable comments about my research, and I am grateful to them all.

I thank all members of the Wireless Communications Laboratory, past and present, especially Barış Özgül, for his friendship and support.

I cannot fail to mention the names of friends that helped me go through tough times: Fulya Kunter, Mehmet İpekoğlu and Nazım Mahmutyazıcıoğlu.

Now that all family members are doctors, my thanks to my family will not end. They have always provided me with the love and support I needed so that I could find my way out whenever confronted with difficult circumstances. My brother, Dr. Murat Güney and my mother, Dr. Mebrure Güney, my sweeties, are my major assets in life, and my father, Opr. Dr. Muzaffer Güney, will always reside in my heart.

This thesis was supported by the Scientific and Technical Research Council of Turkey (TÜBİTAK) Integrated Doctorate Program (BDP), and the TÜBİTAK Scientific Research Project Fund under Contract 105E034.

## ABSTRACT

# ACHIEVABLE RATES AND TRANSCEIVER DESIGN IN ULTRA-WIDEBAND COMMUNICATIONS

In a multipath dominated environment, ultra-wideband (UWB) systems that transmit trains of subnanosecond duration pulses exhibit the desirable property of fine resolution in time of the received paths, which as a result of the impulsive form of the transmitted signal go through fewer amplitude fluctuations than those emanating from systems with narrower bandwidths. Being distributed over a large number of resolvable paths, UWB signal energy is typically collected by the rake receiver.

In this thesis, achievable information rates of time-hopping M-ary pulse position modulation UWB systems using either soft- or hard-decision outputs are calculated first, where one distinguishing characteristic observed for the hard-output systems is that increasing the constellation size is advantageous only at sufficiently large values of the code rate. Next, it is shown that with time division duplex UWB systems, for which channel information is available at the transmitter, it is possible to move about half of the rake fingers to the transmitter, and simultaneously increase the received signal-to-noise ratio (SNR). The impact of the nature of the noise phenomenon on the rake receiver is such that clipper nonlinearities following the rake fingers are needed if non-Gaussian noise is present. To this end, a robust rake receiver is designed and its performance is optimized through the parameters of the nonlinearities. Finally, a robust multipath-combining decorrelating ( $mD$ ) detector is developed for non-Gaussian channels. Corresponding to a structure with further processing of the rake receiver outputs, the robust  $mD$  detector effectively removes the interference from the other users as well as the impulsive noise, and thus the error floor observed with rake receivers and single-user detection at high SNR values and large number of users is avoided.

## ÖZET

### ULTRA-GENİŞBANT İLETİŞİMDE ERİŞİLEBİLİR HIZLAR VE ALICI-VERİCİ TASARIMI

Çok-yolların egemen olduğu ortamlarda altnanosaniye süreli darbe katarları ileten ultra-genişbant (UGB) sistemler, iletilen işaretin dürtün yapısından ötürü daha dar bantgenişlikli sistemlerden kaynaklanana göre daha az genlik dalgalanmalarına maruz kalan alınan yolların zamanda iyi çözünlenebildiği arzulanan özelliği sergilemektedir. Çok sayıda çözünlenebilen yola dağılmasıyla UGB işaret enerjisi sıklıkla tırmık alıcısı tarafından toplanmaktadır.

Bu tezde ilk olarak yumuşak veya sert karar çıkışları kullanan zaman atlamalı M'li darbe konum kiplenimi UGB sistemlerin erişilebilir bilgi hızları hesaplanmaktadır. Burada, sert-çıkışlı sistemler için gözlemlenen ayırdedici bir özellik yıldızkümesi büyüklüğünün artırılmasının sadece yeterince yüksek kod hızlarında yararlı olduğudur. Ardından, kanal bilgisinin alıcıda elde edilebilir olduğu zaman bölüşümlü çift yönlü UGB sistemlerle tırmık parmaklarının yaklaşık yarısının alıcıya taşınabildiği ve aynı zamanda alınan işaret gürültü oranının (İGO) artırılabilirdiği gösterilmektedir. Gürültü olgusunun doğasının tırmık alıcısı üzerindeki etkisi Gauss olmayan gürültü mevcutsa tırmık parmaklarını takiben kırpıcı doğrusalsızlıkların gerekli olduğudur. Bu amaçla, gürbüz bir tırmık alıcısı tasarlanmıştır ve başarımı doğrusalsızlıkların parametreleri vasıtasıyla eniyileştirilmiştir. En son olarak, Gauss olmayan kanallar için gürbüz bir çokyol-birleştirmeli ilintisizleştirilen ( $\zeta\dot{I}$ ) sezici geliştirilmiştir. Tırmık alıcısının çıkışlarının daha fazla işlenmesine karşılık gelen gürbüz  $\zeta\dot{I}$  sezicisi diğer kullanıcılardan kaynaklanan girişimi dürtün gürültüyü olduğu gibi etkinlikle ortadan kaldırmaktadır. Böylece, tırmık alıcıları ve tek-kullanıcı sezimi ile yüksek İGO değerlerinde ve büyük kullanıcı sayılarında gözlemlenen hata tabanları önlenmektedir.

## TABLE OF CONTENTS

ACKNOWLEDGEMENTS . . . . .	iii
ABSTRACT . . . . .	iv
ÖZET . . . . .	v
LIST OF FIGURES . . . . .	viii
LIST OF TABLES . . . . .	xii
LIST OF SYMBOLS/ABBREVIATIONS . . . . .	xiii
1. INTRODUCTION . . . . .	1
1.1. Characteristics of Impulse Radio Signals . . . . .	2
1.2. Research Overview and Contributions . . . . .	4
1.3. Organization of the Thesis . . . . .	7
2. ULTRA-WIDEBAND CHANNEL MODELS AND RAKE COMBINING . . . . .	8
2.1. The IEEE 802.15.3a Standard Channel Model . . . . .	9
2.2. Rake Reception for Impulse Radio Signals . . . . .	12
3. ACHIEVABLE RATES OF M-ARY PPM IMPULSE RADIO . . . . .	15
3.1. UWB System Model . . . . .	17
3.1.1. Statistics of MAI for Asynchronous Users and Rake Reception . . . . .	20
3.1.2. Statistics of IFI for Rake Reception . . . . .	24
3.2. Mutual Information for Impulse Radio in UWB Channels . . . . .	26
3.2.1. Soft-Output M-ary PPM Impulse Radio . . . . .	28
3.2.2. Hard-Output M-ary PPM Impulse Radio . . . . .	31
3.2.3. Arimoto-Blahut Algorithm . . . . .	33
3.2.4. Channel Coding with M-ary PPM . . . . .	35
3.3. Simulation Results . . . . .	37
4. JOINT TRANSMITTER-RECEIVER UWB RAKE DESIGN . . . . .	50
4.1. UWB System Model . . . . .	51
4.2. Transmitter-Receiver Rake Structure for ISI Channels . . . . .	53
4.3. Simulation Results . . . . .	58
5. ROBUST DETECTION OF IMPULSE RADIO SIGNALS IN NON-GAUSSIAN NOISE . . . . .	63

5.1. UWB System Model . . . . .	64
5.2. Robust Detection . . . . .	66
5.2.1. Impulsive Noise and MAI . . . . .	66
5.2.2. Robust Nonlinearity . . . . .	68
5.3. Simulation Results . . . . .	76
6. MULTIUSER DETECTION FOR IMPULSE RADIO IN NON-GAUSSIAN CHANNELS . . . . .	80
6.1. UWB System Model . . . . .	82
6.2. Robust Multiuser Detector Structures for Frequency-Selective Channels	85
6.2.1. The Multipath-Combining Decorrelating ( $mD$ ) Detector . . . . .	87
6.2.2. The Decorrelating Multipath-Combining ( $dM$ ) Detector . . . . .	88
6.2.3. $M$ -Estimation and Robust Decorrelation . . . . .	89
6.2.4. Channel Information . . . . .	92
6.3. Simulation Results . . . . .	94
7. CONCLUSIONS AND FUTURE WORK . . . . .	102
APPENDIX A: DERIVATION OF THE MINIMUM SOFT-OUTPUT $E_b/N_0$ . . . . .	105
REFERENCES . . . . .	106

## LIST OF FIGURES

Figure 2.1.	Impulse response realizations of the IEEE 802.15.3a channel model	13
Figure 3.1.	Timing diagram for impulse radio in the AWGN channel with TH over the whole frame and $N_s = 1$ . . . . .	22
Figure 3.2.	The system model for calculation of achievable information rates .	27
Figure 3.3.	Single-user $\rho_b$ against mutual information for soft-output impulse radio with $M = \{2, 4, 8\}$ , $T_f > \tau_{0,L_0-1}$ and $\tilde{L} = L_0$ . . . . .	38
Figure 3.4.	$(\rho_b)_{\min}$ of soft-output impulse radio against $M$ with $\tilde{L} = L_0$ . . . . .	39
Figure 3.5.	Single-user $\rho_b$ against mutual information for hard-output impulse radio with $M = \{2, 4, 8\}$ , $T_f > \tau_{0,L_0-1}$ and $\tilde{L} = L_0$ . . . . .	40
Figure 3.6.	Mutual information against $E_s/N_0$ (in dB) for soft- and hard-output systems in the CM1 channel with $M = \{2, 4, 8\}$ . . . . .	41
Figure 3.7.	The low SNR region of mutual information against $E_s/N_0$ for soft- and hard-output systems in the CM1 channel with $M = \{2, 4, 8\}$ .	41
Figure 3.8.	Single-user $\rho_b$ against mutual information for soft-output impulse radio with rake reception, $M = \{2, 4, 8\}$ and $T_f > \tau_{0,L_0-1}$ in the CM1 channel, where $\tilde{L} = 4, 8, 16, L_0$ . . . . .	43
Figure 3.9.	Multiple-user $\rho_b$ against mutual information for soft-output impulse radio with $M = \{2, 4, 8\}$ , $K_r = 100$ , $T_f = 100$ ns and $\tilde{L} = L_0$ . . . . .	46

Figure 3.10.	Mutual information for soft-output impulse radio against $K_r$ with $T_f = 100$ ns, $E_s/N_0 = 20$ dB, $M = \{2, 4, 8\}$ , and $\tilde{L} = L_0$ . . . . .	47
Figure 3.11.	Mutual information for soft-output impulse radio against $K_r$ with $T_f = 10$ ns, $E_s/N_0 = 20$ dB, $M = \{2, 4, 8\}$ and $\tilde{L} = L_0$ . . . . .	47
Figure 3.12.	Multiple-user $\rho_b$ against mutual information for hard-output impulse radio with $M = \{2, 4, 8\}$ , $K_r = 100$ , $T_f = 100$ ns and $\tilde{L} = L_0$	48
Figure 4.1.	The normalized SINR values, $\gamma/\gamma_0$ , against $F_t$ for $F = L + 1$ , $T_b > (2L - 1)T_p$ , i.e., no ISI, and different positions of the post-rake fingers . . . . .	60
Figure 4.2.	The normalized SINR values, $\gamma/\gamma_0$ , against $F_t$ for $F = 9, 17, 33$ and $T_b > (L + F_t - 1)T_b$ , i.e., no ISI. Without markers: First arriving paths (4.16). With markers: Middle arriving paths (4.17). Solid curve: All-post rake . . . . .	60
Figure 4.3.	The SINR values for the transmitter-receiver design that combines the first arriving paths, i.e., uses (4.16), against $F_t$ for $F = 33$ , where $E_b/N_0 = 0, 10, 20$ dB, $T_b = 10$ ns and $T_p = 1$ ns . . . . .	61
Figure 4.4.	The SINR values for the transmitter-receiver design that combines the first arriving paths, i.e., uses (4.16), against $F_t$ for $F = 33$ , where $E_b/N_0 = 20$ dB, $T_b = 10$ ns and $T_p = 1$ ns . . . . .	62
Figure 5.1.	The robust rake receiver for impulse radio with $N_s = 1$ . . . . .	67
Figure 5.2.	$P_{e,1}$ against $d$ for $E_b/N_0 = 10$ dB, $R_b = 1$ Mbps, $\epsilon = 0.1$ , $\kappa = \{10, 20, \dots, 100\}$ . . . . .	71

Figure 5.3.	BER for robust and linear receivers for $E_b/N_0 = 10$ dB, $R_b = 1$ Mbps and $\epsilon = 0.1$ in additive non-Gaussian noise . . . . .	72
Figure 5.4.	Numerical calculation of the true pdf of $\zeta$ as $N_s$ is increased . . . . .	73
Figure 5.5.	$P_{e,2}$ against $d$ for $E_b/N_0 = 10$ dB, $R_b = 1$ Mbps, $\epsilon = 0.1$ , $\kappa = \{10, 20, \dots, 100\}$ . . . . .	75
Figure 5.6.	BER for robust and linear receivers for varying $\tilde{L}$ and $E_b/N_0$ when $\kappa = 100$ , $\epsilon = 0.1$ and $K_r = 20$ . . . . .	76
Figure 5.7.	BER for robust and linear receivers for varying $\tilde{L}$ and $E_b/N_0$ when $\kappa = 1$ (Gaussian noise) and $K_r = 20$ . . . . .	77
Figure 5.8.	BER for robust and linear receivers for increasing $K_r$ when $\kappa = 100$ or $\kappa = 1$ (Gaussian noise), $\epsilon = 0.1$ , SNR = 10 dB and $\tilde{L} = 32$ . . . . .	78
Figure 5.9.	BER for robust and linear receivers for increasing $\kappa$ when $\epsilon = 0.1$ , SNR = 10 dB, $K_r = 20$ and $\tilde{L} = 32$ . . . . .	78
Figure 6.1.	BER of the $dM$ detector for varying percentage of captured channel energy with the CM1 model and $K = 20$ at the LR . . . . .	96
Figure 6.2.	BER performances against SNR in the CM1 channel for $K = 20$ at the LR . . . . .	97
Figure 6.3.	BER against $\kappa$ for the $mD$ detectors in the CM1 channel at the LR with $K = 20$ , $P = L_{\max}$ and SNR = 10 dB . . . . .	98
Figure 6.4.	BER performances of the $mD$ detectors against SNR at the LR for the CM1 model and $K = 20$ . . . . .	99

- Figure 6.5. BER performances of the  $mD$  detectors against SNR for the CM1 and the CM4 channels at the LR and HR,  $K = 20$  and  $P = L_{\max}$  . . . . . 100
- Figure 6.6. BER performances of the  $mD$  detectors against  $K$  for the CM1 model at the HR, where  $P = 16$  for the selective and partial detectors and SNR = 10 dB . . . . . 100
- Figure 6.7. BER performances of the  $mD$  detectors against SNR at the LR for the CM1 model,  $K = 20$ ,  $P = 16$  for the selective and partial receivers, and the coherence time of 200  $\mu s$  with  $N_t/N_p = 0.1$  . . . . . 101

## LIST OF TABLES

Table 3.1.	Arimoto-Blahut algorithm for soft-output systems and $M = 8$ . . .	45
Table 3.2.	Arimoto-Blahut algorithm for hard-output systems and $M = 8$ . . .	45
Table 5.1.	The optimal $d$ 's and the corresponding $P_e$ 's predicted via the numerical evaluation of (5.21) . . . . .	74
Table 5.2.	$P_e$ for the suboptimal $d$ 's found by the Gaussian approximation to $\zeta$ (numerical evaluation) . . . . .	74

## LIST OF SYMBOLS/ABBREVIATIONS

<b>A</b>	Orthogonal transformation matrix
<b>A<sub>K</sub></b>	Diagonal matrix of $K$ signal amplitudes
$A_k$	Amplitude of the $k$ th received signal
$A'_k$	Normalized signal amplitude with training
<b>b</b> [ $i$ ]	Vector of $K$ information bits
$b_i$	$i$ th transmitted bit
$b_j^{(k)}$	Data bit in the $j$ th frame of the $k$ th user
<b>C<sub>v</sub></b>	Matrix in the numerator of the generalized Rayleigh quotient to determine $\mathbf{v}_t$
<b>C<sub>w</sub></b>	Matrix in the numerator of the generalized Rayleigh quotient to determine $\tilde{\mathbf{w}}_r$
$\mathcal{C}_h$	Hard-output achievable rate in bits per channel use
$\mathcal{C}_s$	Soft-output achievable rate in bits per channel use
$c_j^{(k)}$	TH sequence element for the $j$ th frame of the $k$ th user
<b>D<sub>v</sub></b>	Matrix in the denominator of the generalized Rayleigh quotient to determine $\mathbf{v}_t$
<b>D<sub>w</sub></b>	Matrix in the denominator of the generalized Rayleigh quotient to determine $\tilde{\mathbf{w}}_r$
$d_\ell$	Trimming parameter of the robust nonlinearity
$d_i^j$	Data symbol in the $(j - i)$ th frame of the 0th user
$d_j^{(k)}$	Data symbol in the $j$ th frame of the $k$ th user
$\text{diag}\{\cdot\}$	Diagonal matrix of the vector argument
$E_b$	Energy per bit
$E_p$	Energy per pulse
$E_s$	Energy per symbol
$E\{\cdot\}$	Expected value
$f_a(\cdot)$	Probability density function of the random variable $a$
$F$	Total number of rake fingers

$F_t$	Number of fingers at the pre-rake structure
$F_r$	Number of fingers at the post-rake structure
$g_i(\cdot)$	Heavy-tailed Gaussian noise pdf
$g_n(\cdot)$	Nominal Gaussian noise pdf
$\mathbf{H}$	Channel matrix for the desired signal
$\mathbf{H}_K$	Block diagonal channel matrix of the $K$ users
$\mathbf{H}_m$	Channel matrix for the $m$ th interfering bit
$H(\cdot)$	Entropy
$\mathbf{h}_k$	Channel vector of the $k$ th user
$h(\cdot)$	Channel impulse response
$h_k(\cdot)$	Channel impulse response of the $k$ th user
$\mathbf{I}_M$	$M \times M$ identity matrix
$I$	Number of interfering symbols (future or past) for the transmitter-receiver rake structure
$I(\cdot ; \cdot)$	Mutual information
$J$	Function maximized by the Arimoto-Blahut algorithm
$j_0$	Channel impulse response length of the desired user as number of frames
$\tilde{j}$	Length of the time window used for rake reception in terms of the number of frames
$K$	Number of multipath components within a cluster
$K$	Number of users for multiuser detection
$K_r$	Number of interfering users for rake reception
$k$	Number of bits in M-ary signaling
$k_h$	Trimming parameter for $\psi_H(\cdot)$
$L$	Number of clusters in the channel impulse response
$L$	Number of paths (length) of the channel impulse response
$L_e$	Effective number of users for the $dM$ detector
$L_k$	Length of the channel impulse response of the $k$ th user
$L_{\max}$	Maximum $L_k$ among $K$ users
$\ln$	Natural logarithm
$\log_a$	Logarithm to the base $a$

$\mathbf{M}_y$	Covariance matrix of $\mathbf{y}$
$\tilde{\mathbf{M}}_y$	Symmetric Toeplitz matrix that has $[r_\alpha^{(0)}(0) \dots r_\alpha^{(0)}(M-1)]^T$ in the first row
$\mathbf{M}_\Xi$	Covariance matrix of $\Xi$
$M$	Constellation size
$\mathcal{M}_\ell$	Set of paths created by all transmitting users excluding the $\ell$ th path of the desired user
$\mathbf{m}_y^i$	Mean vector of $\mathbf{y}$ given the $i$ th symbol is transmitted
$\tilde{\mathbf{m}}_y^i$	$M$ -dimensional vector whose $m$ th element is $r_\alpha^{(0)}(m-i)$
$\mathbf{m}_{\tilde{y}}^i$	Mean vector of $\tilde{\mathbf{y}}$ given the $i$ th symbol is transmitted
$\mathbf{m}_\Xi^i$	Mean vector of $\Xi$ given the $i$ th symbol is transmitted
$m_i$	Mean of $z(x_{j,0})$ due to $g_i(\cdot)$
$m_n$	Mean of $z(x_{j,0})$ due to $g_n(\cdot)$
$m_r$	Mean of $z(x_{j,0})$
$m_{\tilde{y},j}^i$	$j$ th component of $\mathbf{m}_{\tilde{y}}^i$
$N_h$	Number of TH bins
$N_p$	Number of bits in a packet
$N_s$	Number of pulses transmitted per symbol
$N_t$	Number of training bits
$N_0$	One-sided noise power spectral density
$\mathcal{N}(\mu, \sigma^2)$	Normal distribution with mean $\mu$ and variance $\sigma^2$
$\mathbf{n}$	Vector of noise samples
$\mathbf{n}_i$	Vector of noise samples for the $i$ th bit
$n$	Number of channel bits at the output of the channel encoder
$n(\cdot)$	Additive noise component
$n_m$	Noise term in the $m$ th branch
$n_{i,l}$	The $l$ th element of $\mathbf{n}[i]$
$n_{i,m}$	Noise sample at the $m$ th correlator output for the $i$ th bit
$n_{j,\ell}$	Noise sample in $x_{j,\ell}$
$P$	Combined number of paths
$P_{av}$	Average power

$P_e$	Probability of error
$P_{e,1}$	Approximate probability of error using Gaussian assumption
$P_{e,2}$	Exact probability of error using convolution
$P_{e,dM}$	Asymptotic probability of error for the $dM$ detector
$P_{e,mD}$	Asymptotic probability of error for the $mD$ detector
$p(\cdot)$	Probability mass function
$p_i^j$	Difference in TH sequence elements of $j$ th and $(j-i)$ th frames
$p_{k,l}$	Random sign of the $k$ th channel path in the $l$ th cluster
$p(\mathbf{x}_i)^n$	Probability of $\mathbf{x}_i$ at the $n$ th step of Arimoto-Blahut algorithm
$\mathbf{R}_n$	Covariance matrix of $\mathbf{n}$
$R$	Transmission rate
$R_b$	Bit rate
$R_w(\cdot)$	Autocorrelation function of the received pulse waveform
$R_{wv}(\cdot)$	Cross-correlation between $w_{\text{rec}}(\cdot)$ and $v(\cdot)$
$\mathbf{r}$	Received vector
$\mathbf{r}_i$	Received pre-raked signal vector for the $i$ th bit
$\mathbf{r}[i]$	Received multiuser signal vector for the $i$ th bit
$\mathbf{r}_A[i]$	$\mathbf{r}[i]$ in the AWGN channel
$r(\cdot)$	Total received signal
$r_{i,m}$	Correlator output matched to the $m$ th path for the $i$ th bit
$r_{\alpha, \tilde{L}}^{(k)}(\cdot)$	Autocorrelation function of the $k$ th channel impulse response truncated to $\tilde{L}$ paths
$\mathbf{S}_c$	Product of $\tilde{\mathbf{S}}[i]$ and $\mathbf{H}_K$
$\mathbf{S}_c^e$	Estimation error for $\mathbf{S}_c$
$\mathbf{S}_r$	$F_r \times (L + F_t - 1)$ selection matrix that determines which paths are combined at the receiver
$\mathbf{S}_k[i]$	Matrix containing TH codes of the $k$ th user for the $i$ th bit
$\tilde{\mathbf{S}}[i]$	Matrix containing TH codes of $K$ users for the $i$ th bit
$\mathbf{s}$	Received signal vector
$\mathbf{s}_k[i]$	TH spreading vector of the $k$ th user for the $i$ th bit
$s_i(\cdot)$	$i$ th transmitted symbol for orthogonal M-ary PPM

$s_{k,\ell}^i$	$\ell$ th element of $\mathbf{s}_k[i]$
$s_{mi}$	Signal term in the $m$ th branch due to the $i$ th symbol
$s_{\text{rec}}^{(k)}(\cdot)$	Signal received from the $k$ th user
$s_{\text{tr}}(\cdot)$	Transmitted signal
$s_{\text{tr}}^{(k)}(\cdot)$	Signal transmitted by the $k$ th user
$\tilde{s}_{\text{tr}}^{(k)}(\cdot)$	$s_{\text{tr}}^{(k)}(\cdot)$ modified by the receiver antenna
$T_b$	Bit duration
$T_c$	Duration of TH bins
$T_f$	Frame time
$T_l$	$l$ th cluster arrival time
$T_p$	Pulse duration
$t_{k,l}$	Delay of the $k$ th path relative to the $l$ th cluster arrival time
$t_n$	The second derivative Gaussian pulse parameter
$\mathbf{v}_R$	Pre-rake vector of the post-rake only structure
$\mathbf{v}_T$	Pre-rake vector of the pre-rake only structure
$\mathbf{v}_t$	Pre-rake vector of length $F_t$ with arbitrary elements
$\mathbf{v}_t^{\text{opt}}$	Optimal value of $\mathbf{v}_t$ maximizing $\gamma$
$v(\cdot)$	Template signal for the binary PPM correlator
$v_i^2$	Variance of $z(x_{j,0})$ due to $g_i(\cdot)$
$v_n^2$	Variance of $z(x_{j,0})$ due to $g_n(\cdot)$
$v_r^2$	Variance of $z(x_{j,0})$
$v_k$	Gain of the $k$ th pre-rake finger
$\mathbf{w}$	Post-rake vector
$\mathbf{w}_R$	Post-rake vector of the post-rake only structure
$\mathbf{w}_T$	Post-rake vector of the pre-rake only structure
$\mathbf{w}_r$	Post-rake vector of length $L + F_t - 1$ that has $F_r$ nonzero elements
$\tilde{\mathbf{w}}_r$	$F_r \times 1$ vector that contains the nonzero elements of $\mathbf{w}_r$
$w_m$	$m$ th element of the post-rake vector
$\tilde{\mathbf{w}}_r^{\text{opt}}$	Optimal value of $\tilde{\mathbf{w}}_r$ maximizing $\gamma$
$w_{\text{rec}}(\cdot)$	Received pulse waveform

$w_{\text{tr}}(\cdot)$	Transmitted pulse waveform
$w_{j,\ell}$	Combining weight for $x_{j,\ell}$
$\mathbf{X}$	Cross-correlation vector of transmitted PPM signals
$\mathbf{x}$	The estimate of $\mathbf{A}_K \mathbf{b}[i]$ that achieves the LS solution
$\mathbf{x}_i$	Vector $\mathbf{X}$ for the $i$ th transmitted signal
$x_m$	$m$ th component of $\mathbf{X}$
$x_{j,\ell}$	Correlator output for the $\ell$ th selected path of the $j$ th pulse
$\mathbf{Y}$	$M$ -dimensional output of the $M$ -ary correlation receiver
$\tilde{\mathbf{Y}}$	$\mathbf{Y}$ transformed to obtain uncorrelated components
$\mathbf{y}$	Realized value of $\mathbf{Y}$
$\mathbf{y}[i]$	Output of the decorrelator which uses TH codes only
$\tilde{\mathbf{y}}$	Transformed version of $\mathbf{y}$ with uncorrelated components
$y_{j,\ell,m}$	$m$ th correlator output for the $\ell$ th path of the $j$ th pulse
$y_m$	Output of the $m$ th branch of the $M$ -ary correlation receiver
$z(\cdot)$	Output of the robust nonlinearity
$\mathbf{0}_{d_1 \times d_2}$	All-zero matrix of dimension $d_1 \times d_2$
$\alpha_\ell$	Gain of the $\ell$ th path in the channel impulse response
$\alpha_{k,\ell}$	Gain of the $\ell$ th path of the $k$ th user channel
$\beta$	PPM parameter, which is “1” or “-1” when the transmitted bit is a “0” or “1”, respectively
$\beta_k$	Delay of the $k$ th pre-rake finger
$\Gamma$	Cluster decay factor
$\gamma$	SINR of the decision statistic, $\xi$
$\gamma_0$	Bit energy to noise ratio scaled by two
$\gamma_r$	Ray decay factor
$\Delta_{j,j'}^{(k)}$	Random variable determining the $k$ th MAI term in $y_m$
$\delta$	PPM time shift parameter
$\delta_D(\cdot)$	Dirac delta function
$\epsilon$	Impulsive noise parameter which controls the contribution of the impulsive component

$\zeta$	Decision statistic, the sum of $z(x_{j,0})$ for $j = 0, \dots, N_s - 1$
$\eta_m^{(0)}$	IFI term in the $m$ th branch
$\eta_{j,\ell}^{(k)}$	MAI in $x_{j,\ell}$ due to the $k$ th user
$\eta_{j,\ell,m}^{(k)}$	MAI due to user $k$ in $m$ th branch for path $\ell$ of $j$ th pulse
$\eta_m^{(k)}$	MAI term due to the $k$ th user in the $m$ th branch
$\eta_{m,A}^{(k)}$	$k$ th MAI term of the $m$ th branch in the AWGN channel
$\Theta$	Vector of $\theta_k$ 's
$\theta_k$	Product of $A_k$ and $b_i^{(k)}$
$\iota_{k,l}$	Mean value of the amplitude of the $k$ th path in the $l$ th cluster
$\kappa$	The ratio of the variance of the heavier tailed Gaussian pdf to that of the nominal Gaussian pdf
$\Lambda$	Cluster arrival rate
$\lambda$	Arrival rate of a path within each cluster
$\mu$	Mean of $x_{j,0}$ given that a "0" is transmitted
$\Xi$	Hard-output vector for rake reception and M-ary PPM
$\xi$	Decision statistic of the pre-post rake structure
$\xi_m$	$m$ th hard-output statistic for rake reception and M-ary PPM
$\pi_{k,l}$	Channel coefficient of the $k$ th path in the $l$ th cluster
$\varpi_{k,l}$	Fading associated with the $k$ th ray in the $l$ th cluster
$\rho(\cdot)$	Robust function for $M$ -estimation
$\rho_b$	Minimum information bit energy to noise ratio for a code rate
$(\rho_b)_{\min}$	Minimum $\rho_b$ over all code rates
$\rho_H(\cdot)$	Robust function by Huber
$\varrho_l$	Fading associated with the $l$ th cluster
$\Sigma_{\tilde{\mathbf{y}}}$	Covariance matrix of $\tilde{\mathbf{y}}$
$\sigma_i^2$	Variance of $x_{j,0}$ for the heavier tailed Gaussian
$\sigma_{k,\ell}^2$	Variance of MAI for estimation of the $\ell$ th path of the $k$ th user
$\sigma_n^2$	Variance of $x_{j,0}$ for the nominal Gaussian
$\sigma_T^2$	Total noise variance for $M$ -estimation
$\sigma_{\tilde{\mathbf{y}},i}^2$	Component of $\Sigma_{\tilde{\mathbf{y}}}$ in the $i$ th row and column
$\sigma_{\eta,\ell}^{(k)}$	The variance of the total MAI in $x_{j,\ell}$

$\sigma_{\varpi_{k,l}}^2$	Variance of $\pi_{k,l}$ due to the fading on the $k$ th ray
$\sigma_{\varrho_l}^2$	Variance of $\pi_{k,l}$ due to the fading on the $l$ th cluster
$\tau_k$	Asynchronism between the $k$ th transmitter and the receiver
$\tau_k^c$	The part of $\tau_k$ that lies within a chip interval
$\tau_\ell$	Delay of the $\ell$ th path of the channel impulse response
$\tau_{k,\ell}$	Delay of the $\ell$ th path of the $k$ th user channel
$\nu$	Robust nonlinearity parameter for $M$ -estimation
$\Phi(\cdot)$	Cdf of the standard normal distribution
$\phi(\cdot)$	Pdf of the standard normal distribution
$\Omega_0$	Mean energy of the first arriving path
$\chi$	Frame-wise processing gain of impulse radio
$\psi(\cdot)$	Derivative of $\rho(\cdot)$
$\psi_H(\cdot)$	Derivative of $\rho_H(\cdot)$
AWGN	Additive white Gaussian noise
BER	Bit error rate
BPSK	Binary phase shift keying
cdf	Cumulative distribution function
CDMA	Code division multiple access
$dM$	Decorrelating multipath-combining
DPSK	Differential phase shift keying
EGC	Equal-gain combining
FCC	Federal Communications Commission
HR	High rate
IEEE	Institute of Electrical and Electronics Engineers
IFI	Inter-frame interference
i.i.d.	Independent and identically distributed
ISI	Intersymbol interference
LAN	Local Area Network
LOS	Line-of-sight
LR	Low rate

LS	Least squares
MAI	Multiple access interference
Mbps	Megabits per second
MAP	Maximum a posteriori probability
$mD$	Multipath-combining decorrelating
ML	Maximum likelihood
MMSE	Minimum mean-square error
MRC	Maximal ratio combining
NLOS	Non-line-of-sight
ns	Nanoseconds
PAM	Pulse amplitude modulation
PAN	Personal Area Network
pdf	Probability density function
PPM	Pulse position modulation
Pr	Probability
PRC	Principal Ratio Combining
rms	Root-mean-square
SINR	Signal-to-interference and noise ratio
SNR	Signal-to-noise ratio
SV	Saleh-Valenzuela
TDD	Time-division duplex
TH	Time-hopping
U.S.	United States
UWB	Ultra-wideband

## 1. INTRODUCTION

Ultra-wideband (UWB) technology, deemed a viable means for realizing high-speed short-range wireless communication applications, has traditionally been characterized by subnanosecond pulses. Communication systems which transmit signals composed of extremely short duration pulses are referred to as “impulse radio”, where the average time interval separating the pulses is likely to be high compared with the pulse duration [1, 2]. Impulse radio conveys information by changing either the positions or the amplitudes of pulses, which corresponds to pulse position modulation (PPM) and pulse amplitude modulation (PAM), respectively. Multiple users of impulse radio that have different time-hopping (TH) sequences share the same wide frequency band. The starting time of each pulse is shifted according to the TH sequence and catastrophic user collisions are thus avoided.

The impulse radio signal described in [2] occupies an extremely large transmission bandwidth even in the absence of data modulation, as it is the short pulse duration that gives the signal its ultra-wide bandwidth. Although communication applications of UWB technologies using short pulse signals have attracted industry and academia beginning with the 1990s, “baseband carrierless short pulse” techniques have been applied to radar systems since the late 1960s implying that the methods for generating impulse radio signals have in fact existed for almost four decades [3]. Until recently, however, benefits of using signals with ultra-wide bandwidths have only been exploited by the military and government agencies given the lack of appropriate spectrum regulation for commercial applications.

In the spring of 2002, the Federal Communications Commission (FCC) of the United States (U.S.) approved commercial deployment of UWB on an unlicensed basis in the 3.1-10.6 GHz band subject to a modified version of Part 15.209 rules [4]. In order to protect critical applications in adjacent bands, like global positioning and aircraft navigation systems, these rules, which originally limit unintended radiation from devices, are modified for intentional UWB transmissions by placing additional

constraints on their power spectral density as measured at a certain distance from the output of the transmitter antenna. The FCC regulations that allow the legal use of UWB devices have induced similar regulatory and research efforts in Europe and Asia as well, particularly in Japan and Singapore [5]. The novel and unconventional approach underlying the regulation of UWB is based on optimally sharing the existing radio spectrum resources by means of the overlay principle rather than looking for still available but possibly unsuitable new bands [6]. The addition of such a large spectrum for unlicensed use has naturally raised concerns regarding the ability of UWB to coexist with the services it will overlay especially when UWB devices proliferate in the future [7]. Even though the plausibility of this action is still debated, bandwidth that is available for implementation of UWB has enhanced the academic and industrial interest in this old technology.

Based on the anticipation that impulse radio techniques will be used for imaging (imaging of steel bars in concrete or pipes hidden inside walls, surveillance, and monitoring of the heart's contractions [8]), vehicular radar and sensor networks as well as communications, one may appreciate the importance of UWB, as it alone has the potential to create these applications that have not been fully realized with other technologies such as 802.11 Local Area Networks (LAN) and Bluetooth Personal Area Networks (PAN) [7].

### **1.1. Characteristics of Impulse Radio Signals**

In the context of wireless communications, signals with ultra-wide bandwidths have several advantages, the most important being the resistance to multipath interference. Ultra-wide transmission bandwidths and impulsive nature of the transmitted waveforms result in the ability for fine resolution of multipath arrivals, which prevents significant overlap and, hence, reduces possibility of destructive combining [7]. Extensive UWB propagation measurements demonstrate that even in indoor environments impulse radio signals experience a much lower variance in received signal power, i.e., fading, in the presence of multipath than narrowband signals [9]. This effect is understood in the frequency domain by realizing that the bandwidth of the impulse radio

signal is much wider than the coherence bandwidth of the multipath channel so that occasional frequency-selective fades affect only a small portion of the signal power [10].

The extremely fine time resolution of impulse radio signals also enables the development of precise ranging capability at the centimeter level [8, 10], which makes possible the implementation of applications that require an accurate localization [11]. Thus high temporal resolution not only allows radio designs with much lower fading margins than classical narrowband systems, but indicates the potential of impulse radio as the platform that merges precision ranging with data transmissions. Although communication and ranging applications are distinct, location information may be used to improve the security and efficiency of wireless communication networks.

As the bandwidths of impulse radio systems span over a very wide frequency range, transmitted signals undergo relatively low material penetration losses [12]. In particular, due to the fact that impulse radio operates in the lowest frequency band that supports its wide bandwidth, it has the best chance of penetrating materials that tend to be more opaque at higher frequencies [2].

In summary, the key advantages of impulse radio signaling are the following:

- Resistance to multipath interference
- Potential for very high data rates (ultra-short pulses)
- Easier material penetration
- Availability of technology for generation of signals
- High precision ranging at the centimeter level.

The fact that these properties together make impulse radio a very promising technology for establishment of unlicensed indoor wireless communication networks that support high performance data transmission has given rise to this thesis, whose objective is to evaluate the information rates achievable by impulse radio-based communication systems, and to introduce a number of transceiver designs that serve to alleviate some specific problems. While the first design is concerned with the distribu-

tion of a finite number of resources between the transmitter and the receiver such that useful signal components are collected and processed optimally, the second and third designs mitigate impulsive noise and interference present in the indoor environment by using two different but related tools of robust statistics.

## 1.2. Research Overview and Contributions

The evaluation or design of any communication system should start with a fundamental knowledge pertaining to the characteristics of the propagation channel which helps determine the limitations on performance. Typical channel realizations from the study conducted by Intel Corporation over the 2-8 GHz band point to distinctive attributes of a wideband indoor channel [7]. To begin with, it is observed that the multipath spans several nanoseconds in time, which may result in intersymbol interference (ISI) if the pulses are closely spaced in time. Moreover, since the wide bandwidth of the transmitted pulse allows fine resolution of multipath components, receivers may capture the signal energy in these paths by opting to use a rake structure with multiple fingers, where each finger is tuned to a particular path of the channel impulse response.

In the first part of the thesis, the performance of impulse radio is investigated for UWB channels and orthogonal M-ary PPM in terms of the maximum achievable information rate, where the outputs of the M-ary correlation receiver implemented through the rake structure with conventional maximal ratio combining (MRC) are subject to either soft or hard decisions. Applications of UWB technology are likely to be allowed at very low average transmit power levels so as to reduce the additional interference imposed on the systems existing in dedicated bands [4]. Therefore, energy efficient transmission is of utmost importance for UWB systems, where derived from the achievable information rate the minimum information bit energy to noise ratio required for reliable communication is the fundamental information-theoretic parameter that indicates energy efficiency [13]. In this respect, analyzing the achievable rates of impulse radio systems that employ M-ary PPM and rake receivers also gives insights regarding their energy efficiency. The major difference observed between the efficiencies of soft- and hard-output systems is that at low values of the mutual information the minimum

information bit energy-to-noise ratio required for reliable communication increases with the constellation size for the hard-output systems. Furthermore, it is demonstrated that independent of the type of output, achievable rates at medium to large values of signal-to-noise ratio (SNR) are considerably low in UWB channels compared to those in additive white Gaussian noise (AWGN) channels, as the frequency-selectivity of the UWB channel destroys the orthogonality of the transmitted PPM signals. The interference from the other users and the constellation size put additional constraints on the achievable rates at high SNR.

The achievable rates computed in the first part of the thesis constitute the information-theoretical limits of impulse radio systems with rake receivers. However, utilization of rake structures is not confined to be on the receiving side. In particular, it is known for time-division duplex (TDD) systems that rake combining may be performed before transmission by using a pre-rake structure, since channel information is available at the transmitter as well [14]. While the aim of pre-raking is to simplify the receiver structure, by increasing the number of received paths, and hence the diversity gain, such a scheme may in fact enable better detection performance as more of the paths are combined effectively at the receiver. In the second part of the thesis, the performance of an architecture for TDD UWB systems that has a transmitter-receiver pair of rake combining structures is optimized, where the total number of rake fingers to be deployed at the transmitter and the receiver is fixed. It is shown that there exists an optimum distribution of fingers between the two structures for systems with ISI, which maximizes the signal-to-interference plus noise ratio (SINR). Depending on the total number of rake fingers and/or post-rake fingers, i.e., those at the receiver, the optimum placement of post-rake fingers changes as the simulation results demonstrate.

Although the multipath effects of the propagation channel have been extensively investigated, the nature of the noise phenomenon and its impact on impulse radio have thus far been ignored. The traditional approach of considering just the thermal noise, which is modeled as a stationary and memoryless Gaussian random process, does not agree with relevant field measurements. It is reported in [15] that indoor environments, where UWB devices are envisioned to be deployed are subject to im-

pulsive (non-Gaussian) noise produced by office machines such as photocopiers and printers. The conventional linear matched filter exhibits performance deterioration in the presence of non-Gaussian noise of impulsive nature. Therefore, robust procedures are needed so as to combat the deviations in the noise distribution from the nominal Gaussian assumption. A minor perturbation in the noise distribution should cause only a small change in the performance of the robust receiver compared to the ideal Gaussian case.

A robust rake receiver is proposed for impulse radio in the third part of the thesis, which aims to remove the large amplitude outliers that occur due to impulsive noise. The proposed system contains a rake structure for collecting the signal energy dispersed over a large number of paths, and before the paths are merged via MRC, they are passed through nonlinearities to trim the outlier noise components. The robust receiver so designed is shown to outperform the conventional linear rake receiver that consists of only matched filters at its fingers.

The error floor observed at large SNR values as a result of the interference from the other users may be eliminated by resorting to multiuser detection instead of single-user rake reception. The purpose of the last part of the thesis is to introduce the robust multipath-combining decorrelating ( $mD$ ) detector for indoor impulse radio communication systems. The  $mD$  detector ensures strong performance even when the distribution of noise and interference deviates from the nominal Gaussian case. Although multipath combining and decorrelation are both linear operations, elimination of the large amplitudes produced by the impulsive noise is accomplished by means of nonlinear processing of the received signal. These conflicting objectives are realized in essence by making use of  $M$ -estimates in robust statistics. Simulation results demonstrate that whereas the boosting of receiver noise with decorrelation is the major performance limiting factor for the detector which decorrelates paths before multipath combining, the decorrelation that follows multipath combining is crucial with which the development of error floors is avoided. By robustifying the linear  $mD$  detector through  $M$ -estimation, a substantial performance improvement is achieved in additive non-Gaussian noise channels even when channel estimation errors are present.

### 1.3. Organization of the Thesis

Attractive features of impulse radio and the regulatory activities that have caused the recent increase in the interest for UWB communications are the subjects of this introductory chapter, where the objective and overview of the thesis are also covered. The next chapter presents the channel models used in the simulations throughout the thesis, whose characteristics make rake combining a necessity for impulse radio. Hence, some details on rake structures are given in Chapter 2 following the channel models. Chapter 3 provides the information rates achievable by impulse radio with M-ary PPM and rake reception. The distribution of a finite number of rake fingers between the transmitter and the receiver to optimize performance is demonstrated in Chapter 4. The robust rake receiver and the robust  $mD$  detector that employ single-user and multiuser detection, respectively, are introduced and analyzed in Chapters 5 and 6. They are both robust with respect to the deviations of the distribution of the ambient noise from the Gaussian assumption. The last chapter, Chapter 7, is devoted to concluding remarks and suggestions for possible future work.

## 2. ULTRA-WIDEBAND CHANNEL MODELS AND RAKE COMBINING

Unlike wired channels that are generally stationary and predictable, radio channels are extremely random in nature [16]. Reflection, diffraction and scattering are the three basic mechanisms behind electromagnetic wave propagation. Due to multiple reflections from various objects, the signal that has propagated through a wireless channel contains multiple replicas of the original transmitted signal, which is referred to as multipath propagation. As multipath components are created by electromagnetic waves traveling along different paths of varying lengths, they are characterized by different delays and attenuations. Channel modeling is concerned with the description of these parameters that identify the individual multipath components [17]. Modeling of the radio channel, one of the most difficult branches of radio communication engineering, is typically done in a statistical fashion based on measurements made specifically for an intended system or spectrum allocation.

The first and still the most widely used model, flat Rayleigh fading channel, applies when the system bandwidth is so small that the delays of the individual multipath components do not appear in the received signal model. A large number of multipath components interfere at the receiver and collectively determine the amplitude (Rician or Rayleigh depending on whether there is a line-of-sight (LOS) path or not) of the received signal. Although this model is sufficient for narrowband systems, a more accurate description of the multipath components is needed for analysis of systems with ultra-wide bandwidths. To this end, multipath delay axis of the channel impulse response is discretized by dividing it into equal time intervals (bins) whose size is determined by the inverse of the system bandwidth. The power delay profile of this discrete channel model shows how much power arrives within each delay bin. Since the delay bins get smaller as the system bandwidth increases, there may not be enough multipath arrivals that interfere in each bin to justify the Rayleigh fading for the bin amplitudes [17]. Also depending on the bandwidth there may be delay bins

into which no multipath component falls, and thus are empty. All of these effects are taken into account for the channel models developed for UWB PANs introduced next.

### 2.1. The IEEE 802.15.3a Standard Channel Model

The IEEE 802.15.3a Task Group, tasked with defining a PAN physical layer standard based on UWB and compatible with the medium access control standard of IEEE 802.15.3-2003, formed a subgroup for the development of a common UWB channel model, as a unique channel characterization is absolutely necessary when selecting parts of the new standard [17]. The model aims to capture the multipath characteristics of typical indoor environments, where IEEE 802.15.3a devices are expected to operate. In addition to the UWB channel measurements performed in the last couple of years, a number of measurement campaigns were carried out by the participants of the task group. A summary of these measurements can be found in [18].

Among the many indoor channel models considered, the final version adopted for the evaluation of the new standard is the one based on a modified Saleh-Valenzuela (SV) model [19] that best fits the measurements. As a result of the very fine time resolution UWB waveforms provide, reflections from different objects tend to arrive in clusters. For instance, reflections from a desk result in a cluster of paths, which is followed by another cluster created by the wall a few meters behind the desk, etc. This phenomenon is also observed in the SV model even though it is proposed for indoor channels with comparably smaller bandwidths that are on the order of 100 MHz.

In the original SV model, interarrival times between multipath components are exponentially distributed. Moreover, the multipath components are distinguished based on the cluster and the ray within the cluster. Thus four parameters are required to describe each environment: The cluster arrival rate, the ray arrival rate within the cluster, the cluster decay factor and the ray decay factor, where the decay factors are derived from the power delay profile. However, due to ultra-wide bandwidths the amplitude statistics of the paths do not follow a Rayleigh distribution as in the original SV model. The measurements in UWB channels indicate that rather the amplitude

statistics fit either a lognormal or a Nakagami distribution for reasons explained previously. Therefore, before adopting for the IEEE 802.15.3a standard channel model the SV model had to be modified by employing a lognormal amplitude distribution.

The multipath model approved by the IEEE 802.15.3a committee has the following discrete time impulse response [17]

$$h(t) = \sum_{l=0}^{L-1} \sum_{k=0}^{K-1} \pi_{k,l} \delta_D(t - T_l - t_{k,l}), \quad (2.1)$$

where  $\pi_{k,l}$  is the gain of the  $k$ th path in the  $l$ th cluster,  $T_l$  is the delay of the  $l$ th cluster,  $t_{k,l}$  is the delay of the  $k$ th path relative to the  $l$ th cluster arrival time and  $\delta_D(\cdot)$  is the Dirac delta function. The cluster arrivals and the ray arrivals within clusters are exponentially distributed, and thus they have the probability density function (pdf) representations given by

$$f_{T_l|T_{l-1}}(T_l|T_{l-1}) = \Lambda \exp[-\Lambda(T_l - T_{l-1})], \quad l > 0 \quad (2.2)$$

$$f_{t_{k,l}|t_{k-1,l}}(t_{k,l}|t_{k-1,l}) = \lambda \exp[-\lambda(t_{k,l} - t_{k-1,l})], \quad k > 0. \quad (2.3)$$

Here,  $T_l$  is also the arrival time of the first path of the  $l$ th cluster, i.e.,  $t_{0,l} = 0$ ,  $\Lambda$  stands for the cluster arrival rate and  $\lambda$  is the arrival rate of a path within each cluster.

The channel coefficients are determined through

$$\pi_{k,l} = p_{k,l} \varrho_l \varpi_{k,l}. \quad (2.4)$$

Signal inversion caused by reflections is indicated by the variable  $p_{k,l}$ , the random equiprobable + or - signs of the channel coefficients, while the amplitudes of the channel coefficients are lognormally distributed. In particular,  $20 \log_{10} \varrho_l \varpi_{k,l}$  is a normal (Gaussian) random variable with the mean  $\iota_{k,l}$  and the variance  $\sigma_{\varrho_l}^2 + \sigma_{\varpi_{k,l}}^2$ , where  $\sigma_{\varrho_l}^2$  and  $\sigma_{\varpi_{k,l}}^2$  are due to the fading on each cluster and ray, respectively. Such a normal random variable is described shortly with  $\mathcal{N}(\iota_{k,l}, \sigma_{\varrho_l}^2 + \sigma_{\varpi_{k,l}}^2)$ . If the mean energy of the

first arriving path is  $\Omega_0$ , and  $\Gamma$  and  $\gamma_r$  are the cluster decay factor and the ray decay factor, respectively, then the expected value,  $E\{\cdot\}$ , of  $(\varrho_l \varpi_{k,l})^2$  is

$$E [(\varrho_l \varpi_{k,l})^2] = \Omega_0 \exp(-T_l/\Gamma) \exp(-t_{k,l}/\gamma_r). \quad (2.5)$$

Based on (2.5),  $\iota_{k,l}$  are given by

$$\iota_{k,l} = \frac{10 \ln \Omega_0 - 10T_l/\Gamma - 10t_{k,l}/\gamma_r - (\sigma_{\varrho_l}^2 + \sigma_{\varpi_{k,l}}^2) \ln 10}{\ln 10}. \quad (2.6)$$

In the equations above,  $\varrho_l$  reflects the fading associated with the  $l$ th cluster and  $\varpi_{k,l}$  corresponds to the additional fading on the  $k$ th ray of the  $l$ th cluster.

The parameters of the standard channel model have been adjusted to fit the measurements made for a number of different scenarios that consider the existence of a LOS path as well as the distance between the transmitter and the receiver. This in turn has given rise to four channel models. The CM1 model, which is based on LOS channel measurements and the CM2 model, which does not have LOS, have up to 4 m coverage. A longer distance, up to 10 m coverage, is targeted with the CM3 channel in the absence of the LOS path. The CM4 channel model was generated to fit a 25 ns root-mean-square (rms) delay spread to represent an extreme non-line-of-sight (NLOS) multipath channel [18]. When using the channel models, the total average received power of the multipath realizations is normalized to unity in order to provide a fair comparison with other wideband and narrowband systems, which can be done either through normalizing each realization or normalizing the total power averaged over all realizations [17]. Typical realizations from the four channel models are shown in Figure 2.1, where the time resolution is 1 ns. A quick inspection of the figure indicates that the delay spread increases with the distance between the transmitter and the receiver because the propagation paths become more nonuniform as the distance increases [12]. Also, the rms delay increases if the LOS path is absent: The CM1 channel model fits the measurements with 5.28 ns rms delay spread while the CM2 model is designed for those with 8.03 ns [18].

## 2.2. Rake Reception for Impulse Radio Signals

For impulse radio signals that have propagated through channels such as those in Figure 2.1 the useful energy in the multipath components may be combined using rake structures. Specifically, a rake receiver attempts to collect the time-shifted versions of the transmitted impulse radio pulses by providing separate correlators (fingers) for each of the multipath signals [16]. The outputs of the rake fingers are subsequently weighted and combined to form an overall decision statistic. With the MRC scheme, which maximizes the SNR of the decision statistic, each of the signals at the rake finger outputs is weighted in proportion to the finger SNR before being combined. Since this requires knowledge of the channel gains, the variances and the covariances of the noise components in each delay bin, referring to the channel model in (2.1) a total of at least  $2KL$  parameters may have to be estimated.

The rake receiver, which can achieve significant diversity gains in exchange for increased complexity so long as the energy of the resolved multipath components is combined efficiently, may be used for the reception of any pulse based UWB signal. As the complexity of the rake receiver is primarily related to the number and placement of rake fingers, it actually depends on the characteristics of the propagation channel. In particular, the number of rake fingers may be considerably reduced by selecting the most energetic paths, especially with LOS channels. Partial channel information is sufficient when combining the first arriving paths of dense multipath channels, where despite the worsening in performance, receiver complexity is very low compared to the rake that uses every path. As the number of resolved paths increases with the bandwidth of transmitted signals, the complexity of the rake receiver may increase as well [17]. Thus the reduction in the fading margin of multipath components observed with enlarging bandwidth is obtained at the price of a more complex rake receiver.

Another characteristic of the indoor UWB channel which affects rake receiver design is the delay spread that lasts several nanoseconds in time [18]. The implication of such a large multipath delay spread on the performance of the rake receiver is that it is adversely affected if the impulse radio pulses are spaced too closely in time as

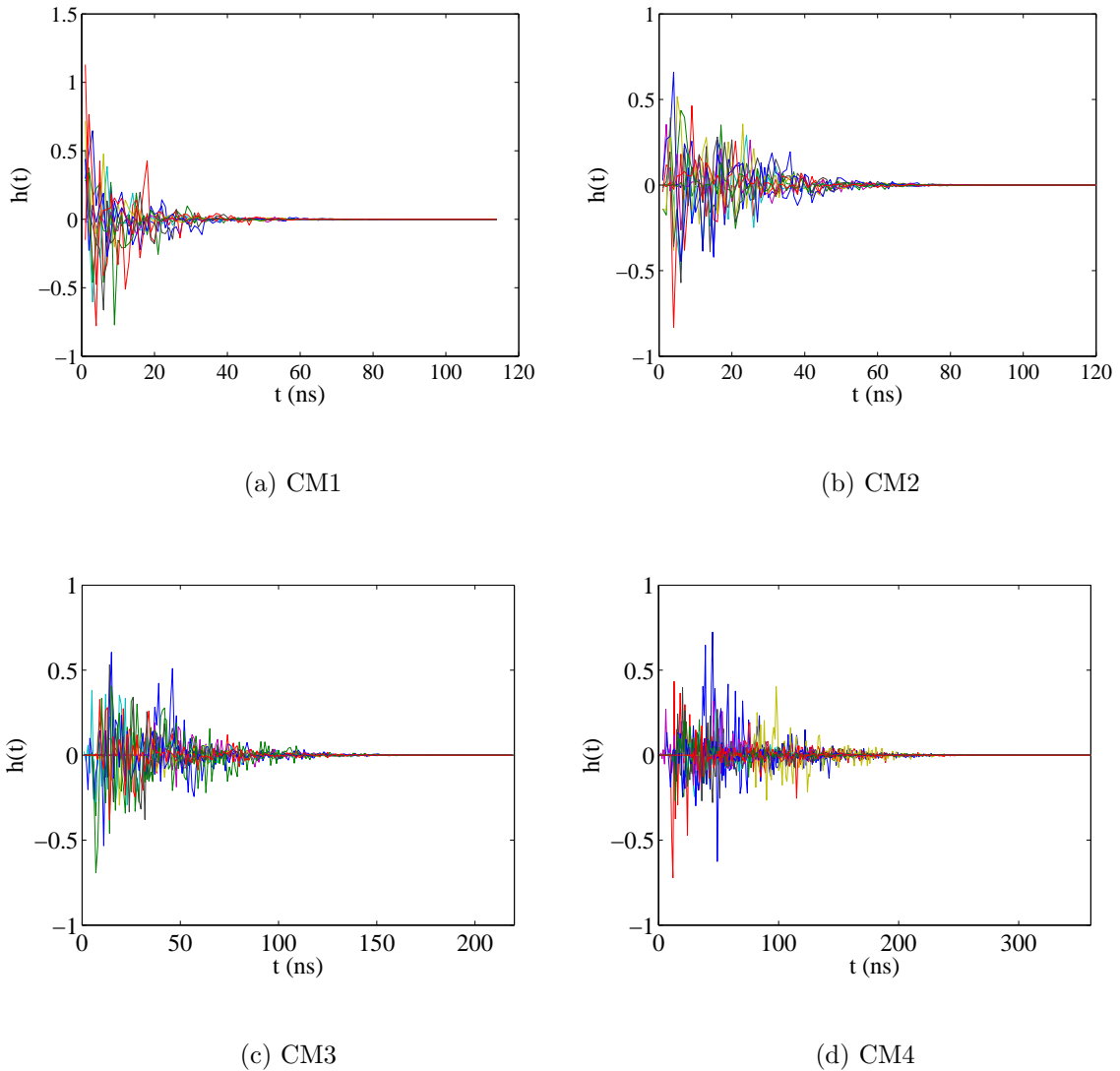


Figure 2.1. Impulse response realizations of the IEEE 802.15.3a channel model

is the case for high data rate applications. The ISI then created can be mitigated by employing equalization after rake combining. On the other hand, the study in [20] indicates that the time spreading induced by the wideband indoor channel leads to a reduction in the ISI variance due to two main reasons: First, the rake finger delays (timing of the correlators) are matched to the arrivals of the desired symbol, and second, the rake finger weights are uncorrelated with the channel coefficients of the interfering symbols. Thus, with limited resources capturing a large number of paths and obtaining the diversity gains predicted by the large multipath delay spread is more critical than the mitigation of the ISI, whose effect on system performance does not vary with increasing number of rake fingers. Benefits of rake reception are

also shown in [21] both in terms of reducing the effects of ISI as well as increasing the overall received signal energy. Even so, when realizing rake structures for imperfectly estimated channel coefficients, there should be an optimum number of paths to combine due to the fact that the signal energy contribution from the weaker paths, which is generally insignificant, may be accompanied by an accumulation of noise at the receiver.

### 3. ACHIEVABLE RATES OF M-ARY PPM IMPULSE RADIO

The capacity of the AWGN channel has been determined by Shannon to be the maximum mutual information achievable between its input and output [22]. In practice, rather than Gaussian signaling, and the theoretically optimal random coding and nearest neighbor decoding rule Shannon has suggested in his proof of the channel capacity theorem as a means for achieving the capacity, simpler modulation and demodulation schemes are preferred instead, mainly because of their computational feasibility [23]. Providing the ultimate transmission rate of communication, Shannon's channel capacity serves as a benchmark to which the performance of communication systems, as given in terms of the achievable information rates, may be compared.

For information-theoretical analysis of the communication applications of impulse radio, whereas multiple accessing is obtained through TH, data modulation is accomplished using PPM as in [1, 2]. The mutual information achieved by this type of signaling over the AWGN channel with M-ary orthogonal PPM and soft M-ary correlation receiver outputs is computed in [24] for single-user communication, and the results are extended to multiple access communication in [25] and [26] using the Gaussian approximation for the multiple access interference (MAI). When evaluating the mutual information of M-ary PPM impulse radio with hard outputs, the inaccuracy of the Gaussian MAI assumption for the AWGN channel leads to an overestimation of the achievable rates as demonstrated in [27], where a more precise statistical analysis of the MAI is developed. Moreover, the high transmission rates foreseen in the AWGN channel with soft outputs are not carried over to UWB systems operating in dense multipath environments: The binary PPM single-user system in [28] apparently has lower rates in NLOS frequency-selective channels in comparison to the rates anticipated in channels with no fading.

In this thesis, the information rates achievable by TH-PPM systems over UWB

channels with optimal single-user detection and either soft or hard outputs are determined in a multiuser setting. Recently, the capacity of soft-output UWB PPM and PAM systems over multipath fading channels has been studied in [29] by first deriving the capacity for an AWGN channel, which is then extended to a fading channel by averaging the SNR over the channel random variables. Similarly, the simplifications in [30], where the investigation covers M-ary PPM that employs soft or hard decoding, allow the treatment of impulse radio as a single-user PPM communication over a flat fading channel subject to AWGN. However, as emphasized previously in [28], studying the random variations in only the received signal energy is not sufficient for frequency-selective channels because the correlation properties of the transmitted signals are also significantly altered by the channel. In particular, the signal and noise components at the output of the M-ary correlation receiver are correlated. Evaluation of the rates achieved by TH-PPM systems over frequency-selective channels is inaccurate and incomplete if the correlation values between the PPM signals and the noise components are not considered, since those directly affect the soft- and hard-output rates, the rules for computing the hard outputs for frequency-selective channels, and the probability distribution of PPM symbols maximizing the mutual information between the input and output of the system. The maximum mutual information with hard outputs and the input symbol probability distribution that achieves it are found by applying the Arimoto-Blahut algorithm for computing the capacity of arbitrary discrete memoryless channels [31, 32]. When generalized for continuous-valued outputs as discussed in [32] and [33], the Arimoto-Blahut algorithm encompasses the soft-output systems under consideration, as well.

The rest of this chapter is organized as follows: The system model for impulse radio as used in this chapter is introduced in the next section along with the statistical characterizations of the MAI and the interframe interference (IFI) for rake reception. Section 3.2 is devoted to the calculation of the mutual information between the input and output of a digital communication system with orthogonal M-ary PPM, which has either soft or hard outputs. The simulation results in Section 3.3 demonstrate the major differences between soft- and hard-output systems in terms of the rates they achieve at various values of SNR.

### 3.1. UWB System Model

The UWB communication system described in this section is configured in such a way that several asynchronous impulse radio users transmit simultaneously over single-user links to communicate with others, where the intended user of any communication link has a rake receiver for performing single-user detection, and the knowledge it has is limited to the user it is trying to communicate with.

Employing TH for multiple access and M-ary PPM for data modulation, the signal transmitted by the  $k$ th user is

$$s_{\text{tr}}^{(k)}(t) = \sqrt{\frac{E_s}{N_s}} \sum_{j=-\infty}^{\infty} w_{\text{tr}}(t - jT_f - c_j^{(k)}T_c - \delta d_{\lfloor j/N_s \rfloor}^{(k)}), \quad (3.1)$$

where  $E_s$  is the symbol energy,  $N_s$  is the number of pulses transmitted per symbol, and each pulse,  $w_{\text{tr}}(t)$ , with duration  $T_p$ , is sent during a frame of  $T_f$  seconds. In each frame, the exact pulse position is determined by the TH sequence element  $c_j^{(k)}$  and the data symbol,  $d_{\lfloor j/N_s \rfloor}^{(k)} \in \{0, \dots, M-1\}$ , both of which are specific to user  $k$ . With  $\lfloor \cdot \rfloor$  denoting the integer floor, data symbol stays identical across  $N_s$  frames, and hence a kind of repetition coding is obtained. The starting time of the  $j$ th pulse is shifted by  $c_j^{(k)}T_c + \delta d_{\lfloor j/N_s \rfloor}^{(k)}$ , where  $c_j^{(k)} \in \{0, 1, \dots, N_h - 1\}$  is chosen randomly.  $N_h$  and  $T_c$  are the number and the duration of the bins to which the pulses are allowed to hop, respectively. The effect of  $\delta$  is such that  $\delta \geq T_p$  is necessary for orthogonal PPM. The frame time and the bin duration are selected to maximize  $N_h$ , and reduce the collision between the pulses of different users:  $T_f = (N_h - 1)T_c + M\delta$  and  $T_c = T_p$ .

Transmitted signals arrive at the receiver through frequency-selective channels due to the wide system bandwidth. The impulse response of the channel experienced by the  $k$ th user is

$$h_k(t) = \sum_{\ell=0}^{L_k-1} \alpha_{k,\ell} \delta_D(t - \tau_{k,\ell}), \quad (3.2)$$

where  $\alpha_{k,\ell}$  and  $\tau_{k,\ell} = \ell T_p$  are the gain and delay of the  $\ell$ th path of the  $k$ th user, respectively. Although the pulses received from different paths are not identical in the sense that the information they carry is frequency-dependent [34], for simplicity of the analysis we assume that the channel merely scales and delays the transmitted signal in a number of different ways, and the receiver antenna modifies the shape of the transmitted pulse so that the  $k$ th received signal is

$$s_{\text{rec}}^{(k)}(t) = \tilde{s}_{\text{tr}}^{(k)}(t) * h_k(t) \quad (3.3)$$

where  $*$  denotes convolution and  $\tilde{s}_{\text{tr}}^{(k)}(t)$  is  $s_{\text{tr}}^{(k)}(t)$  formed using the received pulse waveform,  $w_{\text{rec}}(t)$ , instead of  $w_{\text{tr}}(t)$ . A typical idealized model of the received pulse waveform used especially in the early studies of impulse radio is the unit energy second derivative Gaussian pulse, which is defined as in [2] so that it nominally begins at time zero:

$$w_{\text{rec}}\left(t + \frac{T_p}{2}\right) = \sqrt{\frac{8}{3t_n}} \left[1 - 4\pi \left(\frac{t}{t_n}\right)^2\right] \exp\left\{-2\pi \left(\frac{t}{t_n}\right)^2\right\}. \quad (3.4)$$

The autocorrelation function of the second derivative Gaussian pulse is given by [35]

$$R_w(\tau) = \left[1 - 4\pi \left(\frac{\tau}{t_n}\right)^2 + \frac{4\pi^2}{3} \left(\frac{\tau}{t_n}\right)^4\right] \exp\left\{-\pi \left(\frac{\tau}{t_n}\right)^2\right\}. \quad (3.5)$$

With this model of the received pulse,  $T_p = 2t_n$ , which contains 99.99% of the pulse energy. Representing the asynchronism between the  $k$ th transmitting user and the receiver with  $\tau_k$ , the total received signal is

$$r(t) = s_{\text{rec}}^{(0)}(t - \tau_0) + \sum_{k=1}^{K_r} s_{\text{rec}}^{(k)}(t - \tau_k) + n(t) \quad (3.6)$$

where  $n(t)$  is the AWGN component with two-sided power spectral density  $N_0/2$ . The signal model in (3.6) highlights the fact that there are  $K_r$  users interfering with a desired, e.g., 0th, user. The receiver is assumed to be perfectly synchronized with this user so that it has access to the elements of its TH code and  $\tau_0 = 0$ .

The received signal,  $r(t)$ , is converted by the signal demodulator into an  $M$ -dimensional vector,  $\mathbf{Y} = [y_0 \dots y_{M-1}]^T$ , where  $(\cdot)^T$  denotes the transpose. The vector  $\mathbf{Y}$  is subsequently used by the detector to decide which one of the  $M$  symbols was transmitted [36]. A typical realization of the demodulator is the  $M$ -ary correlation receiver, which is based on the use of  $M$  signal correlators, one for each possible transmitted symbol. To detect the 0th symbol of the desired user that transmits over the channel given by (3.2) for  $k = 0$ , the  $m$ th branch of the  $M$ -ary correlation receiver,  $y_m$ , is structured in the form of a rake:

$$y_m = \sum_{j=0}^{N_s-1} \sum_{\ell=0}^{\tilde{L}-1} \alpha_{0,\ell} \underbrace{\int_0^{\delta} r(t + jT_f + c_j^{(0)}T_c + \tau_{0,\ell} + m\delta) w_{\text{rec}}(t) dt}_{y_{j,\ell,m}} \quad m \in \{0, \dots, M-1\}. \quad (3.7)$$

In (3.7), rake finger outputs, where  $y_{j,\ell,m}$  is the one that corresponds to the  $\ell$ th path of the  $\tilde{L}$  paths used by the rake for the  $j$ th pulse, are merged using the conventional MRC scheme. Conventionally, MRC is implemented to maximize the SNR by assuming that the received paths are subject to independent and identically distributed (i.i.d.) noise components, which gives rise to combining weights that are equivalent to the path gains. In frequency-selective channels the optimality of this combining strategy is violated because of the interference from the other users and frames, which in general is nonuniform and correlated across different paths. It is then necessary to know the channels of the other users and weigh the contributions from different paths as, for instance, in [37] to maximize the SINR of the decision statistic, i.e.,  $y_m$ .

Being disturbed by the channel, the AWGN and the MAI, the  $m$ th component of  $\mathbf{Y}$  contains a signal term determined through the value of the symbol transmitted by the 0th user, which is  $s_{mi}$  for  $d^{(0)} = i$ , an IFI term,  $\eta_m^{(0)}$ , a MAI term in summation,  $\sum_{k=1}^{K_r} \eta_m^{(k)}$ , and a noise term  $n_m$ :

$$y_m = s_{mi} + \eta_m^{(0)} + \sum_{k=1}^{K_r} \eta_m^{(k)} + n_m. \quad (3.8)$$

Since  $R_w(\tau) = 0$  for  $|\tau| \geq T_p$ , with  $\delta = T_p$  the signal term in  $y_m$  is found to be

$$s_{mi} = \sqrt{E_s N_s} r_{\alpha, \tilde{L}}^{(0)}(m - i). \quad (3.9)$$

In (3.9), the signal term in the  $m$ th branch depends on the difference between the branch number and the value of the transmitted symbol, where  $r_{\alpha, \tilde{L}}^{(k)}(l)$  is the autocorrelation function of the truncated channel impulse response of the  $k$ th user at the  $l$ th lag:

$$r_{\alpha, \tilde{L}}^{(k)}(l) = \sum_{\ell=0}^{\tilde{L}-1} \alpha_{k, \ell} \alpha_{k, \ell+l}. \quad (3.10)$$

Analogous to the correlation created between the signal terms, the noise terms in frequency-selective channels are correlated as indicated by

$$\mathbb{E} \{n_m n_{m'}\} = N_s \frac{N_0}{2} r_{\alpha, \tilde{L}}^{(0)}(m' - m) \quad \text{for } m, m' \in \{0, \dots, M - 1\}. \quad (3.11)$$

### 3.1.1. Statistics of MAI for Asynchronous Users and Rake Reception

We resort to the Gaussian approximation of the MAI (and also the IFI) to provide analytical expressions for the achievable information rates of TH-PPM systems, since closed form expressions cannot be evaluated in general when the channel noise is the sum of a Gaussian noise and a non-Gaussian contaminating noise [38]. If none of the interferers dominate the received signal, as when even a coarse power control among the users exists, the MAI can be approximated as a Gaussian random variable with the number of transmitters and received paths going large [39], in which case the mean and the variance sufficiently characterize the MAI.

Previously, moments of

$$\eta_{m,A}^{(k)} = \sum_{j=0}^{N_s-1} \sum_{j'=-\infty}^{\infty} \sqrt{\frac{E_s}{N_s}} R_w((c_j^{(0)} - c_{j'}^{(k)})T_c - \delta d_{\lfloor j'/N_s \rfloor}^{(k)} - \tau_k + (j - j')T_f + m\delta), \quad (3.12)$$

has been evaluated in [2], where  $\eta_{m,A}^{(k)}$  is the signal component at the output of the  $m$ th signal correlator of the M-ary correlation receiver that results from the  $k$ th user in the AWGN channel, i.e., no fading. This has been carried out by computing the conditional expectation over the time asynchronism given the sequence variables and data symbols, and then averaging over the two remaining variables. For analytical convenience, it is assumed in [2] that the time interval over which pulses are allowed to hop is constrained to less than half the frame time

$$N_h T_c < \frac{T_f}{2} - 2T_p. \quad (3.13)$$

With (3.13), it is guaranteed that in the AWGN channel the correlator output for each pulse of the desired user receives interference from exactly one pulse of the interfering user. It is shown in [2] that regardless of TH sequence values and data symbols, the first two moments of  $\eta_{m,A}^{(k)}$  are

$$\mathbb{E} \left\{ \eta_{m,A}^{(k)} \right\} = 0 \quad (3.14)$$

$$\mathbb{E} \left\{ \left( \eta_{m,A}^{(k)} \right)^2 \right\} = \frac{E_s}{T_f} \int_{-\infty}^{\infty} |R_w(\tau)|^2 d\tau. \quad (3.15)$$

Therefore, when calculating statistics of MAI, averaging explicitly over TH codes and data symbols is not necessary for the AWGN channel. Even if the constraint in (3.13) is removed, the expression for the variance of  $\eta_{m,A}^{(k)}$  does not change as an inspection of Figure 3.1 implies. As  $\tau_k$  varies over the range  $[0, T_f)$ , the 0th frame of the desired user is interfered by the 0th and -1st frame of the  $k$ th user with probabilities  $\Pr \left\{ c_0^{(k)} T_c + \delta d_0^{(k)} < c_0^{(0)} T_c + \delta d_0^{(0)} + T_p \right\}$  and  $\Pr \left\{ c_{-1}^{(k)} T_c + \delta d_{-1}^{(k)} + T_p > c_0^{(0)} T_c + \delta d_0^{(0)} \right\}$ , respectively. Since TH codes and data symbols are independently generated, these two probabilities add up to one, which means that the 0th frame of the desired user gets interference from only one frame of the  $k$ th interfering user on the average.

With the frequency-selectivity of the channels under consideration, however, calculation of the exact values for the mean and the variance of the MAI in (3.8) that

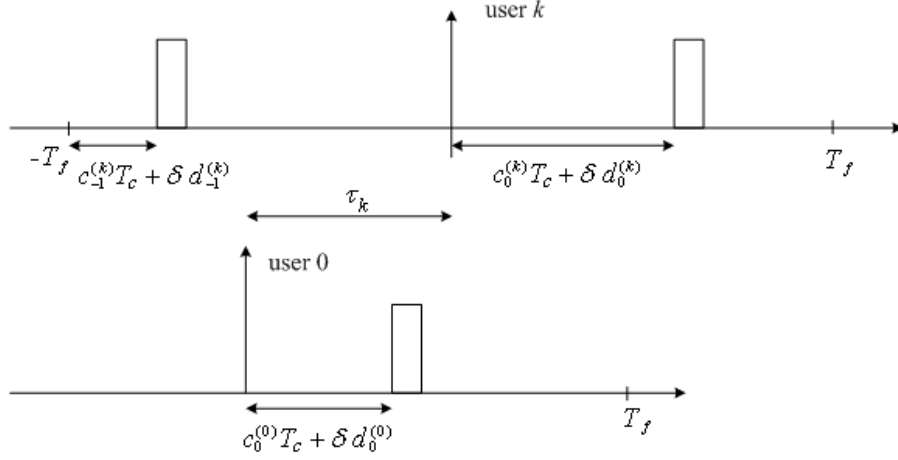


Figure 3.1. Timing diagram for impulse radio in the AWGN channel with TH over the whole frame and  $N_s = 1$

results from the  $k$ th interfering user

$$\eta_m^{(k)} = \sum_{j=0}^{N_s-1} \sum_{\ell=0}^{L-1} \alpha_{0,\ell} \eta_{j,\ell,m}^{(k)} \quad \text{for } k = 1 \dots, K_r \quad (3.16)$$

is computationally prohibitive, for it involves a large number of random terms that are correlated. Specifically,  $\eta_{j,\ell,m}^{(k)}$  in (3.16), the MAI component in  $y_{j,\ell,m}$  due to the  $k$ th user is given by

$$\begin{aligned} \eta_{j,\ell,m}^{(k)} &= \int_0^\delta \sqrt{\frac{E_s}{N_s}} \sum_{j'=-\infty}^{\infty} \sum_{\ell'=0}^{L_k-1} \alpha_{k,\ell'} w_{\text{rec}}(t - j'T_f - c_{j'}^{(k)}T_c - \delta d_{\lfloor j'/N_s \rfloor}^{(k)} - \tau_{k,\ell'} - \tau_k \\ &\quad + jT_f + c_j^{(0)}T_c + \tau_{0,\ell} + m\delta) \times w_{\text{rec}}(t) dt \\ &= \sqrt{\frac{E_s}{N_s}} \sum_{j'=-\infty}^{\infty} \sum_{\ell'=0}^{L_k-1} \alpha_{k,\ell'} R_w(\Delta_{j,j'}^{(k)} + (j - j')T_f + m\delta + \tau_{0,\ell} - \tau_{k,\ell'}) \end{aligned} \quad (3.17)$$

where  $\Delta_{j,j'}^{(k)} = (c_j^{(0)} - c_{j'}^{(k)})T_c - \delta d_{\lfloor j'/N_s \rfloor}^{(k)} - \tau_k$ . Since  $\tau_k$  is related to the times the asynchronous users begin transmission, it is assumed to be uniformly distributed on  $[0, N_s T_f)$  as in [2]. Further assuming that multiple paths of users are independent, which corresponds to ignoring the correlation among the terms in (3.17),  $\eta_m^{(k)}$  is modeled

as a zero-mean Gaussian random variable with variance

$$\mathbb{E} \left\{ (\eta_m^{(k)})^2 \right\} = \frac{E_s}{T_f} r_{\alpha, \tilde{L}}^{(0)}(0) r_{\alpha, L_k}^{(k)}(0) \int_{-\infty}^{\infty} |R_w(\tau)|^2 d\tau. \quad (3.18)$$

This approximate expression treats each path of the desired and interfering users as an independently transmitted pulse in an effort to generalize the derivations that are carried out in [2] for the AWGN channel to include frequency-selective channels as well. The reasoning for frequency-selective channels is that even when the channel creates IFI, i.e.,  $\tau_{k, L_{k-1}} > T_f$ , on the average, each path that originates from the pulse in a particular frame of the desired user is interfered exactly once by each of those that belong to the channel impulse responses of other users. Also, an expression similar to the one in (3.18) appears in [40] for the variance of the MAI caused by an interfering user, where an independent random delay for each arriving path of the user is assumed.

For the received pulse waveform model in (3.4),  $\int_{-\infty}^{\infty} |R_w(\tau)|^2 d\tau = 35t_n/48\sqrt{2}$ . Therefore, the approximate variance of  $\eta_m^{(k)}$  calculated from (3.18) is related to the frame-wise processing gain,  $\chi = T_f/T_p$ , through

$$\mathbb{E} \left\{ (\eta_m^{(k)})^2 \right\} = \frac{E_s}{\chi} \frac{35}{96\sqrt{2}} r_{\alpha, \tilde{L}}^{(0)}(0) r_{\alpha, L_k}^{(k)}(0). \quad (3.19)$$

Thus, the higher the processing gain,  $\chi$ , the better the MAI rejection capability of the UWB system as expected.

The approximate cross-correlation of the MAI due to the  $k$ th user that affects different branches of the M-ary correlation receiver, likewise, is

$$\mathbb{E} \{ \eta_m^{(k)} \eta_{m'}^{(k)} \} = \frac{E_s}{T_f} r_{\alpha, \tilde{L}}^{(0)}(0) r_{\alpha, L_k}^{(k)}(m' - m) \int_{-\infty}^{\infty} |R_w(\tau)|^2 d\tau. \quad (3.20)$$

$\mathbb{E} \{ \eta_m^{(k)} \eta_{m'}^{(k)} \}$  reduces with an enlarging separation between the branches of the M-ary correlation receiver, because, in fact, the correlation among the paths of the  $k$ th user that affects the term,  $r_{\alpha, L_k}^{(k)}(m' - m)$ , becomes lower.

### 3.1.2. Statistics of IFI for Rake Reception

For orthogonal PPM with  $\delta = T_p$  the IFI term in (3.8),  $\eta_m^{(0)}$ , is determined by substituting  $k = 0$  and  $\tau_0 = 0$  in (3.16) and (3.17), which results in

$$\eta_m^{(0)} = \sqrt{\frac{E_s}{N_s}} \sum_{j=0}^{N_s-1} \sum_{\substack{i=-j_0 \\ i \neq 0}}^{\tilde{j}} r_{\alpha, \tilde{L}}^{(0)}(\chi i + p_i^j + m - d_i^j), \quad (3.21)$$

where  $p_i^j = c_j^{(0)} - c_{j-i}^{(0)}$ ,  $d_i^j = d_{\lfloor (j-i)/N_s \rfloor}^{(0)}$ ,  $\tilde{j} = \lfloor \tilde{L}/\chi \rfloor + 1$  and  $j_0 = \lfloor \tau_{0, L_0-1}/T_f \rfloor + 1$ . As before, calculating the exact values of the mean and the variance of the IFI is a difficult task. However, a smaller number of random variables are involved in the expression for  $\eta_m^{(0)}$  with  $N_s = 1$  allowing us to exactly compute its mean for the  $j$ th frame (symbol) as

$$\mathbb{E} \{ \eta_m^{(0)} \} = \sqrt{E_s} \sum_{\substack{i=-j_0 \\ i \neq 0}}^{\tilde{j}} \sum_{d_i^j=0}^{M-1} f_{d_i^j}(d_i^j) \sum_{p_i^j=-(N_h-1)}^{N_h-1} f_{p_i^j}(p_i^j) r_{\alpha, \tilde{L}}^{(0)}(\chi i + p_i^j + m - d_i^j) \quad \text{for } N_s = 1. \quad (3.22)$$

The pdf of  $p_i^j$  that appears in (3.22) is

$$\begin{aligned} f_{p_i^j}(p_i^j) &= \sum_{l=0}^{N_h-1} f_{c_j^{(0)}}(l) f_{p_i^j|c_j^{(0)}}(p_i^j|l) \\ &= \begin{cases} \sum_{l=0}^{N_h-1-|p_i^j|} \frac{1}{N_h^2} & p_i^j \leq 0, \\ \sum_{l=p_i^j}^{N_h-1} \frac{1}{N_h^2} & p_i^j \geq 0 \end{cases} \\ &= \frac{N_h - |p_i^j|}{N_h^2}, \end{aligned} \quad (3.23)$$

where  $f_{c_j^{(0)}}(l) = 1/N_h$  and

$$f_{p_i^j|c_j^{(0)}}(p_i^j|l) = \begin{cases} \frac{1}{N_h} & \text{for } l = 0, \dots, N_h - 1 - |p_i^j| \text{ and } p_i^j \leq 0, \\ \frac{1}{N_h} & \text{for } l = p_i^j, \dots, N_h - 1 \text{ and } p_i^j > 0, \\ 0 & \text{otherwise.} \end{cases} \quad (3.24)$$

The cross-correlation of the IFI in different branches of the M-ary correlation receiver for the  $j$ th frame is given exactly by

$$\begin{aligned}
\mathbb{E} \left\{ \eta_m^{(0)} \eta_{m'}^{(0)} \right\} &= E_s \sum_{\substack{i=-j_0 \\ i \neq 0}}^{\tilde{j}} \sum_{d_i^j=0}^{M-1} f_{d_i^j}(d_i^j) \sum_{p_i^j=-(N_h-1)}^{N_h-1} f_{p_i^j}(p_i^j) \\
&\quad \times r_{\alpha, \tilde{L}}^{(0)}(\chi i + p_i^j + m - d_i^j) r_{\alpha, \tilde{L}}^{(0)}(\chi i + p_i^j + m' - d_i^j) \\
&+ E_s \sum_{\substack{i=-j_0 \\ i \neq 0}}^{\tilde{j}} \sum_{d_i^j=0}^{M-1} f_{d_i^j}(d_i^j) \sum_{\substack{i'=-j_0 \\ i' \neq 0, i}}^{j_0} \sum_{d_{i'}^j=0}^{M-1} f_{d_{i'}^j}(d_{i'}^j) \sum_{p_i^j=-(N_h-1)}^{N_h-1} \sum_{p_{i'}^j=-(N_h-1)}^{N_h-1} f_{p_i^j, p_{i'}^j}(p_i^j, p_{i'}^j) \\
&\quad \times r_{\alpha, \tilde{L}}^{(0)}(\chi i + p_i^j + m - d_i^j) r_{\alpha, \tilde{L}}^{(0)}(\chi i' + p_{i'}^j + m' - d_{i'}^j) \quad \text{for } N_s = 1. \tag{3.25}
\end{aligned}$$

Note that the second moment of  $\eta_m^{(0)}$  is determined from (3.25) using  $m' = m$ . The joint pdf of the random variables,  $p_i^j$  and  $p_{i'}^j$ , in (3.25)

$$f_{p_i^j, p_{i'}^j}(p_i^j, p_{i'}^j) = \frac{1}{N_h} \sum_{\max(0, p_i^j, p_{i'}^j)}^{N_h-1-\max(0, |p_i^j|, |p_{i'}^j|)} \frac{1}{N_h^2} \tag{3.26}$$

is derived from

$$f_{p_i^j, p_{i'}^j}(p_i^j, p_{i'}^j) = \sum_{l=0}^{N_h-1} f_{p_i^j|c_j^{(0)}}(p_i^j|l) f_{p_{i'}^j|c_j^{(0)}}(p_{i'}^j|l) f_{c_j^{(0)}}(l). \tag{3.27}$$

Considering the case where  $N_s > 1$ , the second moment of  $\eta_m^{(0)}$  is approximated using

$$\mathbb{E} \left\{ (\eta_m^{(0)})^2 \right\} = \frac{E_s}{T_f} \sum_{\ell=0}^{\tilde{L}-1} \alpha_{0, \ell}^2 \sum_{\substack{\ell'=0 \\ \ell' \neq \ell}}^{L_0-1} \alpha_{0, \ell'}^2 \int_{-\infty}^{\infty} |R_w(\tau)|^2 d\tau, \tag{3.28}$$

which is obtained by regarding the IFI as if it is created by another interfering user with randomly arriving paths. This also leads to the zero-mean assumption for the IFI. Realizing that the choice  $T_f = (N_h - 1)T_c + M\delta$  prevents the transmission of overlapped pulses, simultaneous arrival of two paths with the same amplitude is prohibited, which

requires the condition  $\ell' \neq \ell$  in (3.28). Similarly, for  $N_s > 1$

$$\mathbb{E} \left\{ \eta_m^{(0)} \eta_{m'}^{(0)} \right\} = \frac{E_s}{T_f} \sum_{\ell=0}^{\tilde{L}-1} \alpha_{0,\ell}^2 \sum_{\substack{\ell'=0 \\ \ell' \neq \ell}}^{L_0-1} \alpha_{0,\ell'} \alpha_{0,\ell'+m'-m} \int_{-\infty}^{\infty} |R_w(\tau)|^2 d\tau. \quad (3.29)$$

While the expressions in (3.22) and (3.25) are exact for  $N_s = 1$ , (3.28) is an approximation of the variance of the IFI for larger values of  $N_s$ , where the IFI is assumed to be zero-mean. The Gaussian assumption for the MAI and the IFI designates Gaussian distributed  $y_m$  with the mean  $s_{mi} + \mathbb{E}\{\eta_m^{(0)}\}$  and a variance, which is the sum of the variances of  $n_m$  and  $\eta_m^{(k)}$  for  $k = 0, \dots, K_r$ . The cross-covariances of branches of the M-ary correlation receiver are arrived at by making use of (3.20) and (3.25), where  $N_s = 1$ . On the other hand, for the analysis of the situations that have  $N_s > 1$ , one should resort to (3.20) and (3.29). Although previous works such as [25] and [26] select  $N_s = 1$  for the simplicity and clarity of the expressions, we prefer it in our performance studies because we are able to employ exact expressions for the IFI moments with  $N_s = 1$ . The implications of this choice on the interpretation of the results are included in Section 3.3.

### 3.2. Mutual Information for Impulse Radio in UWB Channels

The information rates achievable by impulse radio over frequency-selective channels correspond to the maximum mutual information between the input and output of the system in Figure 3.2. The input-output relationship in Figure 3.2 indicates that for orthogonal PPM, each n-bit block at the output of the channel encoder is mapped to one of  $M = 2^n$  mutually orthogonal signal waveforms,  $s_i(t)$ , obtained from (3.1) using  $i = d^{(0)}$ , which also determines

$$x_m = \int_{-\infty}^{\infty} s_i(t) s_m(t) dt = E_s \delta_D(i - m) \quad (3.30)$$

for  $i, m \in \{0, \dots, M-1\}$ . At the receiving end, the demodulator processes the waveform affected by the UWB channel, the noise and the MAI to reduce it to the vector  $\mathbf{Y}$ .

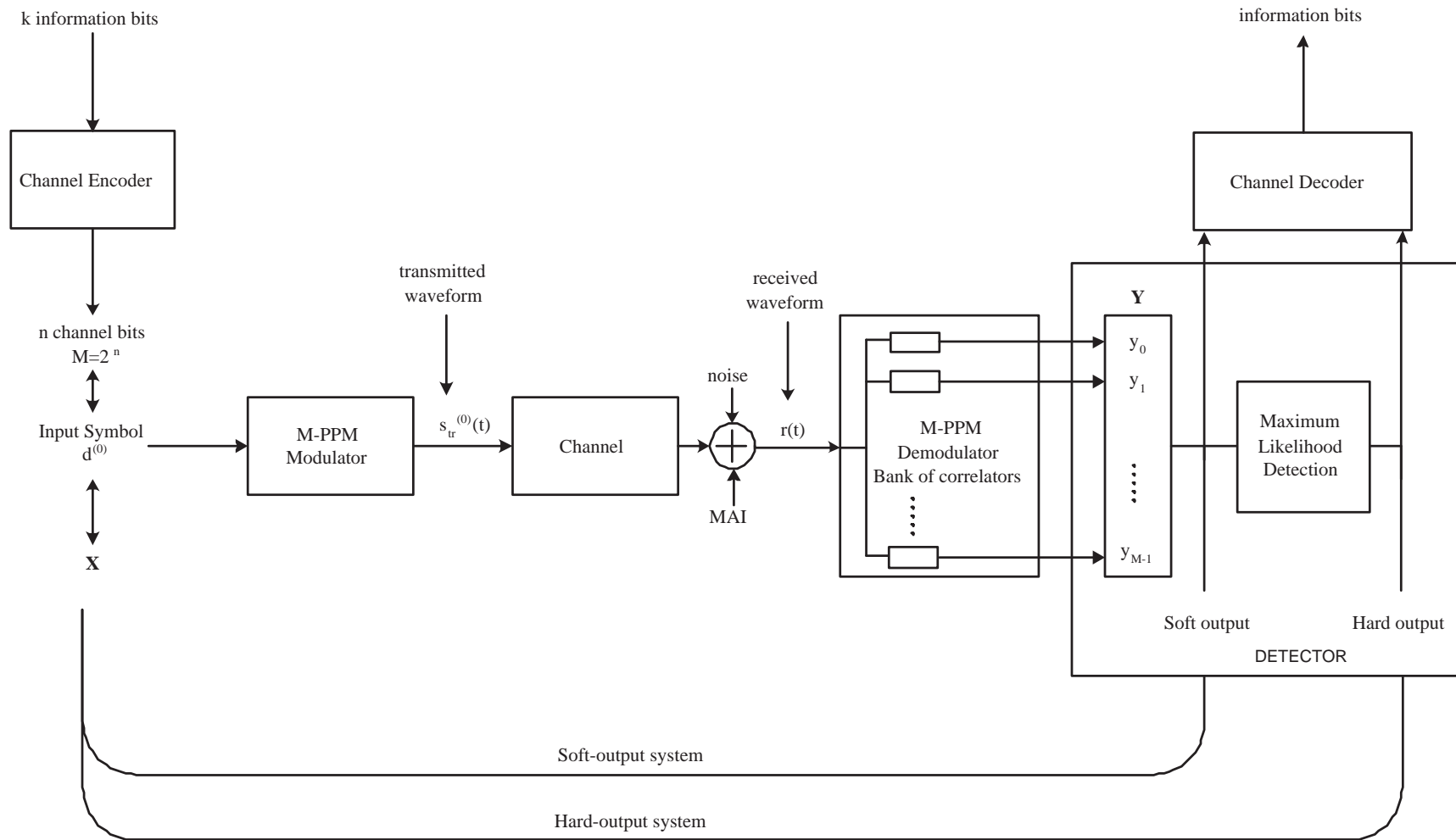


Figure 3.2. The system model for calculation of achievable information rates

The decision process inside the detector may be viewed as some kind of quantization on  $\mathbf{Y}$  [36]. In one of the extreme cases, the detector leaves  $\mathbf{Y}$  as it is. With such soft-decision outputs, it is possible to take advantage of better performing channel codes, which admit soft-decoding algorithms [41]. Alternatively, the detector makes a hard decision by choosing one of the  $M$  symbols as being transmitted.

### 3.2.1. Soft-Output M-ary PPM Impulse Radio

As the channel encoding operation that maps  $k$  information bits to  $n$  channel bits is deterministic, the information carried by those two sets of bits are equivalent. Moreover, because the transmitted symbol,  $d^{(0)}$ , and  $\mathbf{X} \triangleq [x_0 \dots x_{M-1}]^T$  are related by an invertible transformation, the mutual information between  $d^{(0)}$  and  $\mathbf{Y}$  is equivalent to the one between  $\mathbf{X}$  and  $\mathbf{Y}$ , which is

$$I(\mathbf{X}; \mathbf{Y}) = - \sum_{i=0}^{M-1} p(\mathbf{x}_i) \int_{-\infty}^{\infty} f(\mathbf{y}|\mathbf{x}_i) \log_2 \left( \frac{\sum_{j=0}^{M-1} p(\mathbf{x}_j) f(\mathbf{y}|\mathbf{x}_j)}{f(\mathbf{y}|\mathbf{x}_i)} \right) d\mathbf{y} \quad (3.31)$$

where  $\mathbf{y}$  is the realized vector value of  $\mathbf{Y}$  and  $\mathbf{x}_i$  is the vector  $\mathbf{X}$  for the symbol  $i = \{0, \dots, M-1\}$ , which is an  $M$ -dimensional all-zero vector except for the  $(i+1)$ st position that has  $E_s$ . The vector  $\mathbf{x}_i$  is converted by the UWB channel, the AWGN and the MAI into  $\mathbf{y}$ , whose components,  $y_m$  for  $m \in \{0, \dots, M-1\}$ , are correlated due to the receiver noise, the IFI and the MAI. Taking this fact into account, the conditional pdf in (3.31) is given by

$$f(\mathbf{y}|\mathbf{x}_i) = \frac{1}{(2\pi)^{M/2} (\det \mathbf{M}_{\mathbf{y}})^{1/2}} \exp \left[ -\frac{1}{2} (\mathbf{y} - \mathbf{m}_{\mathbf{y}}^i)^T \mathbf{M}_{\mathbf{y}}^{-1} (\mathbf{y} - \mathbf{m}_{\mathbf{y}}^i) \right], \quad (3.32)$$

where  $\mathbf{M}_{\mathbf{y}}$  is the covariance matrix of  $\mathbf{y}$ ,  $\mathbf{m}_{\mathbf{y}}^i$  is the mean vector of  $\mathbf{y}$  given that the  $i$ th symbol is transmitted, and  $\det(\cdot)$  is the determinant. While the element of  $\mathbf{M}_{\mathbf{y}}$  in the  $m$ th row and  $m'$ th column,  $(\mathbf{M}_{\mathbf{y}})_{m,m'}$ , depends on the IFI, the MAI and the noise as

$$(\mathbf{M}_{\mathbf{y}})_{m,m'} = \underbrace{\mathbb{E}\{\eta_m^{(0)} \eta_{m'}^{(0)}\} - \mathbb{E}\{\eta_m^{(0)}\} \mathbb{E}\{\eta_{m'}^{(0)}\}}_{\text{IFI}} + \underbrace{\sum_{k=1}^{K_r} \mathbb{E}\{\eta_m^{(k)} \eta_{m'}^{(k)}\}}_{\text{MAI}} + \underbrace{\mathbb{E}\{n_m n_{m'}\}}_{\text{noise}}, \quad (3.33)$$

the  $m$ th element of  $\mathbf{m}_y^i$  is  $s_{mi} + E\{\eta_m^{(0)}\}$ .

Since the integral in (3.31) has to be performed over a correlated set of jointly Gaussian random variables, computing  $I(\mathbf{X}; \mathbf{Y})$  becomes tedious for large  $M$ . This problem may be circumvented by resorting to a linear transformation of a set of jointly Gaussian random variables that results in statistically independent Gaussian random variables. Specifically, the transformation [42]

$$\tilde{\mathbf{y}} = \mathbf{A}^T \mathbf{y}, \quad (3.34)$$

creates uncorrelated components for  $\tilde{\mathbf{y}} = [\tilde{y}_0 \dots \tilde{y}_{M-1}]^T$  if  $\mathbf{A}$  is an orthogonal matrix consisting of columns that are the eigenvectors of  $\mathbf{M}_y$ . Given that the  $i$ th symbol is transmitted, the mean vector and the covariance matrix of  $\tilde{\mathbf{y}}$ , which we denote by  $\mathbf{m}_{\tilde{\mathbf{y}}}^i$  and  $\Sigma_{\tilde{\mathbf{y}}}$ , respectively, are

$$\mathbf{m}_{\tilde{\mathbf{y}}}^i = \mathbf{A}^T \mathbf{m}_y^i \quad (3.35)$$

$$\Sigma_{\tilde{\mathbf{y}}} = \mathbf{A}^T \mathbf{M}_y \mathbf{A}, \quad (3.36)$$

where  $\mathbf{m}_{\tilde{\mathbf{y}}}^i = [m_{\tilde{y},0}^i \dots m_{\tilde{y},M-1}^i]^T$  and  $\Sigma_{\tilde{\mathbf{y}}} = \text{diag}\{\sigma_{\tilde{y},0}^2, \dots, \sigma_{\tilde{y},M-1}^2\}$  is a diagonal matrix that contains the eigenvalues of  $\mathbf{M}_y$ .

The conditional pdf  $f(\tilde{\mathbf{y}}|\mathbf{x}_i)$  is obtained from (3.32) by replacing  $\mathbf{m}_y^i$  and  $\mathbf{M}_y$  with  $\mathbf{m}_{\tilde{\mathbf{y}}}^i$  and  $\Sigma_{\tilde{\mathbf{y}}}$ , respectively. Due to the fact that  $\Sigma_{\tilde{\mathbf{y}}}$  is a diagonal matrix,  $f(\tilde{\mathbf{y}}|\mathbf{x}_i)$  may also be expressed as

$$f(\tilde{\mathbf{y}}|\mathbf{x}_i) = \frac{1}{(2\pi)^{M/2} \prod_{j=0}^{M-1} \sigma_{\tilde{y},j}} \exp \left[ - \sum_{j=0}^{M-1} \frac{(\tilde{y}_j - m_{\tilde{y},j}^i)^2}{2\sigma_{\tilde{y},j}^2} \right] \quad (3.37)$$

emphasizing that the components of  $\tilde{\mathbf{y}}$  are independent Gaussian random variables.

As uncorrelated components are created by means of an invertible linear transformation,  $I(\mathbf{X}; \tilde{\mathbf{Y}})$  and  $I(\mathbf{X}; \mathbf{Y})$  are equivalent. Based on (3.35), (3.36) and a series of

manipulations, the mutual information between  $\mathbf{X}$  and  $\tilde{\mathbf{Y}}$  is determined to be

$$\begin{aligned}
I(\mathbf{X}; \tilde{\mathbf{Y}}) &= - \sum_{i=0}^{M-1} p(\mathbf{x}_i) \int_{-\infty}^{\infty} f(\tilde{\mathbf{y}}|\mathbf{x}_i) \log_2 \left\{ \sum_{j=0}^{M-1} p(\mathbf{x}_j) \right. \\
&\quad \left. \times \exp \left( \sum_{m=0}^{M-1} \frac{\tilde{y}_m}{\sigma_{\tilde{y},m}^2} (m_{\tilde{y},m}^j - m_{\tilde{y},m}^i) + \frac{(m_{\tilde{y},m}^i)^2 - (m_{\tilde{y},m}^j)^2}{2\sigma_{\tilde{y},m}^2} \right) \right\} d\tilde{\mathbf{y}}.
\end{aligned} \tag{3.38}$$

Although the mutual information is maximized by equiprobable symbols, i.e.,  $p(\mathbf{x}_i) = 1/M$ , for orthogonal signals in the AWGN channel as indicated in [41], the frequency-selectivity of the UWB channel affects the mean of the system output in such a way that the input distribution that maximizes the mutual information for  $M > 2$  depends on the channel realizations of the users engaged. For the AWGN channel, the mean vector of  $\mathbf{Y}$  is  $\mathbf{x}_i$  given the  $i$ th symbol is transmitted. However, if different symbols are transmitted over frequency-selective channels, the mean vector of  $\mathbf{Y}$  does not contain the same elements as shown below for  $M = 4$

$$\mathbf{s}_0 = [r_{\alpha,\tilde{L}}^{(0)}(0) \ r_{\alpha,\tilde{L}}^{(0)}(1) \ r_{\alpha,\tilde{L}}^{(0)}(2) \ r_{\alpha,\tilde{L}}^{(0)}(3)] \tag{3.39}$$

$$\mathbf{s}_1 = [r_{\alpha,\tilde{L}}^{(0)}(1) \ r_{\alpha,\tilde{L}}^{(0)}(0) \ r_{\alpha,\tilde{L}}^{(0)}(1) \ r_{\alpha,\tilde{L}}^{(0)}(2)] \tag{3.40}$$

$$\mathbf{s}_2 = [r_{\alpha,\tilde{L}}^{(0)}(2) \ r_{\alpha,\tilde{L}}^{(0)}(1) \ r_{\alpha,\tilde{L}}^{(0)}(0) \ r_{\alpha,\tilde{L}}^{(0)}(1)] \tag{3.41}$$

$$\mathbf{s}_3 = [r_{\alpha,\tilde{L}}^{(0)}(3) \ r_{\alpha,\tilde{L}}^{(0)}(2) \ r_{\alpha,\tilde{L}}^{(0)}(1) \ r_{\alpha,\tilde{L}}^{(0)}(0)] \tag{3.42}$$

where  $\mathbf{s}_i$  is the mean vector of  $\mathbf{Y}$  given that the  $i$ th symbol is transmitted. The  $\mathbf{s}_i$  are obtained using (3.9) so that IFI is absent. Thus, UWB channels are not symmetric in the sense that the the mean of the output depends on the transmitted symbol. Mathematically stated, the contribution to the mutual information  $I(\mathbf{X}; \mathbf{Y})$  from different transmitted symbols are not identical with frequency-selectivity and the PPM mapping  $\delta = iT_p$ . In such a case, it is not possible to say that the equally-likely symbols maximize the mutual information. Yet, the maximum mutual information and the input symbol distribution that achieves it may be found iteratively for these channels through the Arimoto-Blahut algorithm as discussed in Subsection 3.2.3. At each step

of the algorithm, the part that requires handling an  $m$ -fold integral to perform the expectation operation in (3.38),  $E_{\tilde{\mathbf{y}}|\mathbf{x}_i}\{\cdot\}$ , is evaluated by creating  $\tilde{\mathbf{y}}$  according to the Gaussian distribution in (3.37) and averaging the results.

### 3.2.2. Hard-Output M-ary PPM Impulse Radio

In the AWGN channel, the maximum-likelihood (ML) detector selects the symbol that results in the maximum cross-correlation between  $\mathbf{Y}$  and each of the  $M$  orthogonal signal vectors possibly transmitted,  $\mathbf{x}_i$  for  $i \in \{0, \dots, M-1\}$ , which is mathematically equivalent to [36]

$$\hat{d}^{(0)} = \arg \max_m y_m. \quad (3.43)$$

Correspondingly, the ML signal detector for frequency-selective channels should be designed before the mutual information for hard-output impulse radio is calculated.

The hard-decision rule based on the ML criterion chooses the maximum of  $f(\mathbf{y}|\mathbf{x}_i)$  over the  $M$  symbols:

$$\hat{d}^{(0)} = \arg \max_i f(\mathbf{y}|\mathbf{x}_i). \quad (3.44)$$

Taking the natural logarithm of (3.32), expanding it by observing that

$$\begin{aligned} (\mathbf{y} - \mathbf{m}_y^i)^T \mathbf{M}_y^{-1} (\mathbf{y} - \mathbf{m}_y^i) &= (\mathbf{y} - \mathbf{m}_y^i)^T \mathbf{A} \mathbf{A}^T \mathbf{M}_y^{-1} \mathbf{A} \mathbf{A}^T (\mathbf{y} - \mathbf{m}_y^i) \\ &= (\tilde{\mathbf{y}} - \mathbf{m}_{\tilde{\mathbf{y}}}^i)^T \Sigma_{\tilde{\mathbf{y}}}^{-1} (\tilde{\mathbf{y}} - \mathbf{m}_{\tilde{\mathbf{y}}}^i) \end{aligned} \quad (3.45)$$

and ignoring terms common to all  $i$  results in the following ML decision statistic to be maximized:

$$\xi_i = \tilde{\mathbf{y}}^T \Sigma_{\tilde{\mathbf{y}}}^{-1} \mathbf{m}_{\tilde{\mathbf{y}}}^i - \frac{1}{2} (\mathbf{m}_{\tilde{\mathbf{y}}}^i)^T \Sigma_{\tilde{\mathbf{y}}}^{-1} \mathbf{m}_{\tilde{\mathbf{y}}}^i. \quad (3.46)$$

The detected symbol then is

$$\hat{d}^{(0)} = \arg \max_i \xi_i. \quad (3.47)$$

The mutual information between the input and output of impulse radio with hard decisions that are based on the ML criterion is

$$I(\mathbf{X}; \hat{d}^{(0)}) = H(\hat{d}^{(0)}) - H(\hat{d}^{(0)}|\mathbf{X}), \quad (3.48)$$

where the entropies are

$$\begin{aligned} H(\hat{d}^{(0)}) &= - \sum_{m=0}^{M-1} p(\hat{d}^{(0)} = m) \log_2 p(\hat{d}^{(0)} = m) \\ H(\hat{d}^{(0)}|\mathbf{X}) &= - \sum_{i=0}^{M-1} p(\mathbf{x}_i) \sum_{m=0}^{M-1} p(\hat{d}^{(0)} = m|\mathbf{x}_i) \log_2 p(\hat{d}^{(0)} = m|\mathbf{x}_i) \end{aligned} \quad (3.49)$$

and, thus,

$$I(\mathbf{X}; \hat{d}^{(0)}) = \sum_{i=0}^{M-1} p(\mathbf{x}_i) \sum_{m=0}^{M-1} p(\hat{d}^{(0)} = m|\mathbf{x}_i) \log_2 \frac{p(\hat{d}^{(0)} = m|\mathbf{x}_i)}{\sum_{j=0}^{M-1} p(\mathbf{x}_j) p(\hat{d}^{(0)} = m|\mathbf{x}_j)}. \quad (3.50)$$

Both the probabilities

$$p(\hat{d}^{(0)} = m) = \sum_{i=0}^{M-1} p(\hat{d}^{(0)} = m|\mathbf{x}_i) p(\mathbf{x}_i) \quad (3.51)$$

and the entropy,  $H(\hat{d}^{(0)}|\mathbf{X})$ , depend on  $p(\hat{d}^{(0)} = m|\mathbf{x}_i)$  for  $m = \{0, \dots, M - 1\}$ , which in turn are

$$\begin{aligned} p(\hat{d}^{(0)} = m|\mathbf{x}_i) &= \Pr \{ \xi_m > \xi_p, \forall p \neq m \} \\ &= \int_{-\infty}^{\infty} \int_{-\infty}^{\xi_m} \dots \int_{-\infty}^{\xi_m} f(\xi_m, \underbrace{\xi_0, \dots, \xi_{M-1}}_{\text{excluding } \xi_m} | \mathbf{x}_i) d\xi_m d\xi_0 \dots d\xi_{M-1}, \end{aligned} \quad (3.52)$$

where  $f(\xi_0, \dots, \xi_{M-1} | \mathbf{x}_i)$  is the joint conditional pdf of  $\xi_0, \dots, \xi_{M-1}$  given the  $i$ th symbol is transmitted. The decision statistics,  $\xi_m$ , are normally distributed, since they are linear combinations of Gaussian random variables. Hence it suffices to calculate the mean and the covariance matrix of  $\Xi = [\xi_0 \dots \xi_{M-1}]^T$  for a given  $\mathbf{x}_i$ , which are  $\mathbf{m}_\Xi^i$  and  $\Sigma_\Xi$ , respectively, to obtain the joint conditional pdf mentioned. While the  $m$ th element of  $\mathbf{m}_\Xi^i$  is given by  $(\mathbf{m}_{\hat{y}}^i - \frac{1}{2}\mathbf{m}_{\hat{y}}^m)^T \Sigma_{\hat{y}}^{-1} \mathbf{m}_{\hat{y}}^m$ , the covariance matrix for  $\Xi$  is

$$\Sigma_\Xi = \begin{bmatrix} (\mathbf{m}_{\hat{y}}^0)^T \Sigma_{\hat{y}}^{-1} \mathbf{m}_{\hat{y}}^0 & \dots & (\mathbf{m}_{\hat{y}}^0)^T \Sigma_{\hat{y}}^{-1} \mathbf{m}_{\hat{y}}^{M-1} \\ \vdots & & \vdots \\ (\mathbf{m}_{\hat{y}}^{M-1})^T \Sigma_{\hat{y}}^{-1} \mathbf{m}_{\hat{y}}^0 & \dots & (\mathbf{m}_{\hat{y}}^{M-1})^T \Sigma_{\hat{y}}^{-1} \mathbf{m}_{\hat{y}}^{M-1} \end{bmatrix}. \quad (3.53)$$

The probability in (3.52) can be computed numerically for the multivariate Gaussian with the mean vector  $\mathbf{m}_\Xi^i$  and the covariance matrix  $\Sigma_\Xi$ . These probabilities determine the mutual information we are looking for, as in (3.50).

### 3.2.3. Arimoto-Blahut Algorithm

In this part, firstly the average mutual information  $I(\mathbf{X}; \hat{d}^{(0)})$  is maximized over the input symbol probability distribution using the Arimoto-Blahut algorithm [31, 32]. Defining

$$J = \sum_{i=0}^{M-1} p(\mathbf{x}_i) \sum_{m=0}^{M-1} p(\hat{d}^{(0)} = m | \mathbf{x}_i) \log_2 \frac{p(\mathbf{x}_i | \hat{d}^{(0)} = m)}{p(\mathbf{x}_i)}, \quad (3.54)$$

Arimoto and Blahut prove three facts [32]:

1. Capacity, i.e., the maximum mutual information of hard-output systems in this context, is a double maximum over  $J$ :

$$\mathcal{C}_h = \max_{p(\mathbf{x}_i)} \max_{p(\mathbf{x}_i | \hat{d}^{(0)} = m)} J \text{ bits/symbol}. \quad (3.55)$$

2. For fixed  $p(\mathbf{x}_i)$ ,  $J$  is maximized by

$$p(\mathbf{x}_i|\hat{d}^{(0)} = m) = \frac{p(\mathbf{x}_i)p(\hat{d}^{(0)} = m|\mathbf{x}_i)}{\sum_{j=0}^{M-1} p(\mathbf{x}_j)p(\hat{d}^{(0)} = m|\mathbf{x}_j)}. \quad (3.56)$$

3. For fixed  $p(\mathbf{x}_i|\hat{d}^{(0)} = m)$ ,  $J$  is maximized by

$$p(\mathbf{x}_i) = \frac{2^{\sum_{m=0}^{M-1} p(\hat{d}^{(0)}=m|\mathbf{x}_i) \log_2 p(\mathbf{x}_i|\hat{d}^{(0)}=m)}}{\sum_{j=0}^{M-1} 2^{\sum_{m=0}^{M-1} p(\hat{d}^{(0)}=m|\mathbf{x}_j) \log_2 p(\mathbf{x}_j|\hat{d}^{(0)}=m)}}. \quad (3.57)$$

Merging the second and third facts, an iterative algorithm that converges to the capacity achieving  $p(\mathbf{x}_i)$  is obtained, where  $p(\mathbf{x}_i)^n$  is the value of  $p(\mathbf{x}_i)$  at the  $n$ th step:

$$p(\mathbf{x}_i)^{n+1} = \frac{2^{\sum_{m=0}^{M-1} p(\hat{d}^{(0)}=m|\mathbf{x}_i) \log_2 \frac{p(\mathbf{x}_i)^n p(\hat{d}^{(0)}=m|\mathbf{x}_i)}{\sum_{j=0}^{M-1} p(\mathbf{x}_j)^n p(\hat{d}^{(0)}=m|\mathbf{x}_j)}}}{\sum_{j=0}^{M-1} 2^{\sum_{m=0}^{M-1} p(\hat{d}^{(0)}=m|\mathbf{x}_j) \log_2 \frac{p(\mathbf{x}_j)^n p(\hat{d}^{(0)}=m|\mathbf{x}_j)}{\sum_{k=0}^{M-1} p(\mathbf{x}_k)^n p(\hat{d}^{(0)}=m|\mathbf{x}_k)}}}. \quad (3.58)$$

The outcome of the iterations is the set of  $p(\mathbf{x}_i)$ , and the mutual information it maximizes,  $\mathcal{C}_h$ , where the latter is found by substituting the final  $p(\mathbf{x}_i)$ , obtained from the algorithm, into (3.50).

An analogous theory is developed for continuous probability distributions to maximize the mutual information of systems with soft outputs given in (3.38), and obtain  $\mathcal{C}_s$ , the maximum soft-output rate achievable, in information bits per channel symbol. When the continuous distribution theory developed in [33] is applied to systems with discrete inputs and continuous-valued outputs, it again results in an iterative formula to determine the set of  $p(\mathbf{x}_i)$  that achieves  $\mathcal{C}_s$ , where  $p(\mathbf{x}_i)^{n+1}$  is given by

$$\frac{2^{\mathbb{E}_{\tilde{y}|\mathbf{x}_i} \left\{ \log_2 p(\mathbf{x}_i)^n - \log_2 \left( \sum_{j=0}^{M-1} p(\mathbf{x}_j)^n \exp \left( \sum_{m=0}^{M-1} \frac{\tilde{y}m}{\sigma_{\tilde{y},m}^2} (m_{\tilde{y},m}^j - m_{\tilde{y},m}^i) + \frac{(m_{\tilde{y},m}^i)^2 - (m_{\tilde{y},m}^j)^2}{2\sigma_{\tilde{y},m}^2} \right) \right) \right\}}}{\sum_{j=0}^{M-1} 2^{\mathbb{E}_{\tilde{y}|\mathbf{x}_j} \left\{ \log_2 p(\mathbf{x}_j)^n - \log_2 \left( \sum_{k=0}^{M-1} p(\mathbf{x}_k)^n \exp \left( \sum_{m=0}^{M-1} \frac{\tilde{y}m}{\sigma_{\tilde{y},m}^2} (m_{\tilde{y},m}^k - m_{\tilde{y},m}^j) + \frac{(m_{\tilde{y},m}^j)^2 - (m_{\tilde{y},m}^k)^2}{2\sigma_{\tilde{y},m}^2} \right) \right) \right\}}}} \quad (3.59)$$

The soft- and hard-output algorithms, (3.59) and (3.58), respectively, may both start with the equally-likely symbols assumption, where  $p(\mathbf{x}_i)^0 = 1/M$ .

### 3.2.4. Channel Coding with M-ary PPM

The capacity of the discrete AWGN channel with average power constraint  $P_{av}$  as given in bits per transmission,  $C = 1/2 \log_2(1 + P_{av}/N_0)$ , is achieved by Gaussian input symbols that satisfy the power constraint  $P_{av}$  [23]. This result, together with Shannon's noisy channel coding theorem guarantee that channel codes enabling reliable communication with as small an error probability as desired exist provided that the transmission rate satisfies  $R < C$  [36]. To ensure that the codewords of the capacity achieving channel code satisfy the power constraint, they are generated randomly in such a way that each symbol (element) is i.i.d. according to the Gaussian distribution with variance  $P_{av}$ . For our setting, the maximum number of bits of information the soft- and hard-decision detection systems carry,  $\mathcal{C}_s$  and  $\mathcal{C}_h$ , respectively, play the role of Shannon capacity. These are the rates achievable with random coding and large block lengths of codewords whose elements are i.i.d. M-ary symbols complying with the maximizing input symbol probability distribution found using the Arimoto-Blahut algorithm.

In this thesis, where we examine the performance of optimal channel codes constructed using symbols from the M-ary PPM alphabet over UWB channels, one of the performance indices is the minimum information bit energy-to-noise ratio required for reliable communication. Since impulse radio uses low-power ultra-short pulses for transmission of information, energy efficiency as measured by the energy required to send one bit of information reliably is a very important criterion. In particular, we are interested in the largest possible rate for which reliable communication is possible, or equivalently the smallest possible information bit energy-to-noise ratio, which assures arbitrarily small error probability for a given code rate [43]. Note that there is a one-to-one correspondence between the achievable information rate and the code rate, where for instance the code rate, which is defined to be the ratio of the number of information bits to the number of channel bits, is given by  $\mathcal{C}_s / \log_2 M$  for soft-output systems. Com-

puting the achievable information rates for M-ary PPM first, the minimum information bit energy-to-noise ratio,  $\rho_b$ , and the SNR,  $E_s/N_0$ , are related by

$$\rho_b \triangleq \frac{E_s}{N_0} \frac{1}{\mathcal{C}_s} \quad (3.60)$$

for the soft-output systems, while the  $\rho_b$  for the hard-output systems has  $\mathcal{C}_h$  in (3.60) instead of  $\mathcal{C}_s$ . From (3.60) it is understood that non-optimal codes that have  $R < \mathcal{C}_s$  are less energy efficient, since they need larger values of energy per information bit, and thus operating at the maximum achievable rate determines the minimum normalized energy per information bit.

When evaluating the energy efficiency of impulse radio, we are also interested in the minimum  $\rho_b$  over all code rates. With continuous-valued output channels, the received energy per information bit that is required for reliable communication is usually minimized in the limit of diminishing SNR [44]. The minimum energy-to-noise ratio per information bit required by soft-output impulse radio

$$(\rho_b)_{\min} = \lim_{E_s/N_0 \rightarrow 0} \frac{E_s/N_0}{\mathcal{C}_s(E_s/N_0)} = \frac{1}{\dot{\mathcal{C}}_s(0)} \quad (3.61)$$

is based on the derivative of the rate of transmission

$$\dot{\mathcal{C}}_s(0) = \frac{1}{2 \ln 2} \sum_{i=0}^{M-1} p(\mathbf{x}_i) \sum_{j=0}^{M-1} p(\mathbf{x}_j) (\check{\mathbf{m}}_{\mathbf{y}}^i - \check{\mathbf{m}}_{\mathbf{y}}^j)^T \check{\mathbf{M}}_{\mathbf{y}}^{-1} (\check{\mathbf{m}}_{\mathbf{y}}^i - \check{\mathbf{m}}_{\mathbf{y}}^j), \quad (3.62)$$

where the  $m$ th element of  $\check{\mathbf{m}}_{\mathbf{y}}^i$  is  $r_{\alpha, \bar{L}}^{(0)}(m-i)$  and  $\check{\mathbf{M}}_{\mathbf{y}}$  is a symmetric Toeplitz matrix that has  $[r_{\alpha, \bar{L}}^{(0)}(0) \dots r_{\alpha, \bar{L}}^{(0)}(M-1)]$  in the first row. This result is general enough to cover the AWGN case as well, which has  $\dot{\mathcal{C}}_s(0) = (M-1)/(M \ln 2)$ . The expression for  $\dot{\mathcal{C}}_s(0)$  is derived in Appendix A. Although a closed form formula for  $(\rho_b)_{\min}$  does not exist with hard-output systems, for which the SNR that minimizes  $\rho_b$  is not trivial, it is possible to evaluate the hard-output  $(\rho_b)_{\min}$  numerically by means of simulations as described in the next section.

With the intention to capture the effects of multipath propagation, any distance-dependent losses are not explicitly included in the received signal model given in Section 3.1, and the average energy of the paths is normalized to unity,  $E\{\sum_{\ell=0}^{L_k-1} \alpha_{k,\ell}^2\} = 1$ . This normalization implies that  $E_s$  initially defined in (3.1) for the transmitted signal of the  $k$ th user actually refers to the received symbol energy. Also, notice that, SNR stands for the symbol SNR,  $E_s/N_0$ .

### 3.3. Simulation Results

Achievable information rates of TH-PPM “impulse radio” systems are computed for the IEEE 802.15.3a task group channel models CM1 (0-4 m LOS) and CM4 (4-10 m extreme NLOS) [18]. For each model, results are obtained by averaging over 100 channel impulse response realizations. System parameters are  $T_p = 1$  ns and  $N_s = 1$  for all simulations. In the first part of this section, the effects of MAI and IFI on the achievable information rates are not considered such that Figures 3.3-3.8 show the results for the single-user scenario with  $T_f > \tau_{0,L_0-1}$ .

In Figure 3.3,  $\rho_b$  as defined in (3.60) is displayed against  $\mathcal{C}_s$ , the maximum of the mutual information achieved by soft-output impulse radio. When analyzing the figure, one should be aware that the average energy of the multipaths is normalized to unity with the intention to make the received signal energy equivalent for all channel models, and hence render the comparison between the AWGN and frequency-selective channels fair. However, as opposed to the AWGN channel, the signal and noise components at the output of the M-ary correlation receiver are correlated for frequency-selective channels, where the orthogonality between the transmitted PPM signals is lost due to the time-dispersion of the transmitted waveform over a large number of paths. Although the correlation between the noise components serves to increase the achievable rates (see [45]), depending on the channel realization the correlation between the signal components either improves the rates achieved or acts to diminish them. While a negative correlation between the signal components helps in distinguishing them and increasing the rates, it is more difficult to discern the positively correlated signals. The cumulative effect of these two types of correlation on the  $\rho_b$  required at various M and

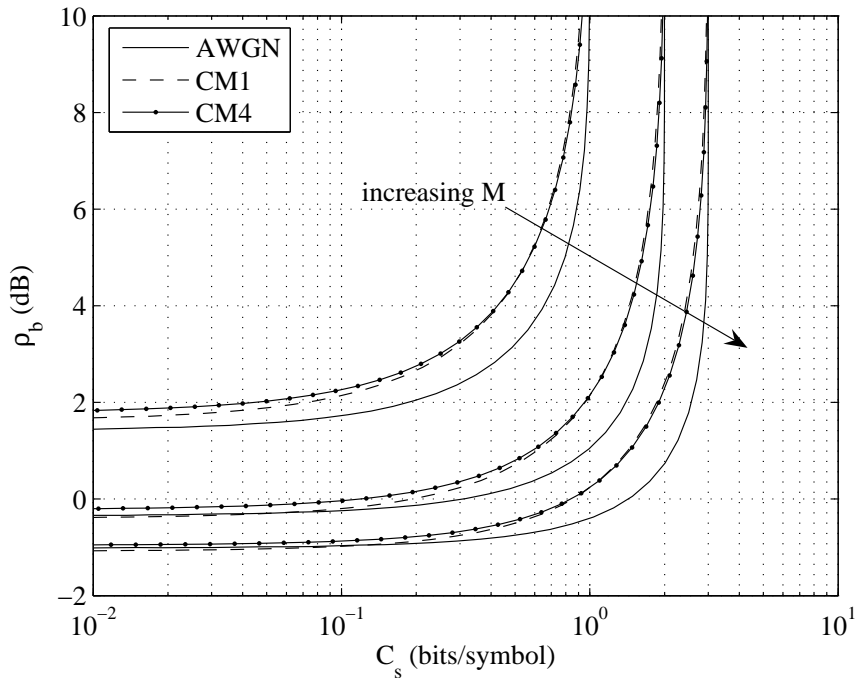


Figure 3.3. Single-user  $\rho_b$  against mutual information for soft-output impulse radio with  $M = \{2, 4, 8\}$ ,  $T_f > \tau_{0,L_0-1}$  and  $\tilde{L} = L_0$

$\mathcal{C}_s$  is observed to be different. For instance, with  $M = 8$  and  $\mathcal{C}_s < 0.1$ , we see that given a particular  $\mathcal{C}_s$ , the  $\rho_b$  of CM1 is lower than the one for the AWGN. On the other hand, at large values of  $\mathcal{C}_s$  the energy that has to be allocated per information bit is lower when transmitting over the AWGN channel compared to those needed in frequency-selective channels.

It is possible to find the soft-output  $(\rho_b)_{\min}$ , which is attained at zero SNR, using Figure 3.3 as  $E_s/N_0$  and, hence,  $\mathcal{C}_s$  goes to zero. In addition to the associated increase in  $(\rho_b)_{\min}$  from  $\ln 2$  to  $M \ln 2 / (M - 1)$  with finite  $M$  due to the orthogonality of the transmitted signals [41], it is seen that  $(\rho_b)_{\min}$  changes further for frequency-selective channels. By employing (3.62), we investigate in Figure 3.4 how  $(\rho_b)_{\min}$  evolves for soft-output impulse radio as  $M$  increases. Instead of growing logarithmically with the SNR, mutual information is a linear function of  $E_s/N_0$  in the low SNR region of interest. Especially as SNR goes to zero, we have  $\mathcal{C}_s = \text{SNR} / (\rho_b)_{\min}$ . Thus for the low SNR region under consideration variations of the received energy do not make the rates achieved in frequency-selective channels lower than those in the AWGN channel when

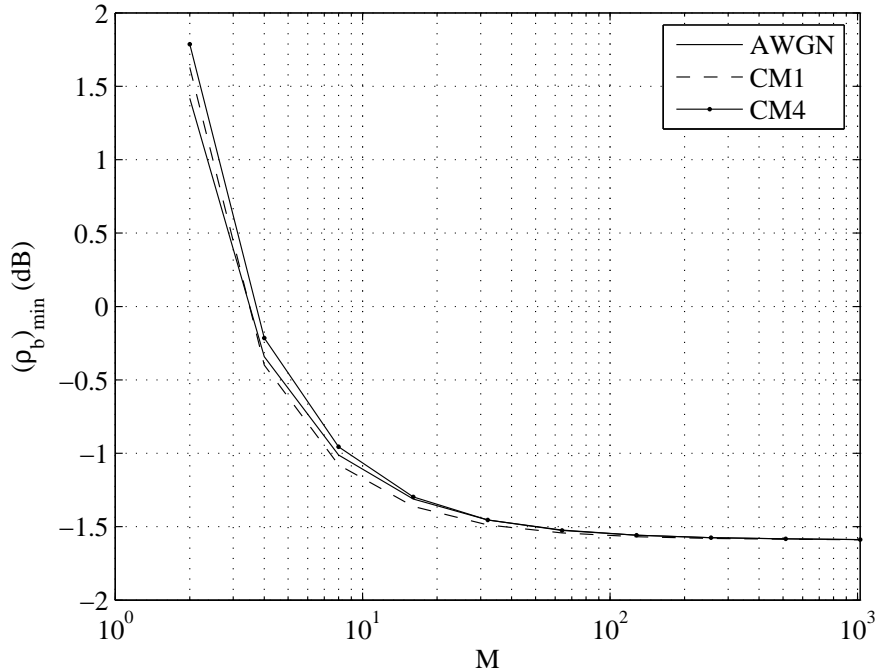


Figure 3.4.  $(\rho_b)_{\min}$  of soft-output impulse radio against  $M$  with  $\tilde{L} = L_0$

averaged over the channel realizations. In fact, as demonstrated in Figure 3.4 there is an insignificant difference between the channel models. We can give a very simple numerical example to exemplify this behavior: Suppose the average of two numbers,  $x_1$  and  $x_2$ , is 2. Then, the average of any linear function of these two numbers is going to remain the same irrespective of their exact values. For instance, with  $y_1 = 3x_1$  and  $y_2 = 3x_2$ , the mean of  $y_1$  and  $y_2$  is 6. However, if  $y_i = \log_2(x_i)$ , then the mean of  $y_1$  and  $y_2$  are less than  $\log_2(2) = 1$  for sure. With  $x_1 = 1.9$  and  $x_2 = 2.1$ , the mean of  $y_1$  and  $y_2$  is  $0.9982 < 1$ . This numerical example also explains the results at large values of SNR, where the frequency-selective channels have lower rates, and thus require larger  $\rho_b$  than the AWGN channel.

The performance of hard-output impulse radio is displayed in Figure 3.5 in terms of  $\rho_b$  against the maximum number of information bits per symbol that are reliably communicated, where  $\rho_b = (E_s/N_0)/\mathcal{C}_h$ , and  $\mathcal{C}_h$  is evaluated using the hard-output Arimoto-Blahut algorithm. The figure shows the minimum information bit energy-to-noise ratio required at a given value of the mutual information, or equivalently the code rate. Although  $\mathcal{C}_h$  is a monotonically increasing function of the SNR (see

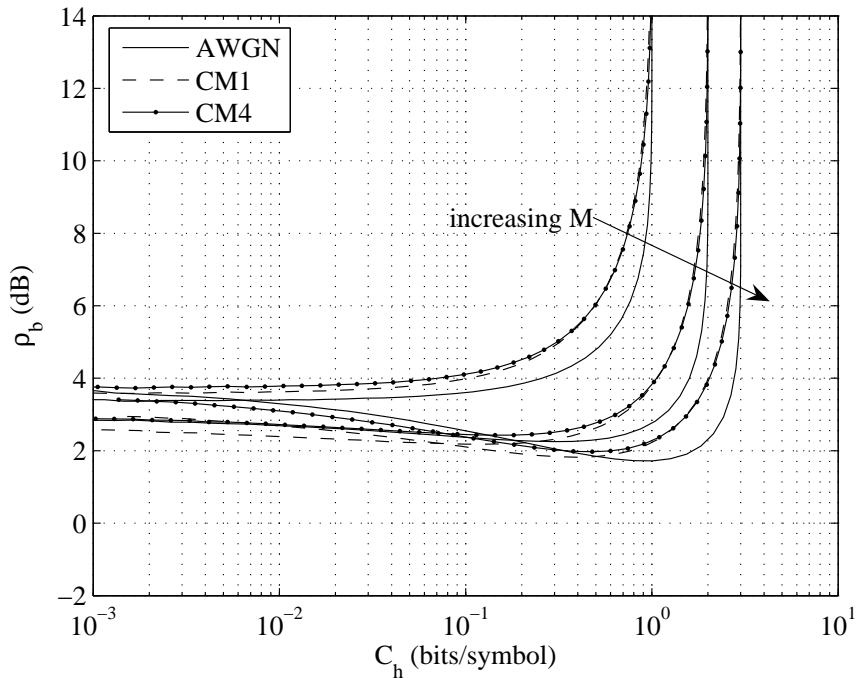


Figure 3.5. Single-user  $\rho_b$  against mutual information for hard-output impulse radio with  $M = \{2, 4, 8\}$ ,  $T_f > \tau_{0,L_0-1}$  and  $\tilde{L} = L_0$

Figures 3.6 and 3.7), it fails to be so when visualized in terms of the energy required per information bit. Figure 3.5 reveals that the  $(\rho_b)_{\min}$  for a particular value of  $M$  is reached at a nonzero value of the mutual information (i.e., SNR) as opposed to soft-output systems that attain  $(\rho_b)_{\min}$  as the mutual information approaches zero. Moreover,  $(\rho_b)_{\min}$  values for hard outputs are approximately 2 dB larger than the corresponding ones involving soft outputs. With  $M = 8$ , to operate at the hard-output  $(\rho_b)_{\min}$ , code rates of approximately  $1/3$ ,  $1/6$  and  $1/7$  are required in the AWGN, CM1 and CM4 channels, respectively, where the code rate is  $\mathcal{C}_h / \log_2 M$ .

Although lower values of mutual information are more efficient in Figures 3.3 and 3.5 with soft outputs in the sense that a small increase in  $\rho_b$  results in a large increase of the mutual information, the efficiency drops rapidly with hard outputs beyond  $(\rho_b)_{\min}$  as the mutual information decreases, especially for  $M > 2$ , where in fact pushing  $\mathcal{C}_h$  to zero causes an increase in  $\rho_b$  significantly above  $(\rho_b)_{\min}$ . On the other hand, as observed in Figure 3.3 increasing  $M$  is always an advantage for soft-output systems, and results in lower values of  $\rho_b$ . While soft-output systems benefit

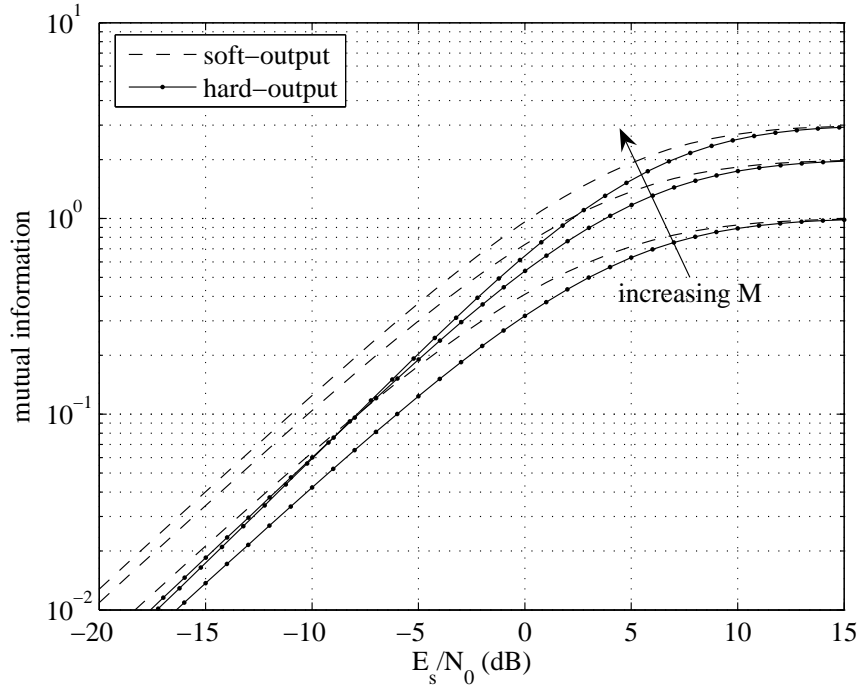


Figure 3.6. Mutual information against  $E_s/N_0$  (in dB) for soft- and hard-output systems in the CM1 channel with  $M = \{2, 4, 8\}$

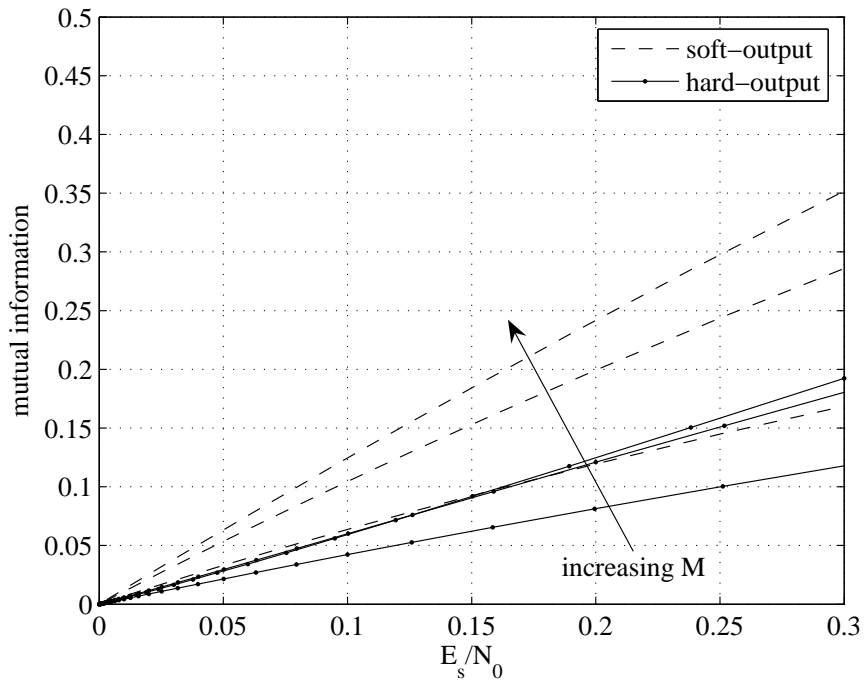


Figure 3.7. The low SNR region of mutual information against  $E_s/N_0$  for soft- and hard-output systems in the CM1 channel with  $M = \{2, 4, 8\}$

from the additional soft information supplied by an increasing number of correlators to improve information rates, as the energy per symbol decreases it becomes more difficult for hard-output systems to decide on the transmitted channel symbol with increasing values of  $M$ , which requires them to discard much of the soft information and make a distinct choice among a larger number of noisy candidates. It is understood from Figure 3.5 that hard-output systems should operate above a critical value of the SNR if increasing  $M$  is to be associated with larger values of the number of information bits transmitted reliably.

Viewed in terms of the code rates, we realize that as the energy per symbol,  $E_s$ , is lowered resulting in low SNR, the code rate also drops as shown in Figures 3.6 and 3.7. In some cases, the performance gain that comes from the increased redundancy obtained by low values of the code rate cannot compensate for the performance loss that results from lowered SNR [46]. In other words, the decay in detection performance at low SNR cannot be overcome by the corresponding increase in the redundancy of the channel code. In such cases, the  $\rho_b$  versus the code rate (mutual information) curve may admit a nonzero solution for the optimal code rate. Examples from literature where this effect is demonstrated include the noncoherent frequency-shift keying case in [43] and the general coherent/noncoherent orthogonal signaling in [47], where spectral efficiency is considered. Notice that the  $\rho_b$  requirements at low rates are dramatically higher than the values at optimal code rates in [43] and [47]. Our results shows a similar trend for M-PPM impulse radio: As the rate becomes lower than the optimal value, the  $\rho_b$  increases. However, the rise in  $\rho_b$  is somewhat marginal, which is less than 2 dB in all cases considered, and it tends to flatten out as the rate goes to zero. Moreover, the phenomenon is limited to hard-output information. Apparently, the performance gain obtained through processing soft information overcomes the low SNR performance loss.

Despite the differences noted above, soft- and hard-output systems exhibit analogous behavior at medium and large values of  $E_s/N_0$ . Specifically, it is seen from Figures 3.3 and 3.5 that the maximum mutual information of M-ary PPM is limited by the constellation size to  $\log_2 M$  bits per channel symbol. Moreover, in frequency-selective channels, the values of  $\rho_b$  required to achieve a certain value of the mutual informa-

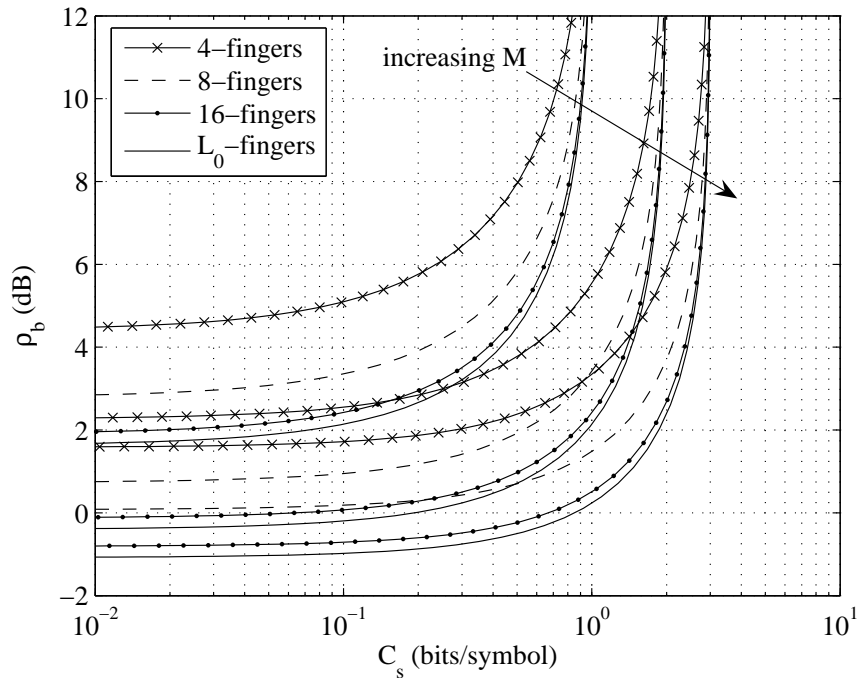


Figure 3.8. Single-user  $\rho_b$  against mutual information for soft-output impulse radio with rake reception,  $M = \{2, 4, 8\}$  and  $T_f > \tau_{0,L_0-1}$  in the CM1 channel, where

$$\tilde{L} = 4, 8, 16, L_0$$

tion are larger than those in the AWGN channel, with both soft- and hard-output systems. Accordingly, the correlation induced by the frequency-selective channel on the previously orthogonal signals turns out to be a disadvantage as the SNR increases.

Limiting the number of rake fingers deteriorates receiver performance. Figure 3.8 indicates the validity of this fact for soft-output systems, where the energy required per bit of information for reliable communication increases as the receiver is equipped with fewer number of fingers.

When computing  $\mathcal{C}_s$  and  $\mathcal{C}_h$ , the probability distribution of input symbols that achieves the maximum mutual information for  $M > 2$  is determined using the Arimoto-Blahut algorithm. It is observed that although the uniform distribution does not maximize the mutual information for a single channel realization, when averaged over the probability distributions found using the Arimoto-Blahut algorithm, the average probability distribution is not very different from the uniform distribution. The difference

is less pronounced for the soft-output systems compared to the hard-output ones, and also as  $E_s/N_0$  increases. Some numerical examples are given in Tables 3.1 and 3.2 for soft- and hard-output systems, respectively, with 32 fingers of the rake structure, where IFI and MAI are absent. In the tables, “maximum” and “pdf” are the maximum mutual information and the pdf of the input symbols calculated using the Arimoto-Blahut algorithm, respectively, and “uniform” is the mutual information obtained by the uniform symbol distribution.

Interference from other users and frames degrades the performance of TH-PPM systems under consideration relative to the single-user link results displayed in Figures 3.3 and 3.5. Although we have argued that the uniformly distributed symbols do not maximize the mutual information, the equiprobable symbols assumption is employed when calculating (3.22) and (3.25) such that  $f_{d_i^j}(d_i^j) = 1/M \forall i$ . The fact that the symbol distribution has to be known before (3.22) and (3.25) are calculated makes the problem of maximizing the mutual information truly difficult unless the uniform distribution is utilized for (3.22) and (3.25): The Arimoto-Blahut algorithm maximizes the mutual information given the means and the variances of the output. The distribution the algorithm finds changes the mean and the variance of the IFI, which in turn change the distribution the algorithm is to determine. However, the iterations between these two stages do not necessarily converge to a maximizing symbol distribution as our simulations have shown. Thus we resort to the equiprobable symbols assumption to calculate (3.22) and (3.25) before the Arimoto-Blahut algorithm is applied, and obtain Figure 3.9, which is fairly appropriate when the results are averaged over different channel realizations.

It is deduced from Figure 3.9 that the soft-output  $(\rho_b)_{\min}$  is determined only through the signal and noise powers, and, therefore, remains unchanged. However, when  $\mathcal{C}_s$  increases, interference dominates performance, and the achievable rates become lower than those indicated by the constellation size. In particular, at sufficiently large values of SNR, the rates for reliable communication are controlled by the number of interfering users. This behavior is demonstrated in Figures 3.10 and 3.11, which have  $E_s/N_0 = 20$  dB with  $T_f = 100$  ns and  $T_f = 10$  ns, respectively. A quick comparison of

Table 3.1. Arimoto-Blahut algorithm for soft-output systems and  $M = 8$

Channel	SNR (dB)	pdf	maximum	uniform
CM1	0	[0.1274 0.1234 0.1243 0.1248 0.1248 0.1244 0.1234 0.1275]	1.8753	1.8735
CM1	10	[0.1252 0.1250 0.1250 0.1248 0.1248 0.1250 0.1250 0.1252]	2.9530	2.9529
CM1	20	[0.1250 0.1250 0.1250 0.1250 0.1250 0.1250 0.1250 0.1250]	3.0000	3.0000
CM4	0	[0.1289 0.1230 0.1241 0.1239 0.1239 0.1241 0.1230 0.1290]	1.3559	1.3540
CM4	10	[0.1253 0.1250 0.1250 0.1247 0.1247 0.1250 0.1250 0.1253]	2.8845	2.8844
CM4	20	[0.1250 0.1250 0.1250 0.1250 0.1250 0.1250 0.1250 0.1250]	2.9999	2.9999

Table 3.2. Arimoto-Blahut algorithm for hard-output systems and  $M = 8$

Channel	SNR (dB)	pdf	maximum	uniform
CM1	0	[0.1277 0.1226 0.1244 0.1252 0.1252 0.1244 0.1227 0.1278]	1.5171	1.5148
CM1	10	[0.1253 0.1250 0.1249 0.1248 0.1247 0.1249 0.1250 0.1253]	2.9181	2.9180
CM1	20	[0.1250 0.1250 0.1250 0.1250 0.1250 0.1250 0.1250 0.1250]	3.0000	3.0000
CM4	0	[0.1300 0.1226 0.1239 0.1234 0.1236 0.1238 0.1226 0.1300]	0.9923	0.9900
CM4	10	[0.1255 0.1249 0.1249 0.1246 0.1246 0.1249 0.1249 0.1255]	2.7960	2.7956
CM4	20	[0.1250 0.1250 0.1250 0.1250 0.1250 0.1250 0.1250 0.1250]	2.9999	2.9999

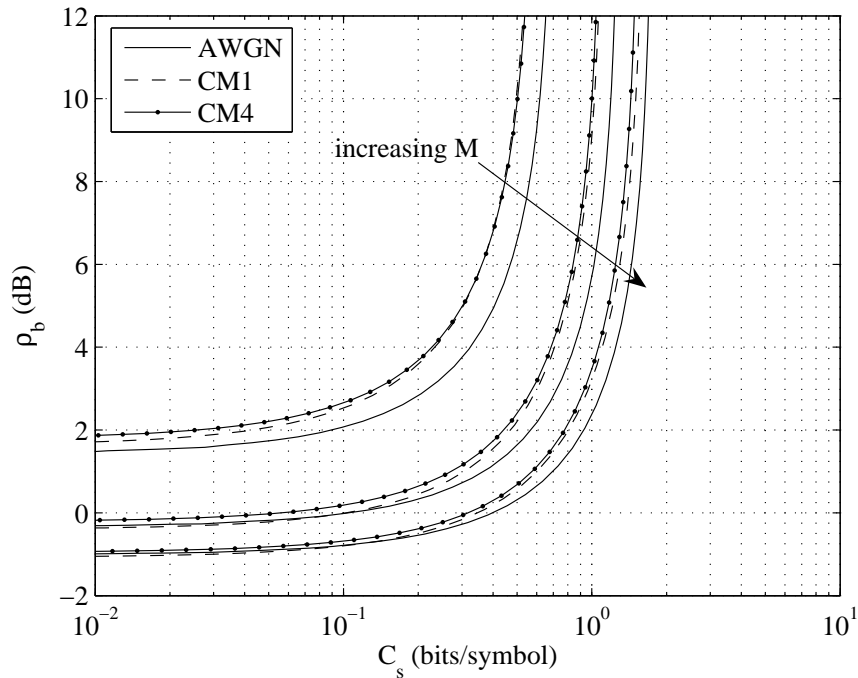


Figure 3.9. Multiple-user  $\rho_b$  against mutual information for soft-output impulse radio with  $M = \{2, 4, 8\}$ ,  $K_r = 100$ ,  $T_f = 100$  ns and  $\tilde{L} = L_0$

the two figures suggest a subtle difference between the CM1 and CM4 models: As the frame time decreases, which gives rise to more severe IFI, and/or the number of users increases, the CM1 model, with a smaller delay spread, outperforms CM4. These two figures also reveal that although lower values of frame time create lower transmission rates in terms of the number of bits per symbol, the degradation in the mutual information seems less critical than the reduction in  $T_f$ .

Our simulation results show that the performance is relatively robust to IFI compared to other effects, and some specific numerical examples are given to illustrate this behavior. For  $E_s/N_0 = 20$  dB and  $M = \{2, 4, 8\}$  with  $T_f = 100$  ns,  $C_s = \{0.9998, 1.9992, 2.9981\}$ , which indicates a rather minor performance degradation compared to the ideal case with no IFI that has  $C_s = \{1, 2, 3\}$ . On the other hand, for  $T_f$  as low as 10 ns, we have  $C_s = \{0.9838, 1.9687, 2.9517\}$ , which is still an insignificant deterioration in performance.

For hard-output systems that are subject to IFI and MAI similar conclusions

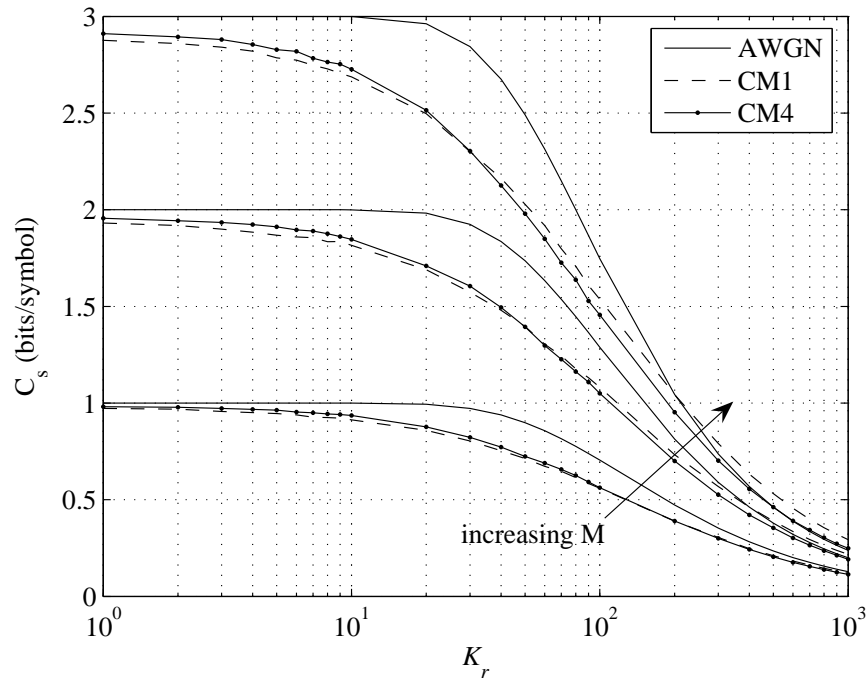


Figure 3.10. Mutual information for soft-output impulse radio against  $K_r$  with  $T_f = 100$  ns,  $E_s/N_0 = 20$  dB,  $M = \{2, 4, 8\}$ , and  $\tilde{L} = L_0$

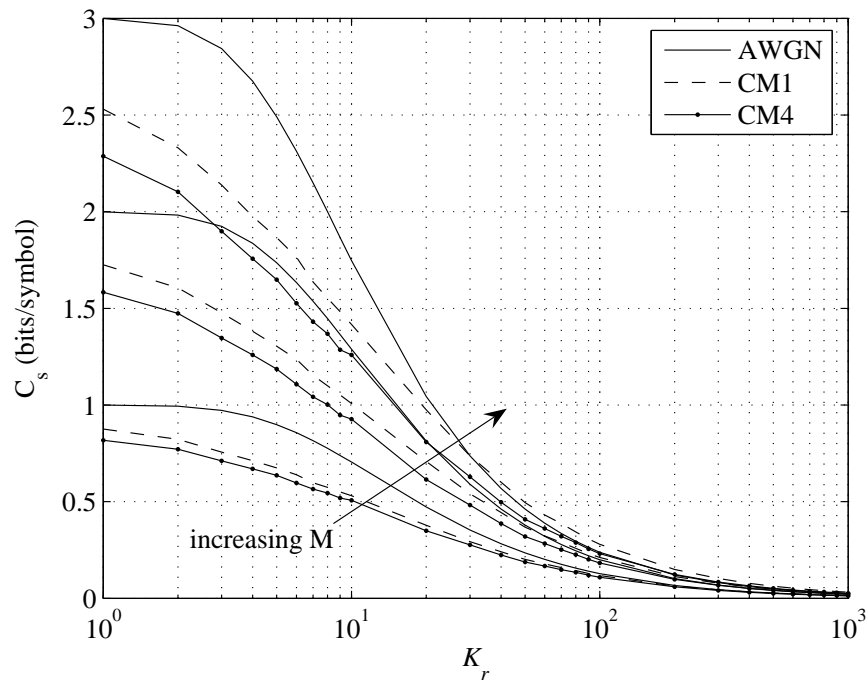


Figure 3.11. Mutual information for soft-output impulse radio against  $K_r$  with  $T_f = 10$  ns,  $E_s/N_0 = 20$  dB,  $M = \{2, 4, 8\}$  and  $\tilde{L} = L_0$

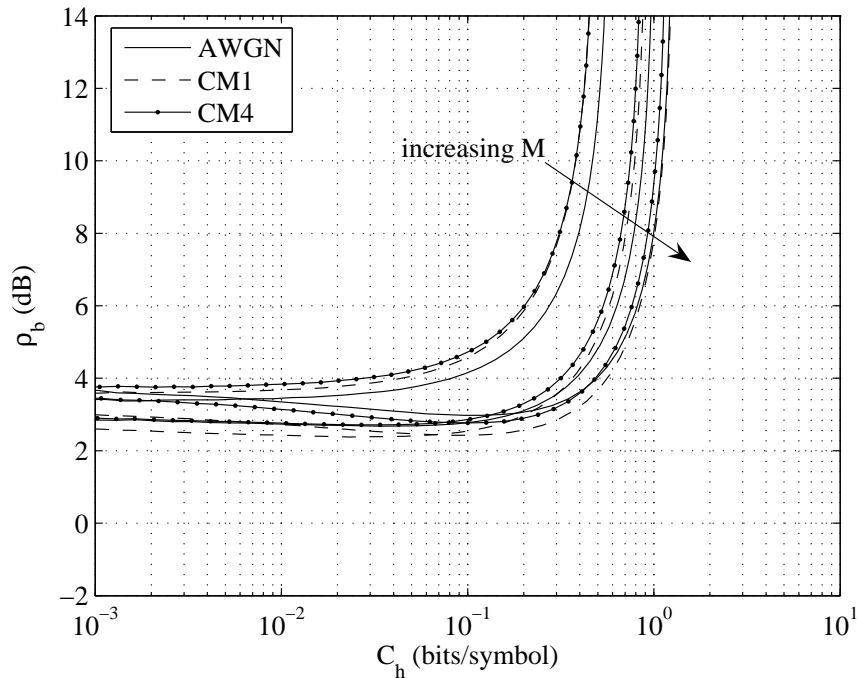


Figure 3.12. Multiple-user  $\rho_b$  against mutual information for hard-output impulse radio with  $M = \{2, 4, 8\}$ ,  $K_r = 100$ ,  $T_f = 100$  ns and  $\tilde{L} = L_0$

concerning the  $\rho_b$  values in the limit of zero SNR and the response of the mutual information to the increasing number of users in the region of large SNR are reached. On the other hand, the hard-output  $(\rho_b)_{\min}$  values that are observed in between those two SNR regions change as demonstrated in Figure 3.12, where  $K_r = 100$  and  $T_f = 100$  ns. Therefore, larger values of  $(\rho_b)_{\min}$  are required for hard-output systems as  $K_r$  increases or rake reception is performed with a limited number of fingers.

When evaluating  $\mathcal{C}_s$  and  $\mathcal{C}_h$ , the Gaussian assumption for the MAI and IFI has been used primarily to obtain closed form expressions. The validity of the Gaussian approximation for the MAI has been studied in several works. As pointed out in [11], which investigates the asymptotic distribution of the correlation receiver output for TH UWB signals, the Gaussian approximation might not be valid when  $N_s$  is too small. On the other hand, we also have to realize that since the study mentioned does not take into account the statistical model for the channels under consideration, it does not violate the conclusions reached in [39] regarding the Gaussianity of the MAI. If the Gaussian assumption for either the MAI or IFI is not accurate in frequency-selective

channels, this implies the following. The calculated mutual information, which assumes Gaussian interference, constitutes a lower bound for soft-output systems, since it is known that with continuous-valued outputs the Gaussian noise minimizes capacity for a given power spectral density [38]. This has also been noted by Shannon in [48], where he has shown the white Gaussian noise to be the worst among all possible noises in this respect. For hard-output systems, the mutual information found is larger than the one that would be obtained if the interference were non-Gaussian as demonstrated in [27] for the AWGN channel, for the hard-output rates depend on the error probabilities in (3.52), and it is known that non-Gaussian MAI is harmful in the sense that the Gaussian approximation predicts lower error probabilities. Mathematically stated, with larger error probabilities in the non-Gaussian case, the entropy  $H(\hat{d}^{(0)}|\mathbf{X})$  in (3.48) is also larger, which results in lower rates. This justification is based on the intuition that the sum of the error probabilities is lower than 1/2, which means that  $H(\hat{d}^{(0)}|\mathbf{X})$  gets larger as the error probability sum increase toward 1/2.

## 4. JOINT TRANSMITTER-RECEIVER UWB RAKE DESIGN

Ultra-wideband systems have a much lower fading margin than narrowband systems, since the wide system bandwidth enables fine resolution in time of the received multipaths [9]. Experimental investigations of the wideband indoor channel lying in the 2-8 GHz band confirm this fact and indicate that rake receivers can achieve significant diversity gains by collecting the total signal energy distributed over a large number of paths [18]. Furthermore, for TDD systems it is possible to move the rake structure from the receiver to the transmitter by making use of the channel information estimated in the reverse link. To be specific, the transmitter scales and delays the original transmitted signal in such a way that the operation of multipath combining is already performed when the signal arrives at the receiver, in which case the receiver may use the conventional design that tunes to a single path [14, 49].

Pre-raked transmission has initially been proposed in [14] for code division multiple access (CDMA) systems, where its performance is shown to be equivalent to the conventional rake receiver over single-user links with moderate data rates. Later studies conducted for UWB systems in particular, such as [50], indicate that pre-raking may lead to suppressed ISI with high data rates, since the MRC stage of rake reception, which boosts interference energy at the receiver, is avoided. This desirable property of pre-raking is accompanied by a larger number of multipaths at the receiver than that exists for the channel impulse response between the transmitter and the receiver. When properly exploited, those paths allow an improved performance compared to the pre-rake or post-rake, i.e., the rake structure at the receiver, only systems. The pre/post-rake structure in [51], for instance, uses an MRC post-rake to collect all of the multipaths. Moving one step further, the eigenprecoder proposed in [52] has its pre- and post-rake weights determined jointly to maximize the SNR at the receiver. The principal ratio combining (PRC) pre/post-rake with a flexible number of pre-rake fingers [53] is a variation of the eigenprecoder.

The PRC pre/post-rake has to have an unlimited number of post-rake fingers for optimum performance, since the received SNR increases with the number of pre-rake fingers, which in turn requires a larger number of post-rake fingers. With this structure an infeasible number of pre- and post-rake fingers may have to be deployed in total at the transmitter and the receiver for UWB channels that tend to be extremely frequency-selective. In this thesis, the problem of how to distribute a fixed total number of rake fingers between the transmitter and the receiver is being addressed. Specifically, it is shown that in the absence of ISI, there is an optimum number of pre-rake fingers, and thus post-rake vectors, that maximizes the received SNR when the post-rake structure combines the first arriving paths. Also, it is demonstrated that the presence of ISI results in a transmitter-receiver design that does not allow a closed form expression for the pre- and post-rake vectors, but rather an iterative algorithm has to be used to arrive at the rake vectors that are optimum in the sense that they maximize the SINR of the decision statistic. Moreover, simulations indicate that depending on the total number of rake and/or pre-rake fingers, the optimum placement of the post-rake fingers becomes a difficult problem, which may even require an exhaustive search in some cases (e.g., as in [54] for a minimum mean-square error (MMSE) post-rake-only system), where combining the first arriving paths does not exhibit sufficient performance.

The rest of this chapter is organized as follows: Section 4.1 introduces the UWB system model used in this chapter. Presented in Section 4.2 is the transmitter-receiver structure which performs rake combining jointly to maximize the SINR at the receiver. Simulation results are described in Section 4.3.

#### 4.1. UWB System Model

Considering an uncoded single-user system which uses binary phase shift keying (BPSK) for data modulation, the signal transmitted after pre-rake processing is

$$s_{\text{tr}}(t) = \sqrt{E_b} \sum_{i=-\infty}^{\infty} b_i \sum_{k=0}^{F_t-1} v_k w_{\text{tr}}(t - iT_b - \beta_k), \quad (4.1)$$

where  $E_b$  is the bit energy,  $b_i \in \{-1, 1\}$  is the  $i$ th bit,  $T_b$  is the bit duration, and  $v_k$  and  $\beta_k$  are the gain and delay of the  $k$ th pre-rake finger, respectively. Note that in order to simplify the analysis the number of pulses transmitted per bit,  $N_s$ , is chosen to be one such that  $T_b = T_f$ . Also, user-dependent quantities are not included in (4.1), and there is no TH of the pulses, since we are investigating a single-user system. However, the results presented in this chapter may be modified to cover the multiuser case as well by resorting to the expressions for the mean and the variance of the MAI derived in the previous chapter.

The transmitted signal propagates through the UWB channel, whose impulse response is modeled as

$$h(t) = \sum_{\ell=0}^{L-1} \alpha_{\ell} \delta_D(t - \tau_{\ell}), \quad (4.2)$$

where  $\alpha_{\ell}$  and  $\tau_{\ell}$  denote the gain and delay of the  $\ell$ th multipath, respectively. Accordingly, the signal received over a single-user link is

$$r(t) = \sqrt{E_b} \sum_{i=-\infty}^{\infty} b_i \sum_{\ell=0}^{L-1} \alpha_{\ell} \sum_{k=0}^{F_t-1} v_k w_{\text{rec}}(t - iT_b - \beta_k - \tau_{\ell}) + n(t) \quad (4.3)$$

at the output of the receiver antenna, where  $w_{\text{rec}}(t)$ , which has duration  $T_p$ , is the received unit energy pulse, and  $n(t)$  is an AWGN component with two-sided power spectral density  $N_0/2$ .

Inspection of (4.3) reveals that since the pre-rake finger delays,  $\beta_k = \tau_{L-1} - \tau_k$ , are obtained from the channel impulse response, for  $\tau_{\ell} = \ell T_p$  the number of multipath components at the receiver is  $L + F_t - 1$ . Representing the received signal at the output of the correlator that is matched to the  $m$ th multipath by

$$r_{i,m} = \int_{iT_b+mT_p}^{iT_b+(m+1)T_p} r(t) w_{\text{rec}}(t - iT_b - mT_p) dt \quad m = 0, \dots, L + F_t - 2, \quad (4.4)$$

the received vector for the  $i$ th bit is written as

$$\mathbf{r}_i = [r_{i,0} \dots r_{i,L+F_t-2}]^T. \quad (4.5)$$

The final decision for the  $i$ th bit, where the post-rake vector  $\mathbf{w} = [w_0 \dots w_{L+F_t-2}]^T$  is used to perform rake combining at the receiving side, is made as in

$$\hat{b}_i = \text{sgn} \{ \mathbf{w}^T \mathbf{r}_i \}. \quad (4.6)$$

## 4.2. Transmitter-Receiver Rake Structure for ISI Channels

The aim in this work is to maximize the SINR for systems with ISI, which perform transmitter-receiver rake processing under the constraint that the total number of rake fingers to be deployed at the transmitter and receiver is fixed as given by

$$F = F_t + F_r \quad (4.7)$$

where  $F$  is the total number of rake fingers, and  $F_t$  and  $F_r$  are the number of fingers at the pre- and post-rake structures, respectively. Although the number of multipaths created in response to pre-raked transmission is  $L + F_t - 1$ , and hence the number of post-rake fingers may be as large as that as indicated in (4.6), we investigate the case, where the number of post-rake fingers is limited to  $F_r < L + F_t - 1$ .

In the following, while the length of the pre-rake vector is the same as the number of pre-rake fingers such that

$$\mathbf{v}_t = [v_{F_t-1} \dots v_0]^T, \quad (4.8)$$

the vector  $\mathbf{w}_r$  represents the post-rake vector of length  $L + F_t - 1$  that has  $F_r$  nonzero elements.

High data rate transmission introduces ISI to the decision statistic for the  $i$ th bit as in

$$\xi = \sqrt{E_b} b_i \mathbf{w}_r^T \mathbf{H} \mathbf{v}_t + \sqrt{E_b} \sum_{\substack{m=-I \\ m \neq 0}}^I b_{i+m} \mathbf{w}_r^T \mathbf{H}_m \mathbf{v}_t + \mathbf{w}_r^T \mathbf{n}_i, \quad (4.9)$$

where  $\xi = \mathbf{w}_r^T \mathbf{r}_i$  is the decision statistic before thresholding,  $I = \lfloor (L + F_t - 1)/\chi \rfloor$  and  $\chi = T_b/T_p$  (remember that  $T_b = T_f$  with  $N_s = 1$ ). The elements of  $\mathbf{n}_i$  are the noise samples

$$n_{i,m} = \int_{iT_b+mT_p}^{iT_b+(m+1)T_p} n(t) w_{\text{rec}}(t - iT_b - mT_p) dt, \quad (4.10)$$

which are zero-mean Gaussian random variables that have variance  $N_0/2$ . In (4.9) the channel matrix for the desired signal component is the  $(L + F_t - 1) \times F_t$  convolution matrix

$$\mathbf{H} = \begin{bmatrix} \alpha_0 & 0 & 0 & \dots & 0 \\ \alpha_1 & \alpha_0 & 0 & \dots & 0 \\ \vdots & \ddots & \ddots & \ddots & \vdots \\ \alpha_{L-1} & & \ddots & & \\ 0 & & & \ddots & 0 \\ \vdots & \ddots & & \ddots & \alpha_0 \\ & & & \ddots & \vdots \\ 0 & \dots & & 0 & \alpha_{L-1} \end{bmatrix}. \quad (4.11)$$

The channel matrices in (4.9) that describe the signals due to interfering bits are derived from  $\mathbf{H}$  as

$$\mathbf{H}_m = \begin{bmatrix} \mathbf{H}(-\chi m + 1 : L + F_t - 1, :) \\ \mathbf{0}_{-\chi m \times F_t} \end{bmatrix}, \quad m < 0, \quad (4.12)$$

$$\mathbf{H}_m = \begin{bmatrix} \mathbf{0}_{\chi m \times F_t} \\ \mathbf{H}(1 : L + F_t - 1 - \chi m, :) \end{bmatrix}, \quad m > 0, \quad (4.13)$$

where  $\mathbf{H}(r_1 : r_2, c_1 : c_2)$  denotes a submatrix of  $\mathbf{H}$  that contains rows  $r_1$  through  $r_2$  and columns  $c_1$  through  $c_2$ , and  $\mathbf{0}_{d_1 \times d_2}$  is an all-zero matrix of dimension  $d_1 \times d_2$ .

With independent and equiprobable bits, the SINR of  $\xi$ , which is denoted by  $\gamma$ , is expressed as

$$\gamma = \frac{|\mathbf{w}_r^T \mathbf{H} \mathbf{v}_t|^2}{\frac{N_0}{2E_b} \mathbf{w}_r^T \mathbf{w}_r + \sum_{\substack{m=-I \\ m \neq 0}}^I |\mathbf{w}_r^T \mathbf{H}_m \mathbf{v}_t|^2}. \quad (4.14)$$

Because the post-rake vector has  $F_r$  non-zero elements, it can also be written as

$$\mathbf{w}_r = \mathbf{S}_r^T \tilde{\mathbf{w}}_r, \quad (4.15)$$

where  $\tilde{\mathbf{w}}_r$  is an  $F_r \times 1$  vector and  $\mathbf{S}_r$  is an  $F_r \times (L + F_t - 1)$  selection matrix that determines which paths, i.e., elements of  $\mathbf{r}_i$ , are combined at the receiver. The paths that arrive first, in the middle and at the end are combined by using the matrices given respectively by

$$\mathbf{S}_r = [\mathbf{I}_{F_r} \quad \mathbf{0}_{F_r \times (L+F_t-F_r-1)}], \quad (4.16)$$

$$\mathbf{S}_r = [\mathbf{0}_{F_r \times F_t-1} \quad \mathbf{I}_{F_r} \quad \mathbf{0}_{F_r \times (L-F_r)}], \quad (4.17)$$

$$\mathbf{S}_r = [\mathbf{0}_{F_r \times (L+F_t-F_r-1)} \quad \mathbf{I}_{F_r}], \quad (4.18)$$

where  $\mathbf{I}_M$  represents an  $M \times M$  identity matrix. By substituting (4.15) in (4.14) and observing that  $\mathbf{S}_r \mathbf{S}_r^T = \mathbf{I}_{F_r}$ , another expression is obtained for  $\gamma$ :

$$\gamma = \frac{|\tilde{\mathbf{w}}_r^T \mathbf{S}_r \mathbf{H} \mathbf{v}_t|^2}{\tilde{\mathbf{w}}_r^T \mathbf{S}_r \mathbf{S}_r^T \tilde{\mathbf{w}}_r \frac{N_0}{2E_b} + \sum_{\substack{m=-I \\ m \neq 0}}^I |\tilde{\mathbf{w}}_r^T \mathbf{S}_r \mathbf{H}_m \mathbf{v}_t|^2} \quad (4.19)$$

$$= \frac{|\tilde{\mathbf{w}}_r^T \mathbf{S}_r \mathbf{H} \mathbf{v}_t|^2}{\tilde{\mathbf{w}}_r^T \tilde{\mathbf{w}}_r \frac{N_0}{2E_b} + \sum_{\substack{m=-I \\ m \neq 0}}^I |\tilde{\mathbf{w}}_r^T \mathbf{S}_r \mathbf{H}_m \mathbf{v}_t|^2}. \quad (4.20)$$

When ISI is present, the joint transmitter-receiver rake design that has a limited

total number of rake fingers is the solution to the problem

$$\{\tilde{\mathbf{w}}_r^{\text{opt}}, \mathbf{v}_t^{\text{opt}}\} = \arg \max_{\tilde{\mathbf{w}}_r, \mathbf{v}_t} \frac{\tilde{\mathbf{w}}_r^T \mathbf{S}_r \mathbf{H} \mathbf{v}_t \mathbf{v}_t^T \mathbf{H}^T \mathbf{S}_r^T \tilde{\mathbf{w}}_r}{\tilde{\mathbf{w}}_r^T \left( \frac{N_0}{2E_b} \mathbf{I}_{F_r} + \sum_{\substack{m=-I \\ m \neq 0}}^I \mathbf{S}_r \mathbf{H}_m \mathbf{v}_t \mathbf{v}_t^T \mathbf{H}_m^T \mathbf{S}_r^T \right) \tilde{\mathbf{w}}_r}. \quad (4.21)$$

The pre-rake and post-rake vectors that are obtained from (4.21) are optimal in the sense that they maximize the SINR of the decision statistic.

Defining  $\gamma_0 \triangleq 2E_b/N_0$  and the matrices

$$\mathbf{C}_v \triangleq \mathbf{S}_r \mathbf{H} \mathbf{v}_t \mathbf{v}_t^T \mathbf{H}^T \mathbf{S}_r^T, \quad (4.22)$$

$$\mathbf{D}_v \triangleq \frac{1}{\gamma_0} \mathbf{I}_{F_r} + \sum_{\substack{m=-I \\ I \neq 0}}^I \mathbf{S}_r \mathbf{H}_m \mathbf{v}_t \mathbf{v}_t^T \mathbf{H}_m^T \mathbf{S}_r^T, \quad (4.23)$$

it is recognized that the expression in (4.21) is in the form of the generalized Rayleigh quotient,

$$\gamma = \frac{\tilde{\mathbf{w}}_r^T \mathbf{C}_v \tilde{\mathbf{w}}_r}{\tilde{\mathbf{w}}_r^T \mathbf{D}_v \tilde{\mathbf{w}}_r}. \quad (4.24)$$

The post-rake vector that maximizes  $\gamma$  for a given value of  $\mathbf{v}_t$  (also  $\mathbf{C}_v$  and  $\mathbf{D}_v$ ) is the principal eigenvector (corresponding to the largest eigenvalue) of the generalized eigenvalue problem  $(\mathbf{C}_v, \mathbf{D}_v)$ , which requires solving for  $\tilde{\mathbf{w}}_r$  that satisfy

$$\mathbf{C}_v \tilde{\mathbf{w}}_r = \gamma \mathbf{D}_v \tilde{\mathbf{w}}_r. \quad (4.25)$$

This result follows from a generalization of the Rayleigh-Ritz theorem and if the inverse of  $\mathbf{D}_v$  exists,  $\tilde{\mathbf{w}}_r$  is the principal eigenvector of  $\mathbf{D}_v^{-1} \mathbf{C}_v$  [55]. In this case, since  $\mathbf{C}_v$  is of rank one, the principal eigenvector is  $\mathbf{D}_v^{-1} \mathbf{S}_r \mathbf{H} \mathbf{v}_t$  corresponding to the eigenvalue  $\mathbf{v}_t^T \mathbf{H}^T \mathbf{S}_r^T \mathbf{D}_v^{-1} \mathbf{S}_r \mathbf{H} \mathbf{v}_t$ .

For the post-rake vector optimal for a given  $\mathbf{v}_t$ , which we have obtained as

$\tilde{\mathbf{w}}_r = \mathbf{D}_v^{-1} \mathbf{S}_r \mathbf{H} \mathbf{v}_t$ , the SINR is given by

$$\gamma = \mathbf{v}_t^T \mathbf{H}^T \mathbf{S}_r^T \mathbf{D}_v^{-1} \mathbf{S}_r \mathbf{H} \mathbf{v}_t. \quad (4.26)$$

Therefore,  $\mathbf{v}_t^{\text{opt}}$  is the solution to the optimization problem

$$\mathbf{v}_t^{\text{opt}} = \arg \max_{\mathbf{v}_t} \mathbf{v}_t^T \mathbf{H}^T \mathbf{S}_r^T \mathbf{D}_v^{-1} \mathbf{S}_r \mathbf{H} \mathbf{v}_t \quad (4.27)$$

This is a very structured problem when there is ISI, since  $\mathbf{D}_v$  contains terms involving  $\mathbf{v}_t$ . It cannot be posed as an eigenvalue problem, which would lead to a closed form expression for  $\mathbf{v}_t^{\text{opt}}$ , and the Rayleigh-Ritz theorem is not applicable. However, under the constraints  $\tilde{\mathbf{w}}_r^T \tilde{\mathbf{w}}_r / P_w = \mathbf{v}_t^T \mathbf{v}_t = 1$ , the optimum pre-rake vector  $\mathbf{v}_t$  for a given  $\tilde{\mathbf{w}}_r$  is obtained by rewriting  $\gamma$  as

$$\gamma = \frac{|\tilde{\mathbf{w}}_r^T \mathbf{S}_r \mathbf{H} \mathbf{v}_t|^2}{\frac{P_w}{\gamma_0} \mathbf{v}_t^T \mathbf{v}_t + \sum_{\substack{m=-I \\ m \neq 0}}^I |\tilde{\mathbf{w}}_r^T \mathbf{S}_r \mathbf{H}_m \mathbf{v}_t|^2} \quad (4.28)$$

$$= \frac{\mathbf{v}_t^T \mathbf{H}^T \mathbf{S}_r^T \tilde{\mathbf{w}}_r \tilde{\mathbf{w}}_r^T \mathbf{S}_r \mathbf{H} \mathbf{v}_t}{\mathbf{v}_t^T \left( \frac{P_w}{\gamma_0} \mathbf{I}_{F_t} + \sum_{\substack{m=-I \\ m \neq 0}}^I \mathbf{H}_m^T \mathbf{S}_r^T \tilde{\mathbf{w}}_r \tilde{\mathbf{w}}_r^T \mathbf{S}_r \mathbf{H}_m \right) \mathbf{v}_t}. \quad (4.29)$$

Defining

$$\mathbf{C}_w \triangleq \mathbf{H}^T \mathbf{S}_r^T \tilde{\mathbf{w}}_r \tilde{\mathbf{w}}_r^T \mathbf{S}_r \mathbf{H}, \quad (4.30)$$

$$\mathbf{D}_w \triangleq \frac{P_w}{\gamma_0} \mathbf{I}_{F_t} + \sum_{\substack{m=-I \\ m \neq 0}}^I \mathbf{H}_m^T \mathbf{S}_r^T \tilde{\mathbf{w}}_r \tilde{\mathbf{w}}_r^T \mathbf{S}_r \mathbf{H}_m, \quad (4.31)$$

the pre-rake vector that maximizes  $\gamma$  for a given  $\tilde{\mathbf{w}}_r$  is found as the principal eigenvector of the matrix  $\mathbf{D}_w^{-1} \mathbf{C}_w$ , which is  $\mathbf{v}_t = \mathbf{D}_w^{-1} \mathbf{H}^T \mathbf{S}_r^T \tilde{\mathbf{w}}_r$ . This results in the optimization problem

$$\tilde{\mathbf{w}}_r^{\text{opt}} = \arg \max_{\tilde{\mathbf{w}}_r} \tilde{\mathbf{w}}_r^T \mathbf{S}_r \mathbf{H} \mathbf{D}_w^{-1} \mathbf{H}^T \mathbf{S}_r^T \tilde{\mathbf{w}}_r. \quad (4.32)$$

Although a closed form expression for  $\tilde{\mathbf{w}}_r^{\text{opt}}$  targeting ISI limited scenarios does not exist either, it is possible to obtain  $\mathbf{v}_t^{\text{opt}}$  and  $\tilde{\mathbf{w}}_r^{\text{opt}}$  jointly using an iterative procedure similar to the approach in [56], which is initialized with the pre- and post-rake vectors for the ISI-free case. In the absence of ISI,  $\mathbf{v}_t^{\text{opt}}$  and  $\tilde{\mathbf{w}}_r^{\text{opt}}$  correspond to the principal eigenvectors of the matrices  $\mathbf{H}^T \mathbf{S}_r^T \mathbf{S}_r \mathbf{H}$  and  $\mathbf{S}_r \mathbf{H} \mathbf{H}^T \mathbf{S}_r^T$ , which follow from (4.27) and (4.32) for  $\mathbf{D}_v = (1/\gamma_0) \mathbf{I}_{F_r}$  and  $\mathbf{D}_w = (P_w/\gamma_0) \mathbf{I}_{F_t}$ , respectively. The solution algorithm can be described as follows.

1. Set the initial value of  $\tilde{\mathbf{w}}_r$  to the optimal ISI-free solution, which is the principal eigenvector of  $\mathbf{S}_r \mathbf{H} \mathbf{H}^T \mathbf{S}_r^T$ .
2. Using  $\tilde{\mathbf{w}}_r$  obtained previously, compute  $\mathbf{D}_w^{-1} \mathbf{H}^T \mathbf{S}_r^T \tilde{\mathbf{w}}_r$ , which becomes the new  $\mathbf{v}_t$ .
3. Update  $\tilde{\mathbf{w}}_r$  to  $\mathbf{D}_v^{-1} \mathbf{S}_r \mathbf{H} \mathbf{v}_t$  based on the latest value of  $\mathbf{v}_t$  from step 2.
4. Evaluate  $\gamma$  according to the expression in (4.26).
5. If the change in  $\gamma$  compared to the outcome of the previous iteration exceeds a preset threshold, compute one more iteration by repeating the procedure in steps 2-5. Otherwise stop the algorithm.

The iterations are guaranteed to converge so that  $\gamma$  reaches a maximum because steps 2 and 3 above both increase the SINR.

### 4.3. Simulation Results

The results for distributing a total fixed number of rake fingers optimally between the transmitter and the receiver so as to maximize the SINR of the decision statistic,  $\xi$ , are presented in this section. Simulations have been performed for the CM1 UWB channel model in [18], where the 1000 channel realizations created are normalized to unity in their average energy as  $E \left\{ \sum_{\ell=0}^{L-1} \alpha_\ell^2 \right\} = 1$ .

The optimal selection of the finger positions of the post-rake, which maximizes the SINR of  $\xi$  for  $F = L + 1$  and  $T_b > (2L - 1)T_p$  is the problem addressed in Figure 4.1. The total number of fingers,  $F$ , in Figure 4.1 is  $L + 1$  so that  $F_r = L$  when  $F_t = 1$ , and similarly  $F_r = 1$  when  $F_t = L$ . Also, the condition  $T_b > (2L - 1)T_p$

ensures that there is no ISI in the figure, where, in other words,  $\gamma$  is the SNR of  $\xi$ . Then  $\gamma$  is the maximum eigenvalue of the matrix  $\mathbf{S}_r \mathbf{H} \mathbf{H}^T \mathbf{S}_r^T$  or equivalently  $\mathbf{H}^T \mathbf{S}_r^T \mathbf{S}_r \mathbf{H}$  scaled by  $\gamma_0$ , which is obtained by evaluating (4.27) or (4.32) for  $\mathbf{D}_v = (1/\gamma_0) \mathbf{I}_{F_r}$  or  $\mathbf{D}_w = (P_w/\gamma_0) \mathbf{I}_{F_t}$ , respectively.

In addition to the post-rake vectors that select paths arriving first, in the middle and at the end as defined in (4.16)-(4.18), the all-post-rake which has  $\mathbf{S}_r = \mathbf{I}_{L+F_t-1}$ , i.e.,  $F_r = L + F_t - 1$ , is included in Figure 4.1. While the all-post-rake structure is equivalent to the eigenprecoder in [52] for  $F_t = L$ , the PRC pre/post-rake design in [53], which considers arbitrary  $F_t$  corresponds to the curve “all” in Figure 4.1. Thus, it is possible to compare the performance of the proposed design with those in previous works using Figure 4.1. It is observed from the figure that for all  $F_t$  the highest  $\gamma$  is obtained by the PRC/post-rake scheme using all post-rake fingers, where  $\gamma$  increases with  $F_t$ , which makes the eigenprecoder the optimum structure in terms of maximizing  $\gamma$ . However, in order to operate at a high  $\gamma$  when  $F$  is constrained to the length of the channel impulse response, it is best to distribute the total number of rake fingers almost equally between the transmitter and the receiver if the first arriving paths are combined at the receiver. For a large number of rake fingers at the transmitter, the figure suggests that selecting the paths that arrive in the middle as in (4.17) improves  $\gamma$ . As the two curves for the “first” and “middle” arriving paths fail to be continuous at large values of  $F_t$ , it is likely that there is a better way to select the finger positions for the post-rake than these two. Note that the form of (4.17) is a generalization of the pre-rake only structure that has a peak at the  $F_t$ th path of the composite channel impulse response with  $L + F_t - 1$  paths if the pre-rake vector of length  $F_t$  consists of the channel coefficients,  $\alpha_\ell$  [57].

The  $\gamma/\gamma_0$  values shown in Figure 4.2 support the previous claim that a more systematic way of selecting the paths at the receiver to form the post-rake fingers is necessary for the proposed transmitter-receiver structure, and that intuition may not be enough. For especially  $F = 9$  the idea of combining the first arriving paths loses its optimality, where the paths that arrive in the middle should be combined as in (4.17) to obtain a larger  $\gamma$ .

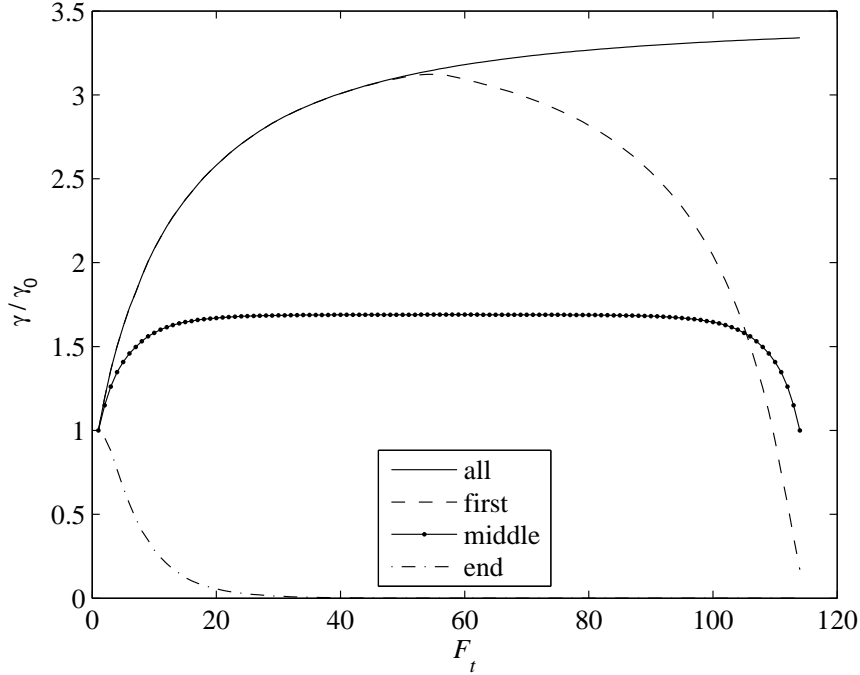


Figure 4.1. The normalized SINR values,  $\gamma/\gamma_0$ , against  $F_t$  for  $F = L + 1$ ,  $T_b > (2L - 1)T_p$ , i.e., no ISI, and different positions of the post-rake fingers

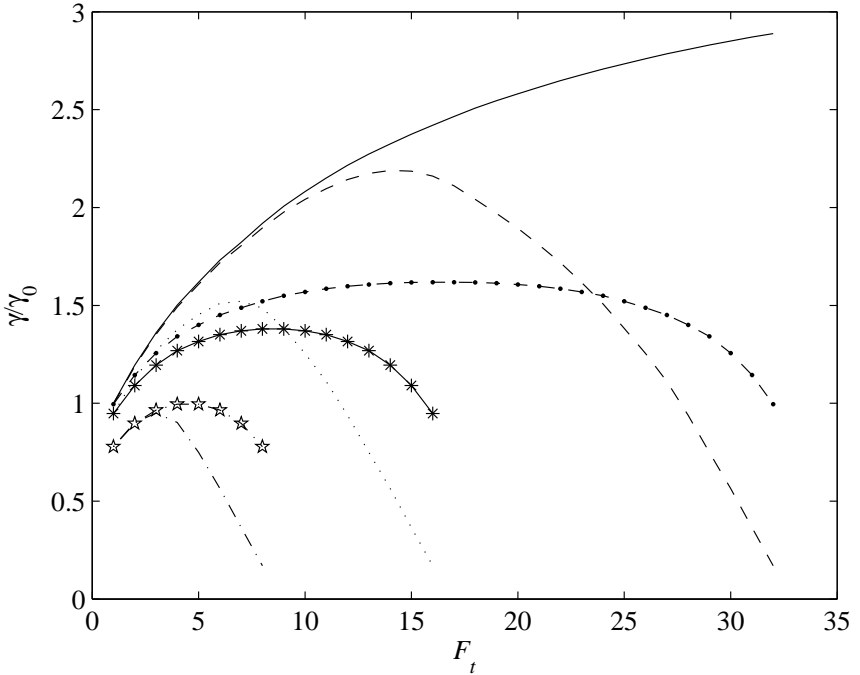


Figure 4.2. The normalized SINR values,  $\gamma/\gamma_0$ , against  $F_t$  for  $F = 9, 17, 33$  and  $T_b > (L + F_t - 1)T_b$ , i.e., no ISI. Without markers: First arriving paths (4.16). With markers: Middle arriving paths (4.17). Solid curve: All-post rake

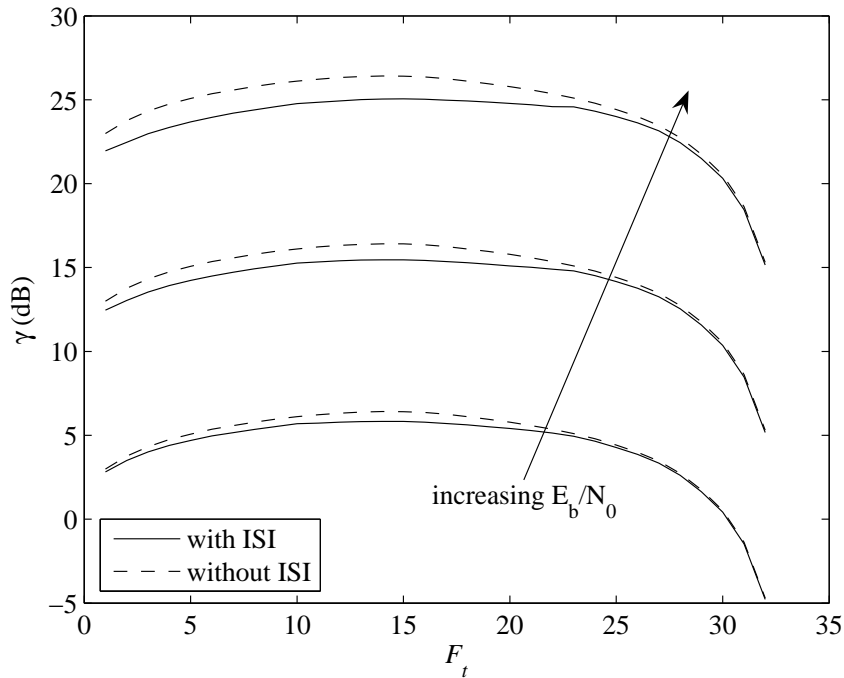


Figure 4.3. The SINR values for the transmitter-receiver design that combines the first arriving paths, i.e., uses (4.16), against  $F_t$  for  $F = 33$ , where  $E_b/N_0 = 0, 10, 20$  dB,  $T_b = 10$  ns and  $T_p = 1$  ns

Displayed in Figure 4.3 are the maximum SINR values achievable in dB for  $F = 33$  and various values of  $E_b/N_0$ , where  $T_b = 10$  ns and  $T_p = 1$  ns. The first arriving paths are combined at the receiver using the matrix in (4.16). It is observed that the effects of ISI are less of a problem when  $E_b/N_0$  is low, and in particular the ISI makes the accurate selection of the optimal  $(F_t, F_r)$  pair (around which the  $\gamma$  curve becomes flatter) less critical at large  $E_b/N_0$  as shown more clearly in Figure 4.4 for  $E_b/N_0 = 20$  dB. Yet another observation is that in general the optimal  $(F_t, F_r)$  pair does not change with ISI, which has been validated by unreported simulations covering other cases.

Finally, these two figures obtained using the iterative algorithm described, Figures 4.3 and 4.4, both point to the fact that moving the rake structure from the receiver to the transmitter helps mitigate ISI as advocated previously in [50]. In Figures 4.3 and 4.4, with  $F_t = 1$  we observe a lowering of the  $\gamma$  value when ISI is present. However, for  $F_t = 32$  the effect of ISI on  $\gamma$  is insignificant.

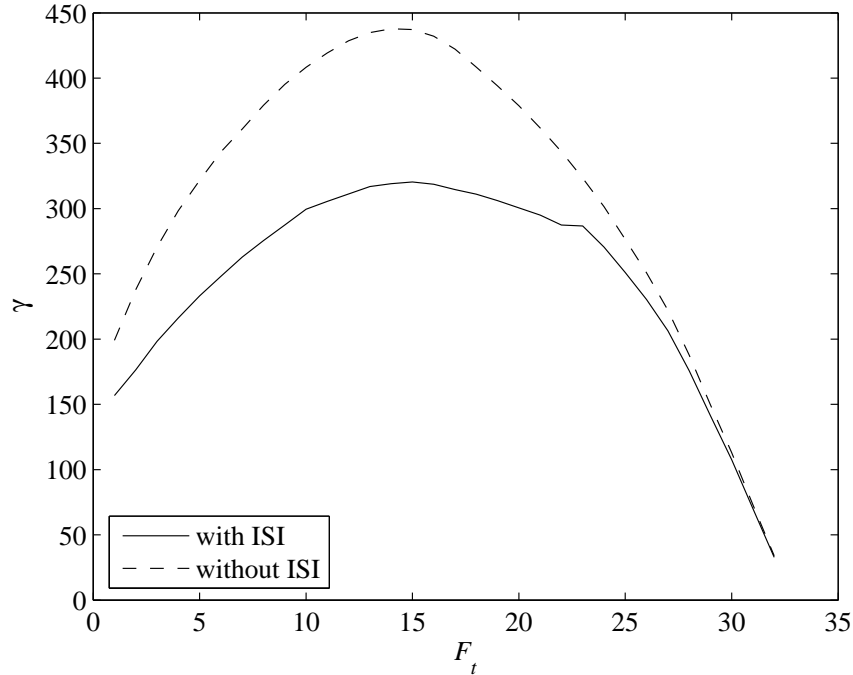


Figure 4.4. The SINR values for the transmitter-receiver design that combines the first arriving paths, i.e., uses (4.16), against  $F_t$  for  $F = 33$ , where  $E_b/N_0 = 20$  dB,

$$T_b = 10 \text{ ns and } T_p = 1 \text{ ns}$$

The single-user performances of the pre-rake and the post-rake only systems are equivalent just for the ISI-free case. The all-post-rake system with MRC has

$$\mathbf{v}_R = 1 \quad (4.33)$$

$$\mathbf{w}_R = [\alpha_0 \dots \alpha_{L-1}]^T, \quad (4.34)$$

where the subscript  $R$  indicates that channel information is employed only at the receiver. When  $\mathbf{v}_T = [\alpha_{L-1} \dots \alpha_0]^T$  with the subscript  $T$  showing that channel information is available only at the transmitter, the  $L$ th received path,  $r_{i,L-1}$ , is in the form of the output of an MRC all-post-rake. Thus, the system with the post-rake vector

$$\mathbf{w}_T = \underbrace{[0 \dots 0]_{L-1}}_{L-1} \underbrace{[1 0 \dots 0]_{L-1}}_{L-1}^T \quad (4.35)$$

is equivalent to the all-post-rake system in terms of single-user performance when ISI is absent, where for the ISI-free case they both have  $\gamma = \gamma_0 \sum_{\ell=0}^{L-1} \alpha_\ell^2$ .

## 5. ROBUST DETECTION OF IMPULSE RADIO SIGNALS IN NON-GAUSSIAN NOISE

Configuration of transceivers, and the selection procedure concerned with the multiple access scheme and the modulation of communication systems are heavily influenced by the transmission channel. An accurate channel characterization enables efficient utilization of the resources and the design of the optimum receiver. The multipath characteristics of the wideband indoor channel lying in the 2-8 GHz band investigated for the IEEE 802.15.3 wireless personal area network standard to be developed and based on a UWB physical layer are such that the total energy is distributed over a large number of paths, which are resolved in time, and the multipath delay spread spans several nanoseconds [18]. Measurement results in [15] demonstrate that the communication channel in typical indoor environments is subject to interference produced by the photocopiers, printers, etc. in the office. Moreover, UWB receivers are also vulnerable to interference from other sources whose operation overlaps with the UWB spectrum. As an example, the IEEE 802.11a wireless local area network standard stipulates a nominal transmission power around 50 mW, which is almost 100 times higher than the total UWB transmission power allowed over its entire spectrum. Despite its relatively narrowband nature, such strong interference can saturate UWB devices and cause drastic performance deterioration [58]. Unlike thermal noise which obeys the AWGN model, channel interference by various sources occurs in high-amplitude bursts and it shows non-Gaussian, impulsive characteristics. A robust receiver is one that performs near-optimal in the presence of nominal Gaussian noise, and does not succumb to occasional bursts of interference outliers. The combined impediment created by noise and interference will hereafter be referred to as impulsive noise.

In this chapter, the performance improvement offered by the robust rake receiver for the frequency-selective UWB channel [18] corrupted with an additive noise process containing impulsive components is investigated in the presence of other UWB users. The robust rake receiver eliminates the effect of impulsive noise by removing the large-

amplitude outliers at the outputs of the matched filters employed by the conventional rake receiver at each of its fingers, which is followed with the conventional MRC. There is a remarkable performance improvement if the rake receiver with MRC is robustified using clipper nonlinearities to eliminate impulsive noise. Also, it is shown that there exists an optimum choice of parameters for the nonlinearities. The Gaussian approximation for the MAI, which is required for calculating the optimal clipping parameters, is demonstrated to hold for equal-power interferers and the UWB channels under consideration with the simulation set-up used in this chapter.

The organization of the rest of this chapter is as follows: The UWB system model is presented in Section 5.1, where there is some overlap with Chapter 3, since the models described in Chapters 3 and 5 are very similar with the major difference being the nature of the noise process. The proposed robust receiver is described in Section 5.2, and Section 5.3 is reserved for the simulation results and discussions.

### 5.1. UWB System Model

An UWB impulse radio system which uses TH for multiple access and binary PPM for data modulation is considered. In this system, the signal transmitted by the  $k$ th user is

$$s_{\text{tr}}^{(k)}(t) = \sum_{j=-\infty}^{\infty} \sqrt{\frac{E_b}{N_s}} w_{\text{tr}}(t - jT_f - c_j^{(k)}T_c - \delta b_{\lfloor j/N_s \rfloor}^{(k)}), \quad (5.1)$$

where  $k = 0, \dots, K_r$  with 0 denoting the desired user,  $E_b$  is the bit energy and  $N_s$  is the number of pulses transmitted per bit. Hence, the energy per pulse is  $E_p = E_b/N_s$ . Each of the pulses,  $w_{\text{tr}}(t)$ , is transmitted during a frame of  $T_f$  seconds and the exact position of the pulses is determined by the time-hopping sequence  $\{c_j^{(k)}\}$  and the data bit  $b_{\lfloor j/N_s \rfloor}^{(k)}$ , both of which are specific to user  $k$ . The  $j$ th pulse is shifted by  $c_j^{(k)}T_c + \delta b_{\lfloor j/N_s \rfloor}^{(k)}$ , where  $c_j^{(k)} \in \{0, 1, \dots, N_h - 1\}$ , and  $N_h$  is the number and  $T_c$  is the duration of the bins to which the pulses are allowed to hop. The data bit stays constant across  $N_s$  frames so that a kind of repetition coding is obtained. There is either no shift, or a shift of  $\delta$

when the bit is a “0” or “1”, respectively. The parameter  $\delta$ , with  $\delta \geq T_p$  for orthogonal PPM, controls the amount of shift for data modulation, where  $T_p$  is the pulse duration in seconds. Here, we have  $\delta = T_p$ ,  $N_h = T_f/2T_p$  and  $T_c = 2T_p$ .

When multiple users are transmitting simultaneously, the received signal is composed of a desired signal term, other signal components resulting from the interfering users and an additive noise process, which occasionally produces large amplitudes. Considering a frequency-selective channel described by the impulse response function in (3.2), which is reproduced here for convenience

$$h_k(t) = \sum_{\ell=0}^{L_k-1} \alpha_{k,\ell} \delta_D(t - \tau_{k,\ell}), \quad (5.2)$$

the received signal due to the  $k$ th user is as in (3.3)

$$s_{\text{rec}}^{(k)}(t) = \tilde{s}_{\text{tr}}^{(k)}(t) * h_k(t). \quad (5.3)$$

The total received signal is thus

$$r(t) = s_{\text{rec}}^{(0)}(t) + \sum_{k=1}^{K_r} s_{\text{rec}}^{(k)}(t - \tau_k) + n(t), \quad (5.4)$$

where  $n(t)$  is the additive white noise process containing impulsive components, and the time asynchronism between the transmitters of different users is represented by the variable  $\tau_k$ . For the assumption that the receiver is perfectly synchronized with the desired (0th) user, it is required to have  $\tau_0 = 0$  in (5.4). One should realize that although they look identical in form, (3.6) and (5.4) are different, since the noise process of (5.4) has impulsive characteristics.

The optimum detector for a single bit of the TH-PPM system in the AWGN is the correlation receiver [2], which can typically be implemented as a rake structure with  $\tilde{L}$  fingers for frequency-selective channels. Among the  $L_0$  paths produced in response to a UWB pulse, the most energetic  $\tilde{L}$  paths can be chosen for combining, which leads to

a selective rake. The decision statistic for the 0th bit is

$$\sum_{j=0}^{N_s-1} \sum_{\ell=0}^{\tilde{L}-1} w_{j,\ell} \underbrace{\int_{jT_f+\tau_{0,\ell}}^{(j+1)T_f+\tau_{0,\ell}} r(t)v(t-jT_f-c_j^{(0)}T_c-\tau_{0,\ell})dt}_{x_{j,\ell}}, \quad (5.5)$$

where  $v(t) = w_{\text{rec}}(t) - w_{\text{rec}}(t - \delta)$  is the template signal for the correlator,  $x_{j,\ell}$  is the correlator output for the  $\ell$ th selected path of the  $j$ th pulse and  $w_{j,\ell}$  is the combining weight for  $x_{j,\ell}$ . The sum in (5.5) is positive if a “0” is sent. The conventional MRC scheme uses the channel gains as the combining weights so that  $w_{j,\ell} = \alpha_{0,\ell}$ . In a frequency-selective environment or in the presence of MAI, this decision rule will not be optimal. The contributions from different frames have different SINRs depending on the TH sequences of the other users, and there is self-interference in the form of IFI and ISI because of multipath [37].

## 5.2. Robust Detection

In this section, a rake receiver that is robust against the impulsive nature of the noise is introduced. The proposed receiver is shown in Figure 5.1. Outputs of each of the matched filters employed by the rake receiver fingers,  $x_{j,\ell}$  in (5.5), should be passed through a nonlinearity before being merged via MRC. The outputs of the rake fingers are determined to be

$$x_{j,\ell} = \sqrt{E_p} \alpha_{0,\ell} \beta + \sum_{k=0}^{K_r} \eta_{j,\ell}^{(k)} + n_{j,\ell}, \quad (5.6)$$

where  $\beta$  takes on the value of “1” or “-1” when the transmitted bit is a “0” or “1”, respectively.

### 5.2.1. Impulsive Noise and MAI

Referring to  $x_{j,\ell}$  in (5.6), there are two terms which should be modeled: The impulsive noise samples  $n_{j,\ell}$  and the MAI expressed by the second term in summation.

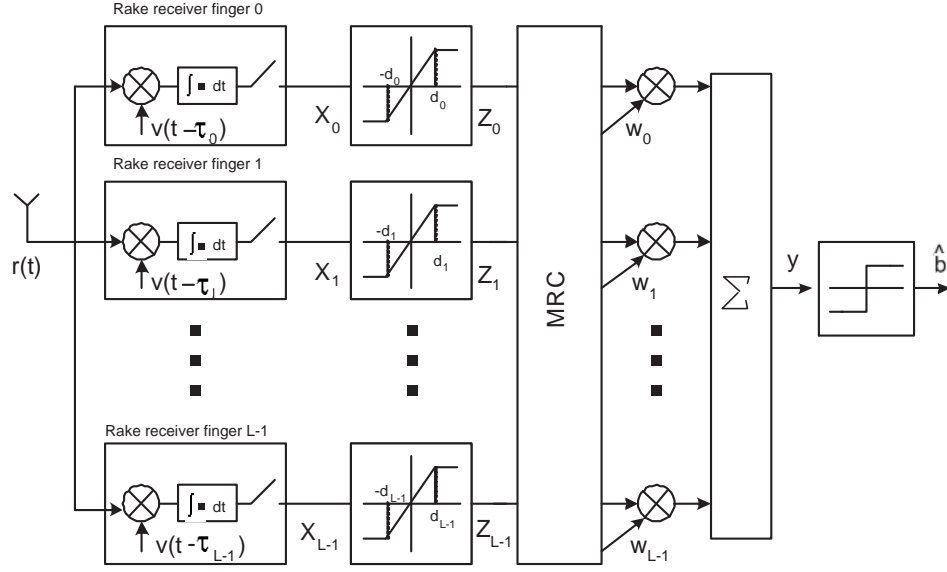


Figure 5.1. The robust rake receiver for impulse radio with  $N_s = 1$

The main assumption about the channel noise is that the samples are i.i.d. so that an impulsive noise source can be studied by modeling its first order pdf [59]. The pdf of the noise model is the mixture of two Gaussians with zero means and different variances, where one is a multiple of the other for the representation of the heavy tail of the distribution which produces large amplitudes. Letting the parameter  $\epsilon \in [0, 1]$  control the contribution of the impulsive component to the density function [59], the noise pdf has the form

$$f_{n_{j,\ell}}(x) = (1 - \epsilon)g_n(x) + \epsilon g_i(x), \quad (5.7)$$

where  $g_n(\cdot)$  is the nominal Gaussian pdf with variance  $N_0$  and  $g_i(\cdot)$  is the heavier tailed Gaussian with variance  $\kappa N_0$  and  $\kappa \geq 1$ . Thus, the noise samples in (5.6),  $n_{j,\ell}$ , have variance  $(1 - \epsilon)N_0 + \epsilon\kappa N_0$ . When  $\kappa = 1$ , the usual AWGN case is obtained. The  $\epsilon$ -mixture model is an approximation to Middleton's Class A noise model pdf [60], which consists of an infinite expansion of Gaussian density functions with different variances and identical means. In [61], it is shown that the first two terms of the expansion sufficiently describe the Class A noise pdf. In addition, the  $\epsilon$ -mixture model is much more tractable than the Class A noise pdf.

As for the MAI, when the number of users is sufficiently large, the combined

effect of the interfering users can be treated as a Gaussian process. Specifically, the MAI term in (5.6) due to the  $k$ th user,  $\eta_{j,\ell}^{(k)}$ , is approximated as a Gaussian random variable with mean zero and variance [40]

$$E[\{\eta_{j,\ell}^{(k)}\}^2] = \frac{1}{T_f} \sum_{m=0}^{L_k-1} \alpha_{k,m}^2 E_p \int_{-\infty}^{\infty} |R_{wv}(\tau)|^2 d\tau, \quad (5.8)$$

where  $R_{wv}(\tau)$  is the cross-correlation between  $w_{\text{rec}}(t)$  and  $v(t)$ :

$$R_{wv}(\tau) = \int_{-\infty}^{\infty} w_{\text{rec}}(t + \tau)v(t)dt. \quad (5.9)$$

The variance in (5.8) is calculated by assuming an independent random delay for each arriving path of each user [40]. The interference term in (5.6) includes self-interference, as well. With such an approximation to MAI, the interference terms in the  $\ell$ th paths of each of the  $N_s$  pulses are assumed to be identical. Thus, the variance of the total MAI at the  $\ell$ th path of any of the  $N_s$  pulses is represented by

$$\sigma_{\eta,\ell}^2 = \frac{1}{T_f} \sum_{k=0}^{K_r} \sum_{m \in \mathcal{M}_\ell} \alpha_{k,m}^2 E_p \int_{-\infty}^{\infty} |R_{wv}(\tau)|^2 d\tau, \quad (5.10)$$

where  $\mathcal{M}_\ell = \{m: m = 0, 1, \dots, L_k - 1, \text{ and } \tau_{0,m} \neq \tau_{0,\ell}\}$ .

### 5.2.2. Robust Nonlinearity

The nonlinearity adopted for UWB signals herein follows the one that is developed for the detection of direct sequence (DS)-CDMA with BPSK [62]. The derivation is based on Huber's mixture model and the log-likelihood ratio between the least favorable pair of density functions in terms of the Kullback-Leibler distance [63]. Accordingly, the rake finger outputs are processed through

$$z(x_{j,\ell}) = \begin{cases} -d_\ell & \text{for } x_{j,\ell} \leq -d_\ell, \\ x_{j,\ell} & \text{for } -d_\ell < x_{j,\ell} < d_\ell, \\ d_\ell & \text{for } x_{j,\ell} \geq d_\ell, \end{cases} \quad (5.11)$$

where  $d_\ell$  is the trimming parameter that needs to be optimized to minimize the probability of error. The parameter depends on the particular multipath  $\ell$ , but not on the particular pulse  $j$  when the white Gaussian assumption for the MAI is used, since the mean and variance of  $x_{j,\ell}$  are  $\alpha_{0,\ell}\sqrt{E_p}$  and  $(1 - \epsilon)N_0 + \epsilon\kappa N_0 + \sigma_{\eta,\ell}^2$ , respectively, independent of  $j$ .

For the additive noise only case, where there is only one path and thus one correlator, the mean of  $x_{j,0}$  given that a “0” is transmitted is

$$E[x_{j,0} | \text{“0” is sent}] \triangleq \mu = \sqrt{E_p}, \quad (5.12)$$

since  $\alpha_{k,0} = 1$  and  $\alpha_{k,m} = 0$  for  $m = 1, \dots, L_k - 1$ ,  $\forall k$ , while its variance is  $\sigma_n^2 = N_0 + \sigma_{\eta,0}^2$ , which is the nominal noise variance without impulsive components plus the MAI variance, or  $\sigma_i^2 = \kappa N_0 + \sigma_{\eta,0}^2$ , the sum of the outlier noise and MAI variances, depending on whether the noise is due to  $g_n(\cdot)$  or  $g_i(\cdot)$ , respectively. On the other hand, the mean and variance of the output of the robust nonlinearity (5.11) are

$$m_r = (1 - \epsilon)m_n + \epsilon m_i \quad (5.13)$$

$$v_r^2 = (1 - \epsilon)v_n^2 + \epsilon v_i^2. \quad (5.14)$$

If  $\phi$  and  $\Phi$  are respectively the pdf and the cumulative distribution function (cdf) of the zero mean, unit variance Gaussian random variable, then  $m_n$  and  $v_n^2$  are

$$m_n = (d + \mu)\Phi\left(\frac{d + \mu}{\sigma_n}\right) - (d - \mu)\Phi\left(\frac{d - \mu}{\sigma_n}\right) - \mu + \sigma_n \left[ \phi\left(\frac{d + \mu}{\sigma_n}\right) - \phi\left(\frac{d - \mu}{\sigma_n}\right) \right], \quad (5.15)$$

$$\begin{aligned} v_n^2 = & 2d^2 - \sigma_n^2 - \mu^2 + (\sigma_n^2 + \mu^2 - d^2) \left[ \Phi\left(\frac{d - \mu}{\sigma_n}\right) + \Phi\left(\frac{d + \mu}{\sigma_n}\right) \right] \\ & - [\sigma_n(d - \mu) + 2\sigma_n\mu] \phi\left(\frac{d - \mu}{\sigma_n}\right) + [-\sigma_n(d + \mu) + 2\sigma_n\mu] \phi\left(\frac{d + \mu}{\sigma_n}\right) - m_n^2, \end{aligned} \quad (5.16)$$

and  $m_i$  and  $v_i^2$  are calculated the same way as  $m_n$  and  $v_n^2$ , by replacing  $m_n$  and  $\sigma_n^2$  with  $m_i$  and  $\sigma_i^2$ , respectively [62].

The decision statistic for the robust detection of TH-PPM signals of a UWB system, which has been corrupted by additive noise only is

$$\zeta = \sum_{j=0}^{N_s-1} z(x_{j,0}). \quad (5.17)$$

Thus, assuming equally likely bits, the theoretical probability of error ( $P_e$ ) for the robust UWB detector in additive non-Gaussian noise is

$$P_e = \Pr \{ \zeta < 0 \mid \text{"0" is sent} \}, \quad (5.18)$$

which can be approximated as

$$P_{e,1} \approx \Phi \left( -\sqrt{N_s} \frac{m_r}{v_r} \right) \quad (5.19)$$

for sufficiently large  $N_s$  by the central limit theorem. The true pdf of the output of the nonlinearity for each pulse  $j$  is

$$f_z(z) = \begin{cases} (1 - \epsilon) \left[ 1 - \Phi \left( \frac{d+\mu}{\sigma_n} \right) \right] + \epsilon \left[ 1 - \Phi \left( \frac{d+\mu}{\sigma_i} \right) \right], & z = -d, \\ \frac{1-\epsilon}{\sqrt{2\pi\sigma_n^2}} \exp \left[ -\frac{(z-\mu)^2}{2\sigma_n^2} \right] + \frac{\epsilon}{\sqrt{2\pi\sigma_i^2}} \exp \left[ -\frac{(z-\mu)^2}{2\sigma_i^2} \right], & -d < z < d, \\ (1 - \epsilon) \left[ 1 - \Phi \left( \frac{d-\mu}{\sigma_n} \right) \right] + \epsilon \left[ 1 - \Phi \left( \frac{d-\mu}{\sigma_i} \right) \right], & z = d. \end{cases} \quad (5.20)$$

The exact probability of error can be calculated from the true pdf of  $\zeta$ , which is the convolution of  $N_s$   $f_z(z)$  functions, by performing

$$P_{e,2} = \int_{-\infty}^0 \underbrace{f_z(z) * \dots * f_z(z)}_{N_s \text{ times}} dz. \quad (5.21)$$

Figure 5.2 shows a plot of the approximate probability of error in (5.19) against the parameter  $d$  of the robust nonlinearity for an additive impulsive noise channel with

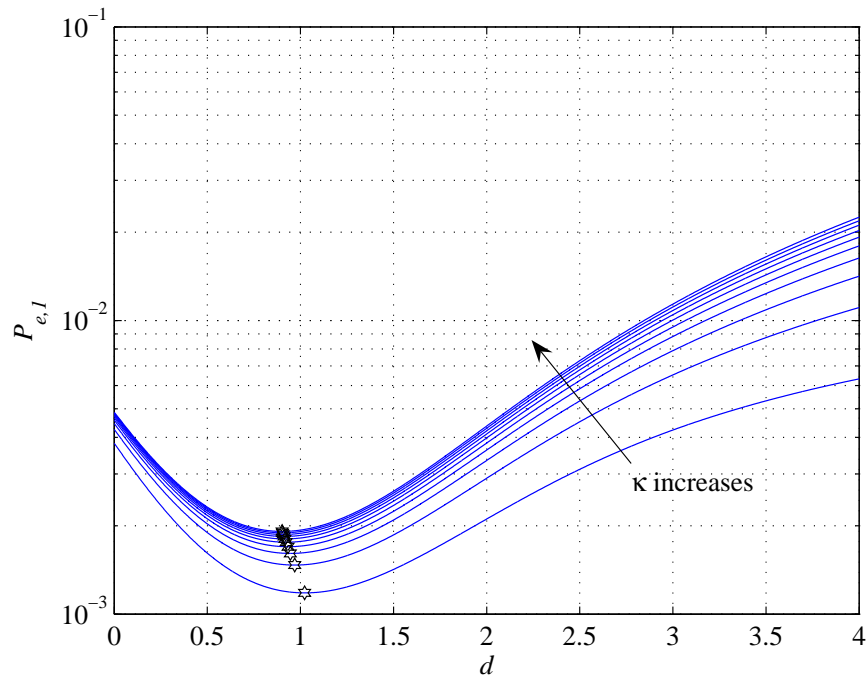


Figure 5.2.  $P_{e,1}$  against  $d$  for  $E_b/N_0 = 10$  dB,  $R_b = 1$  Mbps,  $\epsilon = 0.1$ ,  
 $\kappa = \{10, 20, \dots, 100\}$

$\epsilon = 0.1$  and no interfering users as  $\kappa$  is varied from 10 to 100 in increments of 10. Here, the SNR defined by  $E_b/N_0$  is 10 dB, the bit rate,  $R_b = 1/(N_s T_f)$ , is 1 Mbps,  $T_f = 100$  ns, and  $T_p = 1$  ns so that  $N_s = 10$ . In the extreme case when  $d = \infty$ , there will be no clipping and the robust receiver will be identical to the linear receiver. Therefore, as  $d$  increases, its performance worsens to approach that of the matched filter. Since the  $P_{e,1}$  curves in Figure 5.2 are convex functions of  $d$ , a gradient descent algorithm suffices to find the optimal  $d$  values that minimize  $P_{e,1}$ , which correspond to the minima marked with hexagons in the figure. The optimal  $d$  is almost invariant to the particular value of  $\kappa$ , which implies that the robust UWB system is insensitive to possible errors in the estimation of the outlier strength.

Figure 5.3 shows the superior performance in terms of bit-error rate (BER) of the robust receiver against the linear receiver when the optimal  $d$ 's from Figure 5.2 are used in the simulations. The performance of the robust receiver is not affected very much by the increase in  $\kappa$  for  $\kappa \geq 20$ .

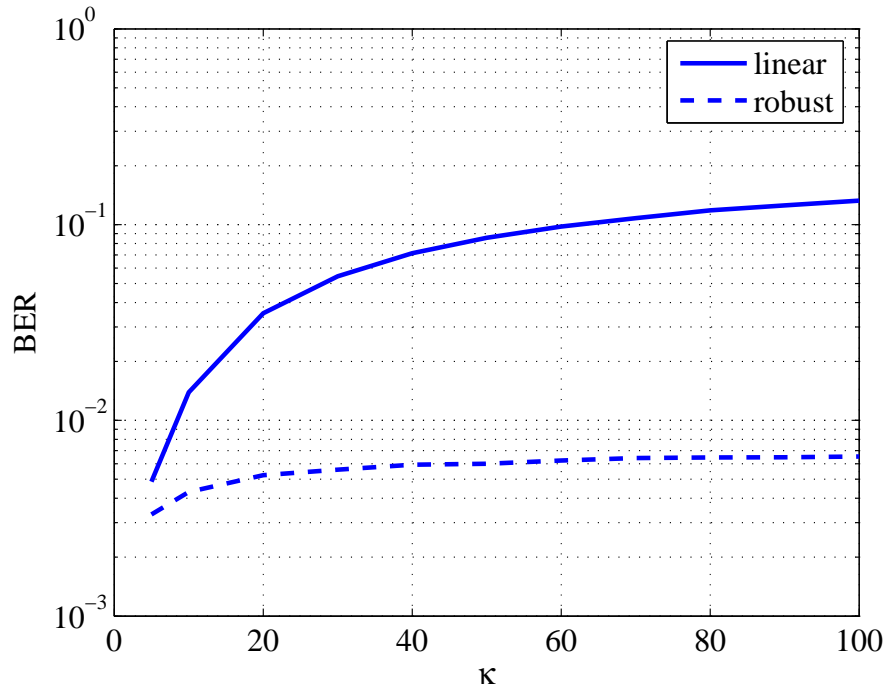
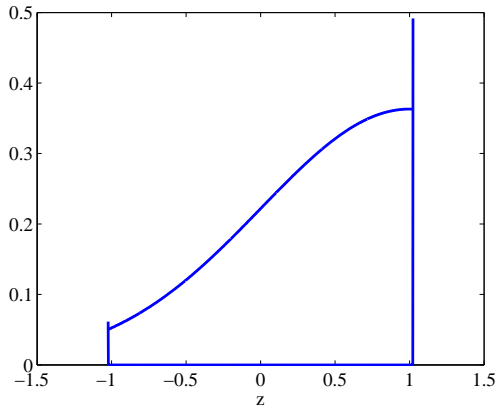
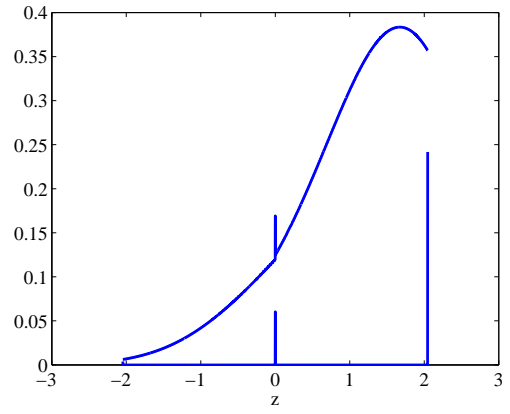
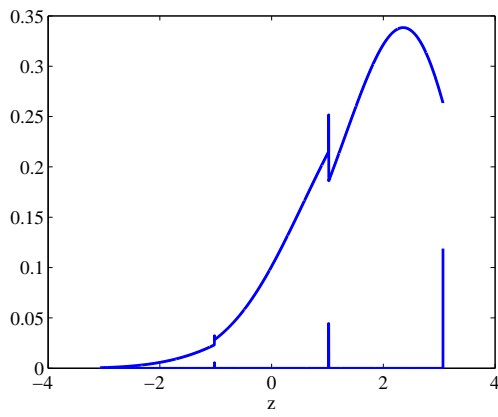
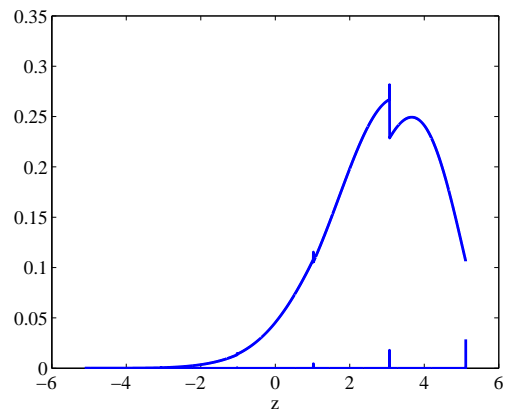
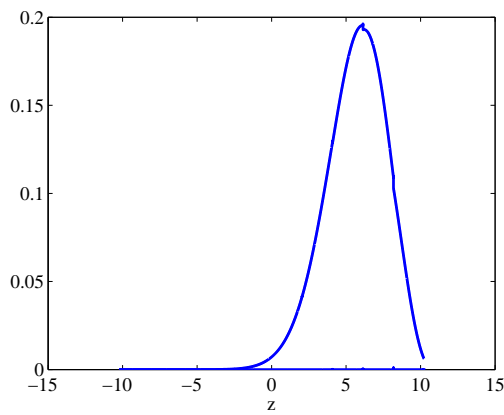
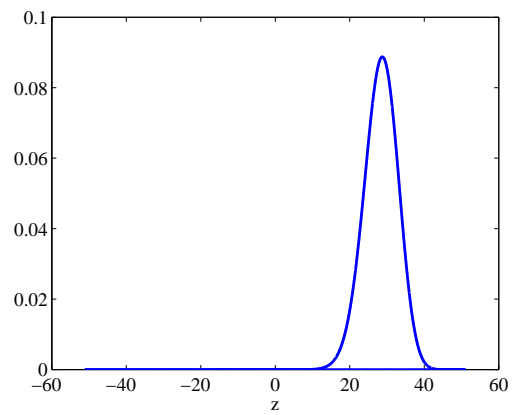


Figure 5.3. BER for robust and linear receivers for  $E_b/N_0 = 10$  dB,  $R_b = 1$  Mbps and  $\epsilon = 0.1$  in additive non-Gaussian noise

Theoretically, the optimum value of  $d$  can be found as the one minimizing  $P_{e,2}$  in (5.21), which can be numerically evaluated. For high data rate applications,  $N_s$  is typically small, and the central limit theorem does not hold in practice. Calculating the true pdf of  $\zeta$  for the case  $\kappa = 10$  and  $d = 1.023$  (i.e., the optimal  $d$  for  $\kappa = 10$  from Figure 5.2), the sequence of pdf's in Figure 5.4 are obtained. The optimal  $d$ 's calculated numerically from (5.21) for the parameters of Figure 5.2 are given in Table 5.1 with their corresponding error probabilities. The numerically computed error probabilities, on the other hand, for the optimal  $d$  values predicted by the Gaussian approximation to  $\zeta$  are in Table 5.2. A comparison of Figure 5.2 and Table 5.2 indicates that the Gaussian assumption for the pdf of  $\zeta$  is not very accurate, and it underestimates the bit error probability. However, the error probabilities listed in Table 5.2 that are obtained by employing the suboptimal  $d$  values calculated from the Gaussian assumption are not very different from the minimum error probabilities in Table 5.1 because the  $P_{e,2}$  curves vary slowly around the minima as shown in Figure 5.5. The results in Table 5.2 are also verified by the simulation outcomes displayed in Figure 5.3. The receiver performance is insensitive to small deviations from the optimal choice of  $d$ , and the suboptimal  $d$

(a)  $N_s = 1$ (b)  $N_s = 2$ (c)  $N_s = 3$ (d)  $N_s = 5$ (e)  $N_s = 10$ (f)  $N_s = 50$ Figure 5.4. Numerical calculation of the true pdf of  $\zeta$  as  $N_s$  is increased

values

Table 5.1. The optimal  $d$ 's and the corresponding  $P_e$ 's predicted via the numerical evaluation of (5.21)

$\kappa$	10	20	30	40	50	60	70	80	90	100
optimal $d$	1.3460	1.2130	1.1620	1.1340	1.1160	1.1020	1.0920	1.0850	1.0780	1.0730
$P_{e,2} (\times 10^{-3})$	3.8716	4.8418	5.3124	5.6041	5.8078	5.9605	6.0805	6.1781	6.2595	6.3288

Table 5.2.  $P_e$  for the suboptimal  $d$ 's found by the Gaussian approximation to  $\zeta$  (numerical evaluation)

$\kappa$	10	20	30	40	50	60	70	80	90	100
Gaussian $d$	1.0230	0.9690	0.9460	0.9330	0.9230	0.9170	0.9120	0.9080	0.9040	0.9020
$P_{e,2} (\times 10^{-3})$	4.0806	5.0062	5.4590	5.7404	5.9392	6.0866	6.2033	6.2982	6.3785	6.4449

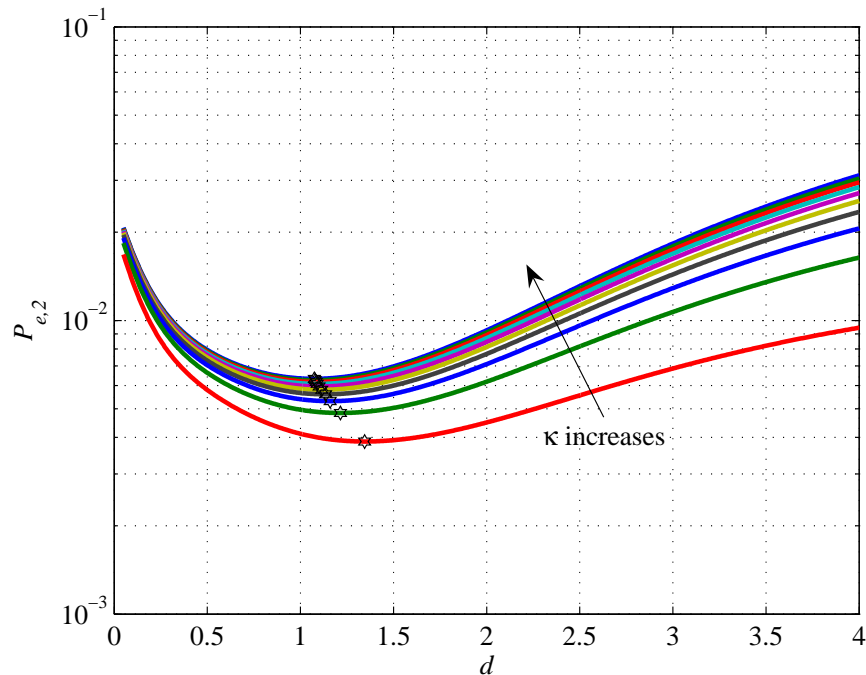


Figure 5.5.  $P_{e,2}$  against  $d$  for  $E_b/N_0 = 10$  dB,  $R_b = 1$  Mbps,  $\epsilon = 0.1$ ,  
 $\kappa = \{10, 20, \dots, 100\}$

values given by the Gaussian approximation are accurate enough. Therefore, the sub-optimal  $d$  values are used in the sequel, since finding the optimal  $d$  is computationally too costly.

In the case of frequency-selective fading, where more than one path for each transmitted pulse is present at the receiver,  $d_\ell$ 's are found separately by using the channel gains and also those of the other users that contribute to the MAI. Setting  $\mu = \alpha_{0,\ell} \sqrt{E_p}$  and calculating the variance terms  $\sigma_n^2$  and  $\sigma_i^2$ , where  $\sigma_{\eta,\ell}^2$  replaces  $\sigma_{\eta,0}^2$ , the parameters in (5.13)-(5.16), as well as  $m_i$  and  $v_i^2$ , are determined. Finally, minimizing the probability of error in (5.19) thus obtained gives the  $d_\ell$ 's we are looking for. The outputs of the rake fingers, whether trimmed using  $d_\ell$  or not, are combined via MRC. For the linear receiver, the decision statistic is the one in (5.5) with  $w_{j,\ell} = \alpha_{0,\ell}$ . The decision rule of the robust rake receiver is as follows:

$$\text{decide} \begin{cases} \text{"0"} & \text{if } \sum_{j=0}^{N_s-1} \sum_{\ell=0}^{L-1} \alpha_{0,\ell} z(x_{j,\ell}) > 0, \\ \text{"1"} & \text{if } \sum_{j=0}^{N_s-1} \sum_{\ell=0}^{L-1} \alpha_{0,\ell} z(x_{j,\ell}) \leq 0. \end{cases} \quad (5.22)$$

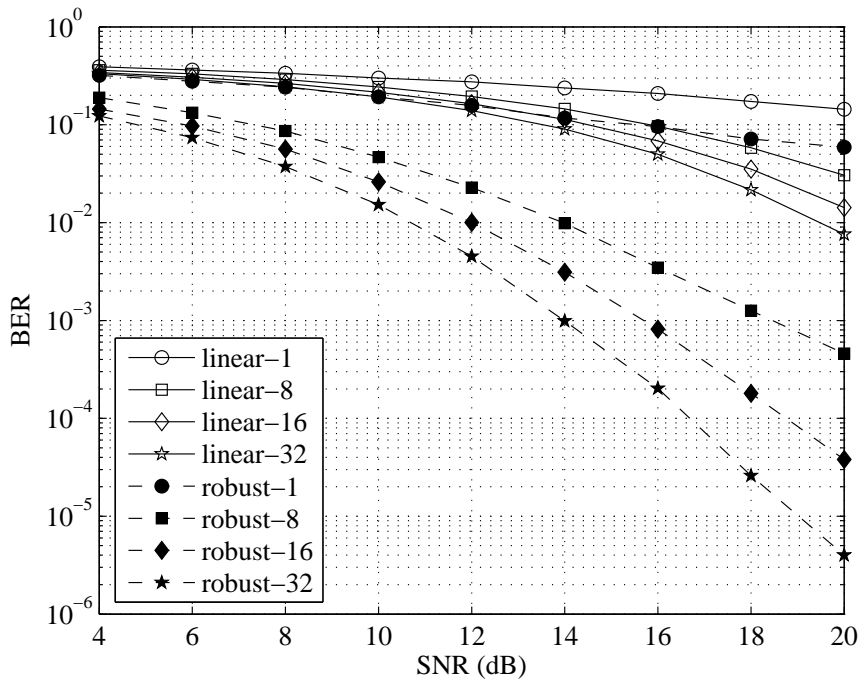


Figure 5.6. BER for robust and linear receivers for varying  $\tilde{L}$  and  $E_b/N_0$  when  $\kappa = 100$ ,  $\epsilon = 0.1$  and  $K_r = 20$

### 5.3. Simulation Results

The performances of the robust and linear rake receivers with MRC are compared for a UWB system in the extreme NLOS frequency-selective channel, CM4, of [18], whose noise process contains impulsive components. For the simulations all users are assumed to be heard with equal power.

In the section, the system parameters are set such that  $R_b = 1$  Mbps,  $T_f = 100$  ns and  $T_p = 1$  ns so that  $N_s = 10$  and  $N_h = 50$ . The channel gains are normalized:  $\sum_{\ell=0}^{L_k-1} \alpha_{k,\ell}^2 = 1, \forall k$ . The effect of increasing  $\tilde{L}$ , the number of fingers for the selective rake receiver, is investigated as the SNR varies from 4 to 20 dB when  $K_r = 20$ . The noise distribution is characterized by  $\kappa = 100$  and  $\epsilon = 0.1$ . Figure 5.6 shows that increasing  $\tilde{L}$  improves the performance of the linear receiver less compared to the robust receiver. With more fingers, it is more likely that noise impulses are included in the sum (5.5). Because no measures are taken against the impulsive noise, the effect of having more fingers is observed as a limited amount of improvement in the low-

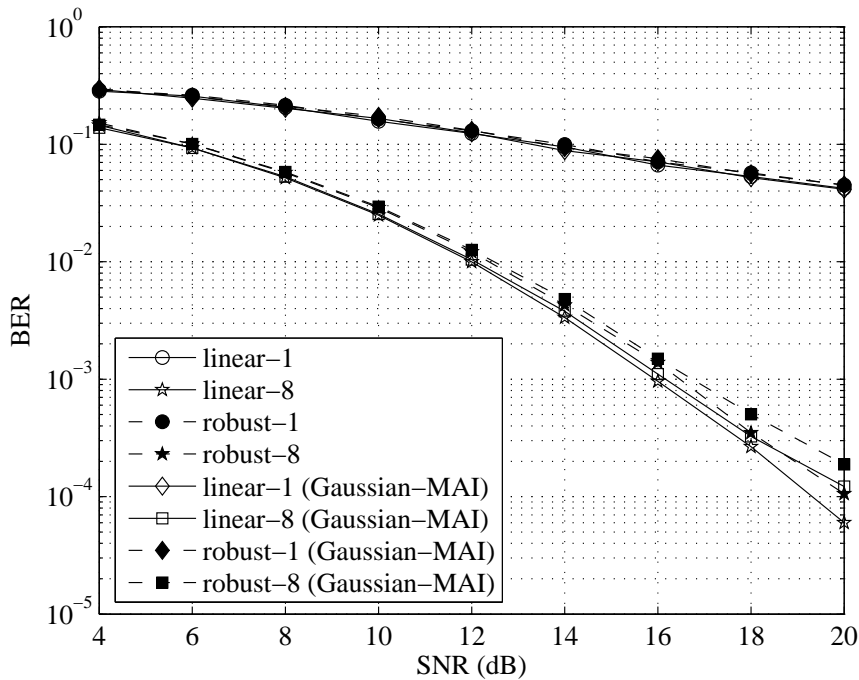


Figure 5.7. BER for robust and linear receivers for varying  $\tilde{L}$  and  $E_b/N_0$  when  $\kappa = 1$  (Gaussian noise) and  $K_r = 20$

to-medium SNR range. The trimming employed by the robust receiver eliminates the effect of the impulsive noise so that the BER can still be decreased as more fingers are used. In fact, the robust UWB system with  $\tilde{L} = 8$  outperforms the linear rake receiver with  $\tilde{L} = 32$  substantially. When  $\tilde{L} = 32$ , the robust receiver is able to outperform the linear receiver by almost an order of magnitude at 10 dB SNR. However, when SNR is increased further, an irreducible error floor due to the equal-power interfering users appears, the onset of which is delayed as  $\tilde{L}$  increases. If the noise process is Gaussian (i.e.,  $\kappa = 1$ ), on the other hand, the BER curve of the robust receiver designed for  $\kappa = 100$  is able to follow the BER curve of the linear receiver, which is optimal when  $\kappa = 1$ , quite closely as shown in Figure 5.7. In this figure, the simulation results of the experiment that confirms the validity of the Gaussian approximation for MAI in Section 5.2 are included as well. For the experiment, white Gaussian noise with variance  $\sigma_{\eta,\ell}^2$  is added to each received path with no interfering users. Thus,  $K_r = 20$  is large enough to assume that the MAI is Gaussian.

The effect of increasing  $K_r$  on the performance of the two types of receivers is

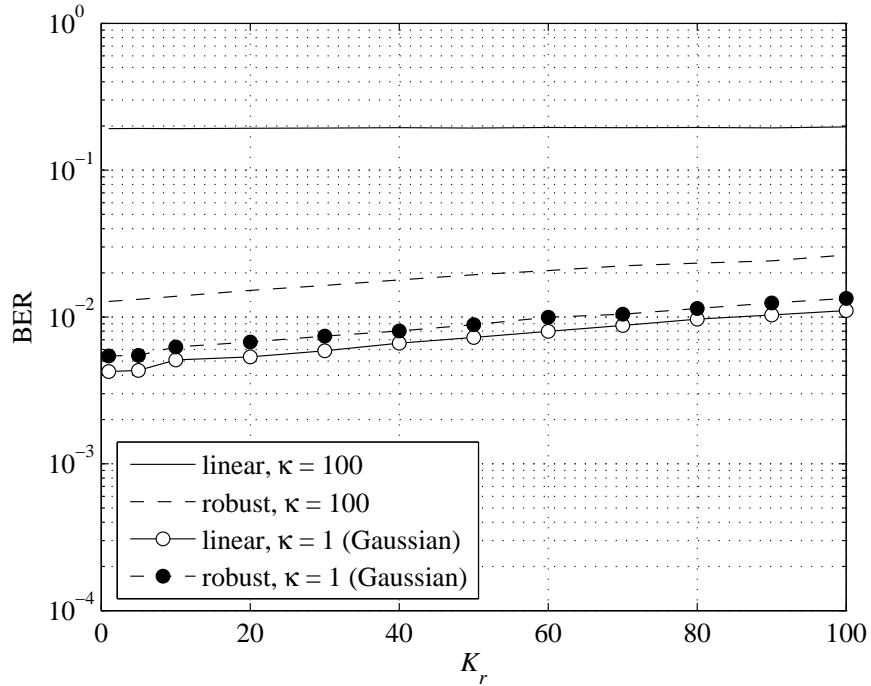


Figure 5.8. BER for robust and linear receivers for increasing  $K_r$  when  $\kappa = 100$  or  $\kappa = 1$  (Gaussian noise),  $\epsilon = 0.1$ , SNR = 10 dB and  $\tilde{L} = 32$

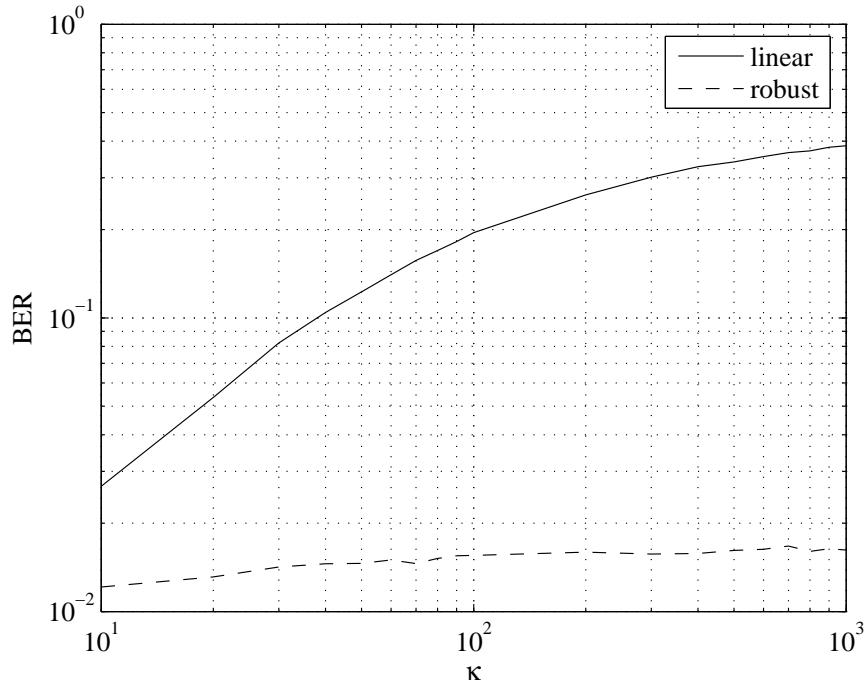


Figure 5.9. BER for robust and linear receivers for increasing  $\kappa$  when  $\epsilon = 0.1$ , SNR = 10 dB,  $K_r = 20$  and  $\tilde{L} = 32$

seen in Figure 5.8, where  $E_b/N_0 = 10$  dB and  $\tilde{L} = 32$ . The noise pdf has  $\kappa = 100$  and  $\epsilon = 0.1$ . The performance of the linear receiver is not affected by the increase in  $K_r$  from 1 to 100 because of the fact that the performance limiting factor for the linear receiver is the impulsive noise and not the MAI. In contrast, as  $K_r$  increases, a performance deterioration is observed for the robust receiver, which is essentially designed to combat the impulsive noise. The increase in  $K_r$  raises the MAI level, which cannot be eliminated by the robust structure with MRC. Eventually, MAI dominates impulsive noise when  $K_r$  is large enough, and the noise floor rises. The BER curve for the robust receiver in impulsive noise with  $\kappa = 100$  is a degraded version of that of the linear receiver in Gaussian noise as demonstrated by Figure 5.8.

When  $\tilde{L}$ ,  $K_r$  and SNR are fixed, and the  $\kappa$  parameter is increased from 10 to 1000 for  $\epsilon = 0.1$ , the performance of the linear receiver diverges from that of the robust receiver for increasing  $\kappa$  as demonstrated in Figure 5.9. The robust receiver exhibits a BER that is essentially independent of the intensity ( $\kappa$ ) of the impulsive noise process.

## 6. MULTIUSER DETECTION FOR IMPULSE RADIO IN NON-GAUSSIAN CHANNELS

In the context of impulse radio-based communication systems, rake receivers and single-user detection may be preferable for asynchronous multiuser transmissions with power control, since the signal energy from undesired users is, on the average, low owing to the autocorrelation properties of UWB pulses. On the other hand, synchronization enables employment of multiuser detection, which prevents the error floor observed with single-user reception at high SNR values and large number of users. Previously, a robust rake receiver that clips the large amplitudes created by the impulsive noise is proposed for asynchronous multiuser impulse radio UWB systems and its performance is optimized by assuming that the MAI is Gaussian.

In this chapter, the  $M$ -estimation technique found in robust statistics is used to develop the robust multipath-combining decorrelating ( $mD$ ) detector for impulse radio, whose performance is immune to deviations of noise from Gaussian to impulsive.  $M$ -estimate based multiuser detection is applied to DS-CDMA and frequency-selective channels in [64] for simultaneous elimination of the structured MAI and impulsive noise, where frequency-selectivity implies only a few Rayleigh fading paths with unknown gains. The decorrelating multipath-combining ( $dM$ ) detector in [64] applies equal-gain combining (EGC) for differential detection of differential phase shift keying (DPSK) signals and decorrelates the received paths before multipath combining. While the decorrelator removes MAI completely, it emphasizes receiver noise and the decorrelation loss increases with the number of users. The number of significant paths, with the enlargement of which the effective number of users for the decorrelation stage of the  $dM$  detector is enhanced, is usually on the order of a hundred with NLOS indoor UWB channels. To circumvent the noise boosting problem for such extremely frequency-selective channels, multipath-combining, which reduces the effective number of users to the actual number of transmitting users, has to precede decorrelation. By exploiting this specific characteristic of the UWB channel the robust multiuser detector

structure suggested for impulse radio here (the  $mD$  detector) happens to be unique and unambiguously distinct from those considered in the previous works on CDMA.

For completeness of the analysis the effects of the availability and the accuracy of the channel information on the performance of the  $mD$  detector are studied by means of simulations. Simulation results indicate that the performance degradation associated with the inaccuracy or the incompleteness of channel information is negligible compared to the gain afforded by the robust design. Moreover, impulsive noise is demonstrated to be beneficial to the performance of the robust detector revealing the well-known least favorability of the Gaussian channel [65]. Whereas in the absence of fading, non-Gaussian noise is shown in [65] to be detrimental to the performance of conventional CDMA systems designed to combat Gaussian noise, the current work indicates that the time spreading of impulse radio signals over a large number of paths as induced by the UWB channel renders the linear system performance invariant to the shape of the noise distribution.

Another contribution of this thesis is the establishment of effective channel impulse response lengths for the users detected with the  $dM$  structure, which serves to optimize its performance whenever sufficiently accurate channel information available. In particular, for this detector there is an optimal number of paths that maximizes the gain in combined signal energy over the loss in decorrelation due to noise emphasis. The optimal number of paths specified in terms of the percentage of channel energy captured is determined to depend on the SNR, where with larger SNR the optimal number of decorrelated paths increases.

The rest of the chapter is organized as follows. In Section 6.1, the UWB system model for multiuser detection is presented. The derivation of  $M$ -estimation based multiuser detector structures for frequency-selective UWB channels with impulsive noise is covered in Section 6.2. Simulation results are given in Section 6.3, where the robust multiuser detector structures are compared to the robust rake structure introduced in the previous chapter, as well.

### 6.1. UWB System Model

In this chapter, multiuser detection of  $K$  users, which employ TH for multiple access and BPSK for data modulation, is considered. The signal transmitted by the  $k$ th user is

$$s_{\text{tr}}^{(k)}(t) = \sum_{j=-\infty}^{\infty} b_{\lfloor j/N_s \rfloor}^{(k)} w_{\text{tr}}(t - jT_f - c_j^{(k)}T_c), \quad (6.1)$$

where each pulse is sent during a frame of  $T_f$  seconds and the exact pulse position is determined only by the TH sequence  $\{c_j^{(k)}\}_{j=-\infty}^{\infty}$  specific to user  $k$  with  $c_j^{(k)} \in \{0, 1, \dots, N_h - 1\}$  chosen randomly. Typically, we have  $N_h T_c \leq T_f$  and  $T_c = T_p$ . For each bit,  $b_i^{(k)}$ ,  $N_s$  pulses are allocated so that a kind of repetition coding is obtained. This, in addition, determines the bit rate,  $R_b = 1/(N_s T_f)$ .

The signal transmitted by each user goes through a frequency-selective UWB channel. The signal from the  $k$ th user, which propagates over the channel

$$h_k(t) = \sum_{\ell=0}^{L_k-1} \alpha_{k,\ell} \delta_D(t - \tau_{k,\ell}) \quad (6.2)$$

is received as

$$s_{\text{rec}}^{(k)}(t) = A_k \sum_{j=-\infty}^{\infty} b_{\lfloor j/N_s \rfloor}^{(k)} \sum_{\ell=0}^{L_k-1} \alpha_{k,\ell} w_{\text{rec}}(t - jT_f - c_j^{(k)}T_c - \tau_{k,\ell}), \quad (6.3)$$

where  $A_k > 0$  is the signal amplitude. The total received signal

$$r(t) = \sum_{k=1}^K s_{\text{rec}}^{(k)}(t) + n(t), \quad (6.4)$$

where  $n(t)$  is the additive noise component, is passed through a linear filter matched to the received pulse,  $w_{\text{rec}}(t)$ , and the output of this filter is sampled every  $T_c$  seconds [66]. A guard time exists between information symbols equal to the length of the channel impulse response so that ISI is avoided [37]. The vector of samples for the  $i$ th bit,  $\mathbf{r}[i]$ ,

is of length  $N_s N_h + L_{\max} - 1$ , where  $L_{\max} = \max_k L_k$ , and its discrete-time model is

$$\mathbf{r}[i] = \bar{\mathbf{S}}[i] \mathbf{H}_K \mathbf{A}_K \mathbf{b}[i] + \mathbf{n}[i], \quad (6.5)$$

where  $\mathbf{H}_K = \text{diag}\{\mathbf{h}_1, \dots, \mathbf{h}_K\}$  is a  $\sum_{k=1}^K L_k \times K$  block diagonal matrix with elements  $\mathbf{h}_k = [\alpha_{k,0} \ \dots \ \alpha_{k,L_k-1}]^T$ , the vector containing the path gains of the  $k$ th user,  $\mathbf{A}_K = \text{diag}\{A_1, \dots, A_K\}$ ,  $\mathbf{b}[i] = [b_i^{(1)} \ \dots \ b_i^{(K)}]^T$  and  $\mathbf{n}[i]$  is the vector of noise samples. The matrix  $\bar{\mathbf{S}}[i] = [\mathbf{S}_1[i] \ \dots \ \mathbf{S}_K[i]]$  in (6.5) gives information about the TH sequences of the users for the  $i$ th bit, where  $\mathbf{S}_k[i]$  is an  $(N_s N_h + L_{\max} - 1) \times L_k$  matrix

$$\mathbf{S}_k[i] = \begin{bmatrix} s_{k,0}^i & 0 & 0 & \dots & 0 \\ s_{k,1}^i & s_{k,0}^i & 0 & \dots & 0 \\ \vdots & & \ddots & \ddots & \vdots \\ s_{k,N_s N_h - 1}^i & & & & \\ 0 & & & \ddots & 0 \\ \vdots & & & \ddots & s_{k,0}^i \\ & & & & s_{k,1}^i \\ & & & \ddots & \vdots \\ 0 & \dots & & 0 & s_{k,N_s N_h - 1}^i \\ 0 & \dots & & & 0 \\ \vdots & & & & \vdots \\ 0 & \dots & & & 0 \end{bmatrix}, \quad (6.6)$$

whose  $L_k$ th column is

$$\left[ \underbrace{0 \ \dots \ 0}_{L_k - 1} \ s_{k,0}^i \ s_{k,1}^i \ \dots \ s_{k,N_s N_h - 1}^i \ \underbrace{0 \ \dots \ 0}_{L_{\max} - L_k} \right]^T \quad (6.7)$$

and  $s_{k,\ell}^i$  computed as [66]

$$s_{k,\ell}^i = \begin{cases} 1, & \text{if } c_{(i-1)N_s + \lfloor \ell/N_h \rfloor}^{(k)} = \ell - \lfloor \frac{\ell}{N_h} \rfloor N_h, \\ 0, & \text{otherwise} \end{cases} \quad (6.8)$$

form the TH spreading vector  $\mathbf{s}_k[i] = [s_{k,0}^i \cdots s_{k,N_s N_h - 1}^i]^T$ .

Since  $\mathbf{r}[i]$  is obtained from  $r(t)$  by using a linear filter matched to  $w_{\text{rec}}(t)$ , unless the received signals from the transmitting users,  $s_{\text{rec}}^{(k)}(t)$ , are chip-synchronous with the receiver, the collected signal energy from some of the users may be insufficient for detection. This observation is especially valid for UWB systems using the second derivative Gaussian pulse in (3.4) which has very low autocorrelation values at nonzero lags. Specifically, representing the asynchronism between the receiver and the  $k$ th transmitter with  $\tau_k$ , the received path with the gain  $\alpha_{k,\ell}$  will be distributed between two samples of the discrete-time received signal as  $\alpha_{k,\ell} R_w(\tau_k^c)$  and  $\alpha_{k,\ell} R_w(T_c - \tau_k^c)$ , where  $\tau_k^c \in [0, T_c)$  is the part of  $\tau_k$  that lies within a chip interval. Thus, as in [67], to take advantage of multiuser detection techniques, the asynchronism between the receiver and the users, if it exists, should be limited to only a few integral multiples of the chip duration (i.e.,  $T_c, 2T_c$ , etc.), the effect of which may be incorporated into the received signal model by adjusting  $L_{\text{max}}$ .

Denoted by  $n_{i,l}$  for  $l = \{0, \dots, N_s N_h + L_{\text{max}} - 1\}$ , the elements of  $\mathbf{n}[i]$  are assumed to be i.i.d. random variables so that the impulsive noise source can be studied by modeling its first order pdf as in [59] and the robust rake receiver case. Being simple, the independent noise samples assumption upper bounds the error performance of the receiver, for if properly modeled, the correlation between the noise samples can be exploited to improve the detector design and obtain a more complex structure than the one considered in this chapter which probably yields a better performance [68].

The assumed pdf for the noise samples,  $f_{n_{i,l}} \forall l$ , is a mixture of two Gaussians with zero means and different variances, where the one that has the larger variance represents the interference producing large amplitudes:

$$f_{n_{i,l}} = (1 - \epsilon)\mathcal{N}(0, N_0/2) + \epsilon\mathcal{N}(0, \kappa N_0/2). \quad (6.9)$$

Notice that the  $\epsilon$ -mixture model in (6.9) has been used previously to derive the pdf of the noise samples at the output of the rake fingers given in (5.7).

## 6.2. Robust Multiuser Detector Structures for Frequency-Selective Channels

In this section, multiuser detection techniques for TH-BPSK impulse radio and non-Gaussian frequency-selective channels are presented. The objective of multiuser detection is to detect the user bits in (6.5), which are the elements of  $\mathbf{b}[i]$ , simultaneously by making use of the received signal structure. Initially a simple linear multiuser detector, the standard linear decorrelator for the AWGN channel, is introduced below from which the more complex  $M$ -estimation based robust multiuser detectors for frequency-selective channels are developed.

For unknown signal amplitudes,  $A_k$ , and the AWGN channel, the discrete-time received signal,  $\mathbf{r}_A[i]$ , can be written as

$$\mathbf{r}_A[i] = \bar{\mathbf{S}}[i] \mathbf{A}_K \mathbf{b}[i] + \mathbf{n}[i], \quad (6.10)$$

since  $\mathbf{H}_K$  is a  $K \times K$  identity matrix when there is no fading. The transmitted bits can be recovered error-free in the absence of noise through

$$\hat{b}_i^{(k)} = \left( \text{sgn} \left\{ (\bar{\mathbf{S}}[i]^T \bar{\mathbf{S}}[i])^{-1} \bar{\mathbf{S}}[i]^T \mathbf{r}_A[i] \right\} \right)_k, \quad (6.11)$$

where  $(\cdot)_k$  denotes the  $k$ th element, and the  $(\bar{\mathbf{S}}[i]^T \bar{\mathbf{S}}[i])^{-1}$  decorrelates users and removes MAI completely [69]. Meanwhile, for the realistic noisy case the noise covariance matrix is scaled by  $(\bar{\mathbf{S}}[i]^T \bar{\mathbf{S}}[i])^{-1}$ , which implies larger noise sample variances unless the TH sequences are orthogonal. The detector that performs (6.11) is the standard linear decorrelator and it also achieves the ML solution to the estimation of  $\mathbf{A}_K \mathbf{b}[i]$  from (6.10) when there are no prior distributions available for  $A_k$  and  $b_i^{(k)} \forall k$  [70]. Moreover, the linear decorrelator output is identical in form to the vector  $\mathbf{x}$ , which is the estimate of  $\mathbf{A}_K \mathbf{b}[i]$  that achieves the solution to the least-squares (LS) problem [70]

$$\min_{\mathbf{x} \in \mathcal{R}^K} \|\bar{\mathbf{S}}[i] \mathbf{x} - \mathbf{r}_A[i]\|, \quad (6.12)$$

where  $\|\cdot\|$  denotes the  $\mathcal{L}_2$  norm and  $\mathcal{R}^K$  is the set of  $K$ -dimensional real vectors. Thus the linear decorrelator is optimal in the AWGN channel according to the ML and the LS criteria.

As the measurement results have shown that the indoor environments, where most UWB devices are envisioned to be deployed are subject to impulsive noise, the AWGN assumption which causes the LS solution described above to be optimal is not valid for indoor UWB communications. Furthermore, the fact that the performance and the optimality of the LS solution depend strictly on the Gaussian noise assumption and the high computational complexity of the ML solution to the estimation of  $\mathbf{A}_K \mathbf{b}[i]$  from (6.10) with non-Gaussian  $\mathbf{n}[i]$  both make the search for other estimation methods necessary. The most favored estimation method to address the impulsive noise case is the robust version of the LS solution found in robust statistics. Particularly, in [63] the LS solution is robustified with respect to deviations from Gaussianity of the elements of  $\mathbf{n}[i]$  by using  $M$ -estimation, which has led to the robust LS solution for  $\epsilon$ -contaminated Gaussian models that also include the  $\epsilon$ -mixture model in (6.9).

The equivalence between the LS solution and the linear decorrelator output is exploited in [65] to obtain the robust decorrelator for impulsive CDMA channels. The idea of robust decorrelation is extended to noncoherent demodulation of DPSK signals transmitted via flat-fading CDMA channels with unknown gains and embedded in impulsive noise [71]. The robust multiuser detector in [64] designed for frequency-selective CDMA channels with only a few paths does not require channel estimation because multiple paths of DPSK signals are decorrelated and the paths arising from the same user in two adjacent bit intervals are subsequently differentially equal-gain combined.

One of the objectives of this work is to demonstrate that when extreme frequency-selectivity comes into play for robust decorrelation of UWB BPSK signals, two distinct routes can be taken by applying multipath combining and decorrelation stages in any order. It is shown next that different choices for the unknown parameters of the linear regression model constructed from (6.5) lead to two distinct robust detectors, one of

which is related to the design in [64].

### 6.2.1. The Multipath-Combining Decorrelating ( $mD$ ) Detector

By defining  $\theta_k \triangleq A_k b_i^{(k)}$ , the matrix  $\mathbf{A}_K$  and the vector  $\mathbf{b}[i]$  in (6.5) are replaced by a single vector  $\boldsymbol{\Theta} = [\theta_1 \cdots \theta_K]^T$  of unknown parameters. Information about the TH codes and path gains are represented with a single matrix  $\mathbf{S}_c = \bar{\mathbf{S}}[i]\mathbf{H}_K$ . The  $k$ th column of  $\mathbf{S}_c$  is the multipath spreading vector of the  $k$ th user,  $\mathbf{S}_k[i]\mathbf{h}_k$ , which is  $\mathbf{s}_k[i]$  convolved with the channel impulse response,  $\mathbf{h}_k$ . Thus, the received signal model is the linear regression model

$$\mathbf{r}[i] = \mathbf{S}_c \boldsymbol{\Theta} + \mathbf{n}[i]. \quad (6.13)$$

The LS solution

$$\hat{\boldsymbol{\Theta}} = \arg \min_{\boldsymbol{\Theta} \in \mathcal{R}^K} \|\mathbf{r}[i] - \mathbf{S}_c \boldsymbol{\Theta}\| \quad (6.14)$$

is the same as the linear decorrelator output:

$$\hat{\boldsymbol{\Theta}} = (\mathbf{S}_c^T \mathbf{S}_c)^{-1} \mathbf{S}_c^T \mathbf{r}[i]. \quad (6.15)$$

This decorrelator, which we term the  $mD$  detector as a result of its similarity to the one in [72] proposed for DPSK signals and CDMA systems, has optimum near-far resistance properties if the path gains and TH codes of the users are known perfectly. The  $mD$  detector contains a bank of filters matched to the multipath signals, which is followed by a decorrelator. Each matched filter is a rake receiver with conventional MRC. Hence, the detector performs separate multipath combining for each user before decorrelating the signals from different users. The bit decision rule for the  $mD$  detector is given by

$$\hat{b}_i^{(k)} = \left( \text{sgn} \left\{ \hat{\boldsymbol{\Theta}} \right\} \right)_k. \quad (6.16)$$

### 6.2.2. The Decorrelating Multipath-Combining (*dM*) Detector

Because each column of  $\bar{\mathbf{S}}[i]$  may be viewed as the spreading vector of one of the received paths, the  $\sum_{k=1}^K L_k$  paths from  $K$  users are decorrelated by performing

$$\mathbf{y}[i] = (\bar{\mathbf{S}}[i]^T \bar{\mathbf{S}}[i])^{-1} \bar{\mathbf{S}}[i] \mathbf{r}[i] \quad (6.17)$$

$$= \mathbf{H}_K \mathbf{A}_K \mathbf{b}[i] + (\bar{\mathbf{S}}[i]^T \bar{\mathbf{S}}[i])^{-1} \bar{\mathbf{S}}[i] \mathbf{n}[i]. \quad (6.18)$$

This time only the TH sequences are utilized at the decorrelation stage through which the vector  $\mathbf{H}_K \mathbf{A}_K \mathbf{b}[i]$  is estimated. As  $\mathbf{y}[i]$  contains the vector

$$\mathbf{H}_K \mathbf{A}_K \mathbf{b}[i] = [\alpha_{1,0} \theta_1 \cdots \alpha_{1,L_1-1} \theta_1 \cdots \alpha_{K,0} \theta_K \cdots \alpha_{K,L_K-1} \theta_K]^T \quad (6.19)$$

embedded in noise, we proceed with maximal ratio combining of paths, for which  $\mathbf{H}_K$  is the matrix of weighting coefficients. The  $k$ th bit detected with the described *dM* structure is

$$\hat{b}_i^{(k)} = (\text{sgn} \{ \mathbf{H}_K^T \mathbf{y}[i] \})_k, \quad (6.20)$$

where in fact the sign of  $\sum_{\ell=0}^{L_k-1} \alpha_{k,\ell}^2 \theta_k$  albeit corrupted with additive noise is determined. On the other hand, the decorrelator outputs  $\mathbf{y}[i]$  can be combined so as to maximize the SNR, which also optimizes the BER performance for each user under the Gaussian noise assumption. The decision rule that maximizes the SNR for the  $k$ th user is

$$\hat{b}_i^{(k)} = \left( \text{sgn} \left\{ \mathbf{h}_k^T (\bar{\mathbf{S}}[i]^T \bar{\mathbf{S}}[i])_{\sum_{k'=1}^{k-1} L_{k'}+1: \sum_{k'=1}^k L_{k'}, \sum_{k'=1}^{k-1} L_{k'}+1: \sum_{k'=1}^k L_{k'}} \right. \right. \\ \left. \left. \times (\mathbf{y}[i])_{\sum_{k'=1}^{k-1} L_{k'}+1: \sum_{k'=1}^k L_{k'}} \right\} \right)_k \quad (6.21)$$

where  $(\mathbf{X})_{i:j,m:n}$  is a matrix containing those elements of the matrix  $\mathbf{X}$  in rows  $i$  through  $j$  and columns  $m$  through  $n$ . The combining rule in (6.21) is based on the well-known idea of matched filtering of known signals in additive noise. The signal corrupted by

an additive noise process

$$\mathbf{r} = \mathbf{s} + \mathbf{n}, \quad (6.22)$$

where  $\mathbf{s}$  is the signal and  $\mathbf{n}$  is the noise process with covariance matrix  $\mathbf{R}_n$ , is estimated by the filter matched to  $\mathbf{s}$ , which is  $\mathbf{R}_n^{-1}\mathbf{s}$ :

$$\hat{\mathbf{s}} = \mathbf{s}^T \mathbf{R}_n^{-1} \mathbf{r}. \quad (6.23)$$

The overall SNR, on the other hand, is maximized by the filter matched to  $\mathbf{y}[i]$ ,  $\bar{\mathbf{S}}[i]^T \bar{\mathbf{S}}[i] \mathbf{H}_K$ , which coincides with rake reception:  $\mathbf{S}_c^T \mathbf{r}[i]$ .

The  $dM$  detector above is proposed for BPSK signals. If, on the other hand, no channel information is available at the receiver, DPSK signaling should be preferred. Then, the bit decisions are made according to

$$\hat{b}_i^{(k)} = \text{sgn} \left\{ \sum_{l=\sum_{k'=1}^{k-1} L_{k'}+1}^{\sum_{k'=1}^k L_{k'}} (\mathbf{y}[i-1])_l (\mathbf{y}[i])_l \right\}. \quad (6.24)$$

Here, the decorrelator output of the previous bit,  $\mathbf{y}[i-1]$ , serves as the noisy channel estimate for the detection of the current bit. The  $dM$  detector proposed for DPSK signals and robustified in [64] corresponds to (6.24). For a better comparison with the  $mD$  detector, the detector structure equivalent to the detection rule in (6.20) is considered in the simulation results section.

### 6.2.3. $M$ -Estimation and Robust Decorrelation

Robust versions of the linear  $mD$  and  $dM$  detectors are obtained by robustifying decorrelation parts of both detectors, for which the robust LS solution in [63] is employed. Instead of minimizing a sum of squares as in the LS solution, a sum of less rapidly increasing function,  $\rho$ , of the residuals is minimized to obtain the robust  $mD$

detector for impulsive noise channels with

$$\hat{\Theta} = \arg \min_{\Theta \in \mathcal{R}^K} \sum_{n=1}^{N_s N_h + L_{\max} - 1} \rho \left( (\mathbf{r})_n - \sum_{k=1}^K (\mathbf{S}_c)_{nk} \theta_k \right), \quad (6.25)$$

where  $(\cdot)_{nk}$  denotes the element of the matrix argument in the  $n$ th row and  $k$ th column. The declared robustness stems from the fact that when the function  $\rho$  increases less rapidly with its argument, the high amplitude outliers unpredicted by the Gaussian distribution, which were emphasized by squaring, are incorporated into the decision statistic in lesser amounts.

If  $\rho$  is convex and  $\psi$  is the derivative of  $\rho$ ,  $\theta_k$ 's which satisfy

$$\sum_{n=1}^{N_s N_h + L_{\max} - 1} \psi \left( (\mathbf{r})_n - \sum_{k=1}^K (\mathbf{S}_c)_{nk} \theta_k \right) (\mathbf{S}_c)_{np} = 0, \quad p = 1, \dots, K, \quad (6.26)$$

are the  $M$ -estimates of  $\theta_k$ . The function  $\rho = -\log f_{n_i, n}$  for  $n = \{0, \dots, N_s N_h + L_{\max} - 1\}$  leads to the maximum-likelihood ( $M$ ) estimate, which gives this type of estimates their name [63]. The bit decisions are made as in (6.16). Similarly, through finding the elements of  $\mathbf{y}[i]$  for which

$$\sum_{n=1}^{N_s N_h + L_{\max} - 1} \psi \left( (\mathbf{r})_n - \sum_{l=1}^{\sum_{k=1}^K L_k} (\bar{\mathbf{S}}[i](\mathbf{y}[i]))_l \right) (\bar{\mathbf{S}}[i])_{np} = 0, \quad p = 1, \dots, \sum_{k=1}^K L_k, \quad (6.27)$$

holds, the robust decorrelator part of the  $dM$  detector is obtained. The bit decisions in (6.20) are based on this robust estimate of  $\mathbf{y}[i]$ .

The  $M$ -estimates  $\hat{\Theta}$  and  $\hat{\mathbf{y}}[i]$  above are asymptotically normal and unbiased as  $N_s N_h \rightarrow \infty$  [63]. As the covariance matrices for these estimates  $v^2 (\mathbf{S}_c^T \mathbf{S}_c)^{-1}$  and  $v^2 (\bar{\mathbf{S}}[i]^T \bar{\mathbf{S}}[i])^{-1}$  for  $\hat{\Theta}$  in (6.26) and  $\hat{\mathbf{y}}[i]$  in (6.27), respectively, depend on the parameter

$$v^2 \triangleq \frac{\int \psi^2(x) f(x) dx}{(\int \psi'(x) f(x) dx)^2}, \quad (6.28)$$

the function  $\rho(x)$  and its derivative  $\psi(x)$  affect the performances of the  $mD$  and  $dM$  detectors through  $v^2$ . The asymptotic probability of error of the  $mD$  detector for the  $i$ th bit of the  $k$ th user with equiprobably transmitted bits is

$$P_{e,mD} = \Pr \left\{ \hat{\theta}_k < 0 \mid \{c_j^1, \dots, c_j^K\}_{j=iN_s}^{(i+1)N_s-1}, \mathbf{h}_1, \dots, \mathbf{h}_K \text{ and "1" is sent} \right\} \quad (6.29)$$

$$= \Phi \left( -\frac{A_k}{v \sqrt{\left( (\mathbf{S}_c^T \mathbf{S}_c)^{-1} \right)_{kk}}} \right). \quad (6.30)$$

The effect of the robust nonlinearity,  $\psi(x)$ , on the performance of the  $dM$  detector is similar although the  $M$ -estimate,  $\hat{\mathbf{y}}[i]$ , is maximal ratio combined before bit decision making. The asymptotic error probability of the  $dM$  detector for the  $k$ th user is

$$P_{e,dM} = \Phi \left( -\frac{A_k \sum_{\ell=0}^{L_k-1} \alpha_{k,\ell}^2}{v \sqrt{\left( \mathbf{H}_K^T (\bar{\mathbf{S}}[i]^T \bar{\mathbf{S}}[i])^{-1} \mathbf{H}_K \right)_{kk}}} \right). \quad (6.31)$$

For a fixed total noise variance,  $\sigma_T^2 = ((1 - \epsilon) + \epsilon\kappa)N_0/2$ , the asymptotic performances of the linear  $mD$  and  $dM$  detectors in (6.30) and (6.31), respectively, with  $\rho(x) = x^2$  and  $v^2 = \sigma_T^2$  are invariant to the changes in  $\kappa$  and  $\epsilon$  parameters of the  $\epsilon$ -mixture noise model pdf [65]. The advantage of  $M$ -estimation is the ability to reduce the effective noise variance at the output of the detectors by manipulating the parameter  $v^2$ . While the ML estimator minimizes  $v^2$  for a specified noise pdf, the function by Huber,  $\rho_H(x)$ , minimizes the maximal asymptotic variance of the estimator over the set of  $\epsilon$ -contaminated Gaussian models with arbitrary contamination pdf [65]. The derivative of  $\rho_H(x)$  is given by [63]

$$\psi_H(x) = \frac{\partial \rho_H(x)}{\partial x} = \begin{cases} -k_h & x < -k_h \sigma^2, \\ \frac{x}{\sigma^2} & -k_h \sigma^2 \leq x \leq k_h \sigma^2, \\ k_h & x > k_h \sigma^2. \end{cases} \quad (6.32)$$

The trimming parameter in  $\psi_H(x)$ ,  $k_h$ , is obtained through the equality it satisfies:

$\phi(k_h\sigma)/k_h\sigma - \Phi(-k_h/\sigma) = \epsilon/2(1 - \epsilon)$ .  $M$ -estimates in (6.26) and (6.27) are both computed with the modified residuals method in [63].

#### 6.2.4. Channel Information

In analogy with practical rake receivers, which employ a limited number of multipath components, the scenarios that differ from the ideal case of perfect knowledge of all of the channel impulse responses are investigated as well. The high temporal resolution of UWB multipath components at the receiver enables the modeling of each fading component with a log-normal distribution, which dictates less amplitude fluctuations in comparison to Rayleigh fading commonly adopted for narrowband systems [18]. Log-normal distribution of multipath components and exponential power decay profile of the channel impulse response designate that the first arriving paths should contain more energy on the average [73]. Thus, it suffices to estimate the initial few arrivals for constructing receivers with low complexity. On the other hand, if the number of multipath components for combining is to be restricted, it is best to use the whole channel impulse response to select the paths carrying most of the energy. Based on the type of the channel information used, the aforementioned receivers are called partial and selective, respectively.

If the entire channel information is not used for  $mD$  detection due to such practical reasons as those listed above, additional interference from the other users will impose on the single-user bit decisions. Let  $\hat{\mathbf{S}}_c$  denote the estimate of  $\mathbf{S}_c$ , where partial or selected channel information is used. The decorrelator output for  $mD$  detection with  $\hat{\mathbf{S}}_c$  is

$$\hat{\boldsymbol{\Theta}} = \left(\hat{\mathbf{S}}_c^T \hat{\mathbf{S}}_c\right)^{-1} \hat{\mathbf{S}}_c^T \mathbf{S}_c \boldsymbol{\Theta} + \left(\hat{\mathbf{S}}_c^T \hat{\mathbf{S}}_c\right)^{-1} \hat{\mathbf{S}}_c^T \mathbf{n}. \quad (6.33)$$

Through (6.33), it is observed that the impact of the MAI on the estimates  $\hat{\theta}_k$  becomes more severe as the degree of mismatch between  $\mathbf{S}_c$  and  $\hat{\mathbf{S}}_c$  increases. Decomposing  $\mathbf{S}_c$  as  $\mathbf{S}_c = \hat{\mathbf{S}}_c + \mathbf{S}_c^e$ , the asymptotic error probability of the  $k$ th user equipped with the

$mD$  detector becomes:

$$P_{e,mD} = \Phi \left( -\frac{A_k + \left( \left( \hat{\mathbf{S}}_c^T \hat{\mathbf{S}}_c \right)^{-1} \hat{\mathbf{S}}_c^T \mathbf{S}_c^e \boldsymbol{\Theta} \right)_k}{v \sqrt{\left( \left( \hat{\mathbf{S}}_c^T \hat{\mathbf{S}}_c \right)^{-1} \right)_{kk}}} \right), \quad (6.34)$$

where the second term in the numerator is the residual MAI created by the lower energy paths, which is another source of performance degradation for the  $mD$  detector constructed with incomplete channel information.

Imperfect channel information from the channel estimator degrades the detector performance further by lowering the received SNR: While high energy paths are suppressed, noise energy is accumulated. A simple channel estimator is considered for the analysis of the sensitivity of the detector to channel estimation errors. The data-aided correlator type estimate for the  $\ell$ th path of the  $k$ th user is given by

$$\hat{\alpha}_{k,\ell} = \frac{1}{N_t N_s} \sum_{j=0}^{N_t N_s - 1} \int_{\tau_{k,\ell}}^{\tau_{k,\ell} + T_p} r(t + jT_f + c_j^{(k)} T_c) w_{\text{rec}}(t - \tau_{k,\ell}) dt, \quad (6.35)$$

where  $N_t$  is the number of training bits. The expected value of  $\hat{\alpha}_{k,\ell}$  is

$$\mathbb{E} \{ \hat{\alpha}_{k,\ell} \} = A'_k \alpha_{k,\ell}. \quad (6.36)$$

Here,  $A'_k = A_k \sqrt{1 - N_t/N_p}$  with  $N_p$  denoting the number of bits in a packet. The transmission of each packet occurs within the coherence time of the UWB channel, which along with the bit rate determines  $N_p$ . The anticipated speed of moving users, 1 m/s, with a maximum frequency of 10 GHz, results in a maximum Doppler frequency of 30 Hz. This, in turn, implies coherence times in the order of 30 ms [74]. Resulting from both the noise and the MAI, the channel estimate in (6.35) has variance  $(\sigma_T^2 + \sigma_{k,\ell}^2) / N_t N_s$  with

$$\sigma_{k,\ell}^2 = \frac{1}{T_f} \sum_{k'=1}^K \sum_{m \in \mathcal{M}_\ell} \alpha_{k',m}^2 (A'_{k'})^2 \int_{-\infty}^{\infty} |R_w(\tau)|^2 d\tau, \quad (6.37)$$

where  $\mathcal{M}_\ell = \{m: m = 0, 1, \dots, L_{k'} - 1, \text{ and } \tau_{k',m} \neq \tau_{k,\ell}\}$ . For (6.37), an independent random delay for each arriving path of each user is assigned, and the IFI and the MAI are assumed to be Gaussian [40]. For synchronous transmissions,

$$\sigma_{k,\ell}^2 = \frac{1}{N_h} \sum_{k'=1}^K \sum_{m \in \mathcal{M}_\ell} \alpha_{k',m}^2 (A'_{k'})^2. \quad (6.38)$$

The mean and the variance are sufficient for a full statistical description of  $\hat{\alpha}_k$  if it is modeled to have the normal distribution as in this work. The error probability expression in (6.34) includes the effect of channel estimation errors as well if channel impulse responses formed with normally distributed  $\hat{\alpha}_{k,\ell}$ , where

$$\hat{\alpha}_{k,\ell} \sim \mathcal{N} (A_{k'} \alpha_{k,\ell}, (\sigma_T^2 + \sigma_{k,\ell}^2) / N_t N_s) \quad (6.39)$$

are used when constructing  $\hat{\mathbf{S}}_{\mathbf{c}}$ .

The  $dM$  detector uses channel information to combine paths effectively and improve the SNR. Since decorrelation is achieved before combination of paths, partial or selective  $dM$  detectors and channel estimation do not result in residual MAI as in the  $mD$  detector. The lowering of the SNR due to channel estimation is the only additional source of performance degradation for the  $dM$  detector. The asymptotic error probability expression for the  $k$ th user, which has incomplete and/or estimated channel information is given by

$$P_{e,dM} = \Phi \left( - \frac{A_k \sum_{\ell=0}^{L_k-1} \hat{\alpha}_{k,\ell} \alpha_{k,\ell}}{v \sqrt{\hat{\mathbf{H}}_K^T (\hat{\mathbf{S}}[i]^T \hat{\mathbf{S}}[i])^{-1} \hat{\mathbf{H}}_K}} \right). \quad (6.40)$$

### 6.3. Simulation Results

In this section, the performance of the  $mD$  detector is examined for such different system parameters as the number of users, transmission rates and channel models. In addition, simulations with incomplete and/or inaccurate channel information are car-

ried out to demonstrate whether the  $mD$  detector maintains its superior performance or not, if channel state is estimated.

For the simulations UWB system has either a low rate (LR) with  $T_f = 100$  ns,  $T_p = 1$  ns,  $R_b = 1$  Mbps or a high rate (HR) determined by  $T_f = 10$  ns,  $T_p = 1$  ns,  $R_b = 10$  Mbps. The impulsive noise is assumed to act in accordance with the  $\epsilon$ -mixture model in (6.9), and unless stated otherwise, the noise model has  $\kappa = 100$  and  $\epsilon = 0.01$ . The effect of the change in the shape of the noise distribution on the receiver performance is investigated by holding  $\sigma_T^2$  constant as  $\kappa$  and  $\epsilon$  vary. The simulated UWB channel models are among the ones considered by the IEEE 802.15.3a task group, which are the CM1 and the CM4 models for the 0-4 m LOS and extreme NLOS situations, respectively. The user channels created for each simulation are statistically equivalent and the coherence time of the channels is 200  $\mu$ s. The expression for the SNR is

$$\text{SNR} = \frac{A_k^2 N_s}{N_0} \text{E} \left\{ \sum_{\ell=0}^{L_k-1} \alpha_{k,\ell}^2 \right\}. \quad (6.41)$$

Typically, the average received power of the multipaths is normalized to unity such that  $\text{SNR} = A_k^2 N_s / N_0$  holds [17].

The detection performance of the  $dM$  detector is substantially affected by the total length of the channel impulse responses of the users, since the estimate  $\hat{\mathbf{y}}[i]$  is obtained by inverting an  $\sum_{k=1}^K L_k \times \sum_{k=1}^K L_k$  matrix. As  $\sum_{k=1}^K L_k$  increases, the decorrelation loss due to the boosting of the receiver noise becomes more severe, but for a given channel impulse response the SNR improves further with larger number of combined paths. These two conflicting outcomes favor an effective channel impulse response length,  $L_e$ , that optimizes performance. Knowledge of the channel impulse response is restricted to those first arriving paths, which contain a certain percentage of the energy of the channel impulse response. Figure 6.1 shows the average BER performance of the  $dM$  detector with MRC at various SNR values in dB against the percentage of energy captured of the channel impulse response for the CM1 channel.

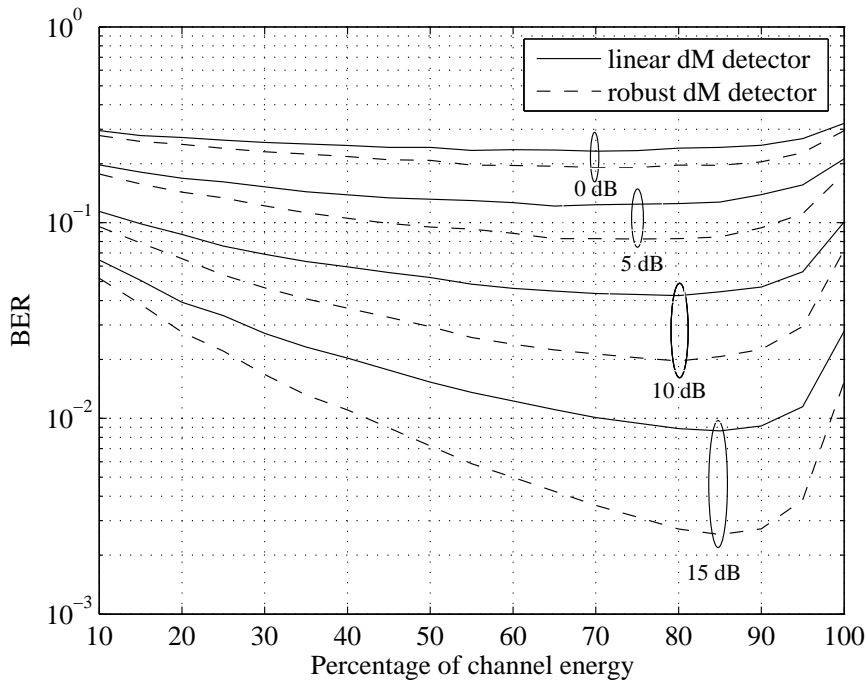


Figure 6.1. BER of the  $dM$  detector for varying percentage of captured channel energy with the CM1 model and  $K = 20$  at the LR

According to Figure 6.1, for 0 dB SNR the initial multipath components that accumulate 70% of the channel energy minimize the error probability in (6.40) with the matrix  $\bar{\mathbf{S}}[i]$  constructed to decorrelate those paths only. For larger percentage values, receiver noise emphasis is more significant than the residual interference from the  $\sum_{k=1}^K L_k$  received paths. Moreover, it is understood from Figure 6.1 that  $L_e$  increases with SNR in such a way that it empirically satisfies  $0.7 + 0.01 \times \text{SNR}(\text{dB})$  in terms of the percentage of channel energy captured. Intuitively as SNR increases, the additional contribution to the captured signal energy outweighs the detrimental effect of more severe noise emphasis with larger total number of decorrelated paths.

The  $mD$  detector achieves the best performance in Figure 6.2 for all SNR, where a UWB system with  $T_f = 100$  ns,  $T_p = 1$  ns and  $R_b = 1$  Mbps is considered. Although the performance of the  $dM$  detector is optimized for each SNR as described above, it is comparable to that of the robust rake receiver with single-user detection and synchronous transmissions for the 0-10 dB SNR range. Here,  $P$  denotes the combined number of paths. While the performance limiting factor for the robust rake receiver is

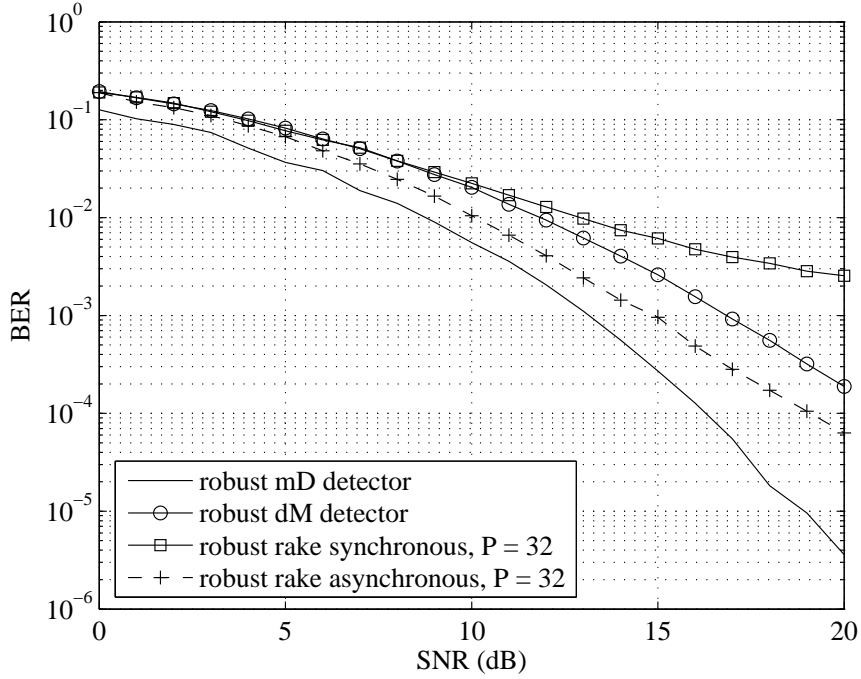


Figure 6.2. BER performances against SNR in the CM1 channel for  $K = 20$  at the LR the MAI with an error floor observed at large SNR, it is the decorrelation loss for the  $dM$  detector, which decorrelates a large number of paths. Hence, the combining rule in (6.21) does not improve the performance of the  $dM$  detector with MRC. The robust rake designed for asynchronous multiuser UWB systems exhibits a good performance with asynchronous transmissions, but due to the MAI it does not achieve BER values on the order of  $1 \times 10^{-5}$  at practical SNR values. It is necessary to use multiuser detection as in the  $mD$  detector to decrease the BER to such low values.

The asymptotic probability of error calculations show that the performance of the linear  $mD$  detector is not affected by the changes in the  $\epsilon$ -mixture noise pdf parameters,  $\epsilon$  and  $\kappa$ , for large processing gain,  $N_s N_h$ . The simulation results in Figure 6.3 reveal that the processing gains of impulse radio UWB systems are large enough to guarantee a performance level that is invariant to the distribution of the noise process. However, in Figure 6.3, the performance of the robust  $mD$  detector improves with  $\kappa$ , as the effective noise variance at the output of the detector decreases with  $\sigma_T^2$  held constant [65]. The advantage of the robust detector is that it removes large amplitudes created by the impulsive noise component. The effective noise variance at the output of the

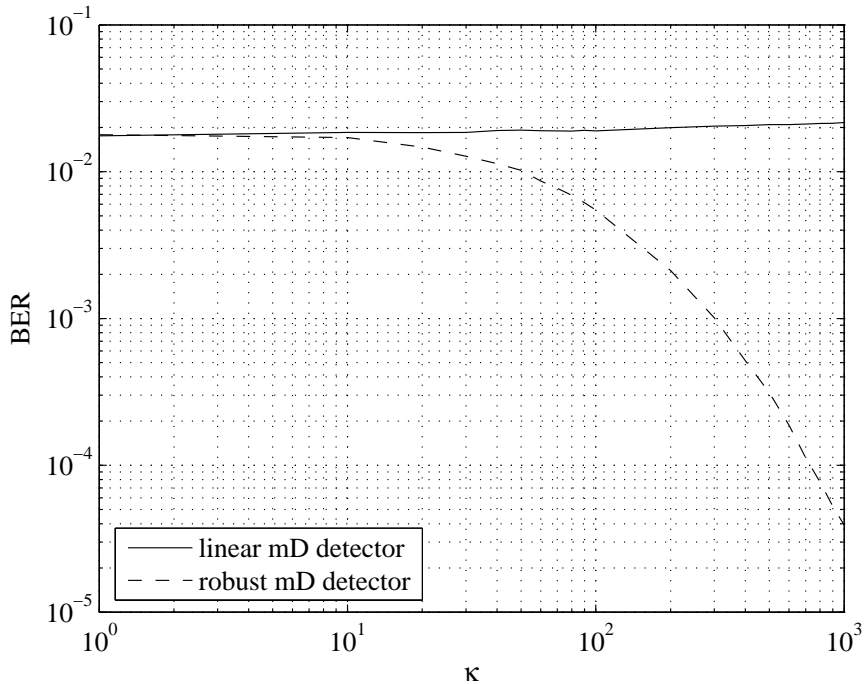


Figure 6.3. BER against  $\kappa$  for the  $mD$  detectors in the CM1 channel at the LR with  $K = 20$ ,  $P = L_{\max}$  and SNR = 10 dB

robust detector is related to the nominal Gaussian component with the smaller variance. When  $\kappa = 1$ , the robust detector designed with  $\epsilon = 0.01$  has a performance slightly worse than but otherwise equivalent to that of the linear detector designed for Gaussian channels.

The non-Gaussian nature of noise plus interference is beneficial to the proposed robust design for all SNR values included in Figure 6.4, where  $\epsilon = 0.01$  and  $\kappa = 100$ . For such a mild deviation from the Gaussian distribution, the robust  $mD$  detector outperforms the conventional detector by almost an order of magnitude at 15 dB. The performance difference in Figure 6.4 of the selective and partial detectors is attributable to a more pronounced interference effect for the partial detector. A partial knowledge of the channel impulse response leads to an inaccurate estimate,  $\hat{\mathbf{S}}_{\mathbf{c}}$ , such that an error floor is induced for the robust partial detector. With lower  $P$ , the gain afforded by the robust detector decreases, since for low  $P$  the major performance limiting factors are the residual MAI and IFI, which become more significant with lower  $T_f$  and larger  $R_b$ .

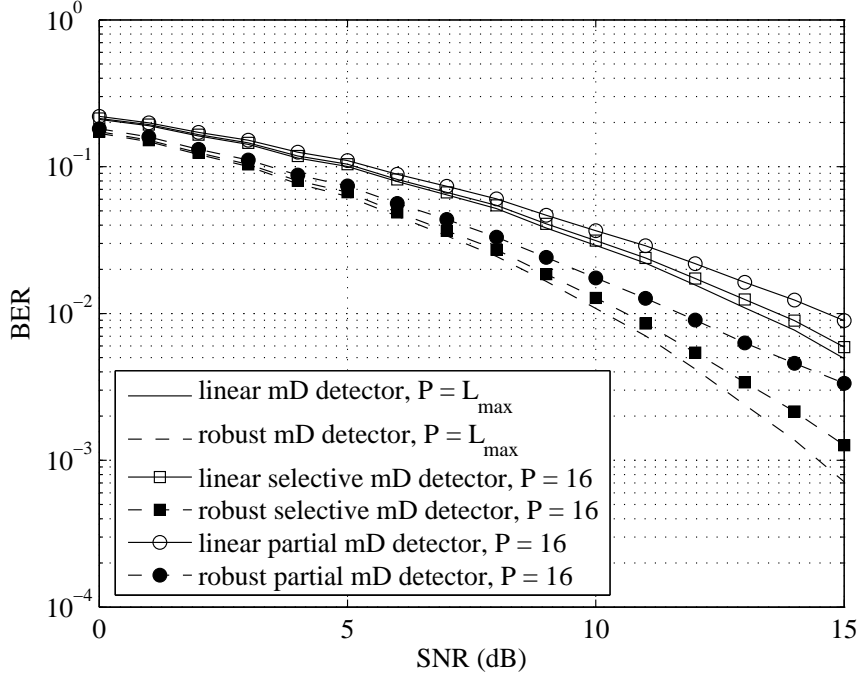


Figure 6.4. BER performances of the  $mD$  detectors against SNR at the LR for the CM1 model and  $K = 20$

As displayed in Figure 6.5, a higher bit rate is linked with a larger number of errors for the  $mD$  detector. For lower rate systems, the processing gain is larger, which improves performance. Besides the transmission rate, the performance of the detector is influenced by the channel model. The diversity gain for the NLOS CM4 channel that has a large number of paths is much higher in comparison to the CM1 channel, which is LOS. In Figure 6.5, the best performance is achieved by the low rate system in the CM4 channel.

The MAI rejection capability of the  $mD$  detector is seen in Figure 6.6 for increasing  $K$ . The figure highlights the importance of the selection mechanism employed by the selective receiver. While the performance of the partial detector is influenced by the IFI with  $T_f = 10$  ns, the robust selective detector substantially outperforms the linear  $mD$  detector for all  $K$  in the figure. When  $K$  gets as large as 50, the effect of the IFI on the robust partial detector becomes comparable to the effect of the impulsive noise on the the linear  $mD$  detector and they almost have the same BER.

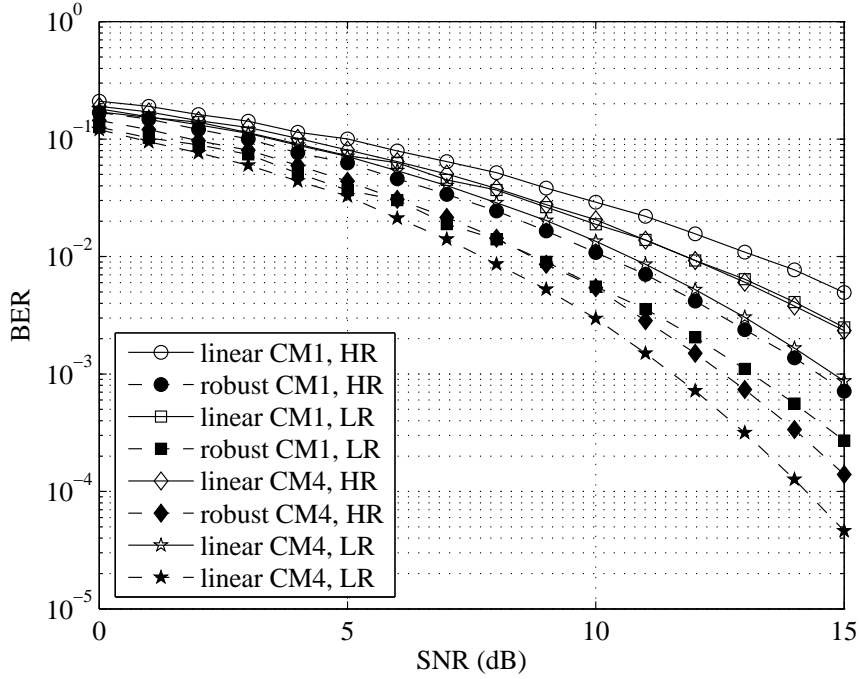


Figure 6.5. BER performances of the  $mD$  detectors against SNR for the CM1 and the CM4 channels at the LR and HR,  $K = 20$  and  $P = L_{\max}$

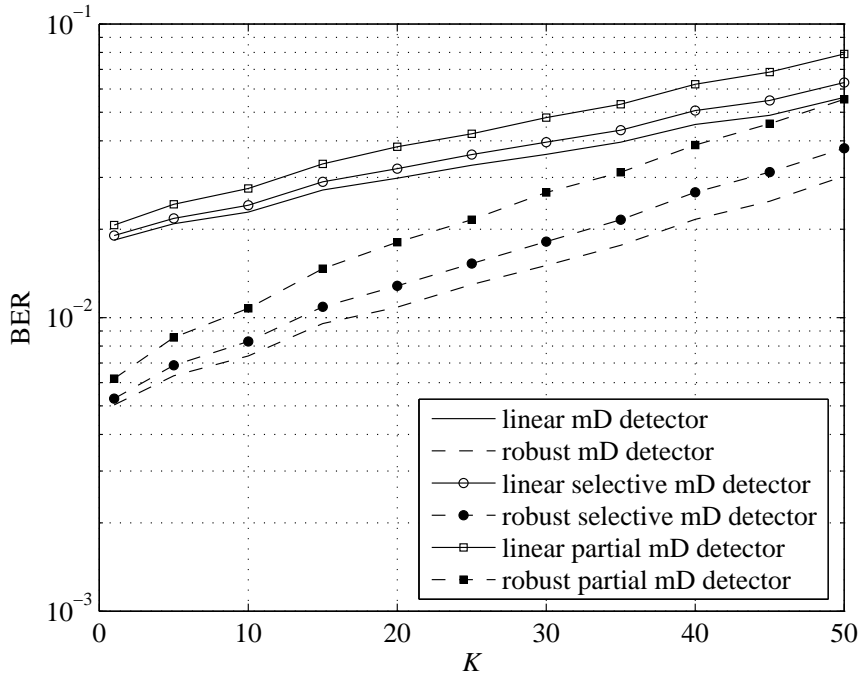


Figure 6.6. BER performances of the  $mD$  detectors against  $K$  for the CM1 model at the HR, where  $P = 16$  for the selective and partial detectors and  $\text{SNR} = 10$  dB

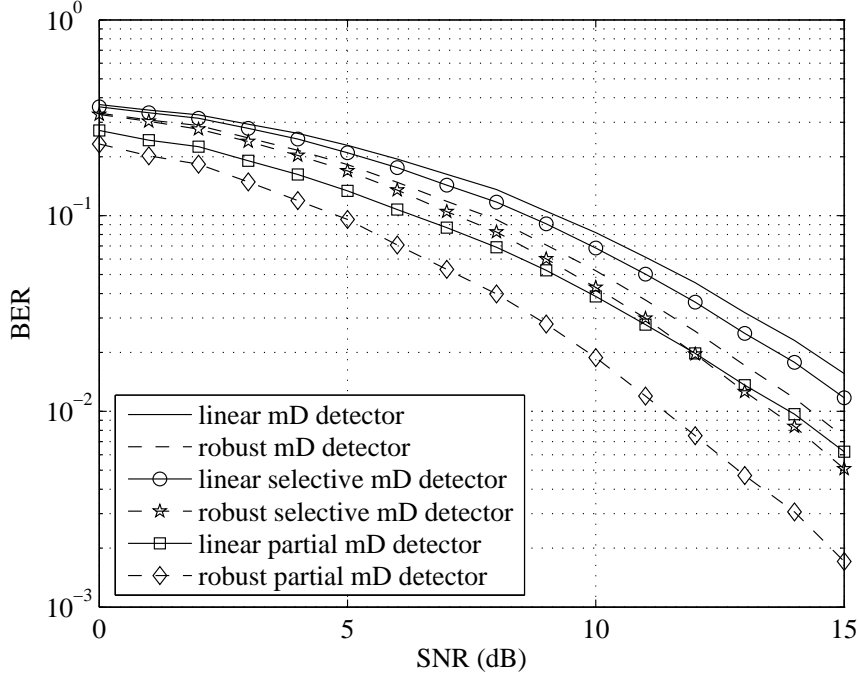


Figure 6.7. BER performances of the  $mD$  detectors against SNR at the LR for the CM1 model,  $K = 20$ ,  $P = 16$  for the selective and partial receivers, and the coherence time of  $200 \mu s$  with  $N_t/N_p = 0.1$

The selection mechanism of the selective detector causes performance deterioration when the channel state is estimated because the artificial high energy paths created by the channel noise are chosen for combining and noise energy is accumulated at the receiver. The output SNR significantly degrades as more of the weak paths that contribute little signal energy are combined with large weights. In contrast, the partial detector with predetermined path arrival times suffers a limited performance loss. These are demonstrated in Figure 6.7, where the  $mD$  detector using every path has the worst performance.

## 7. CONCLUSIONS AND FUTURE WORK

Impulse radio-based UWB technology is expected to be employed at the physical layer of future generation networks which will provide high-speed short-range connectivity. However, in order to satisfy this goal UWB systems have to overcome a number of challenges. This thesis aims to address certain aspects related to the physical layer performance of impulse radio-based communication systems.

In the first part of the thesis, the information rates achieved by TH-PPM “impulse radio” systems over UWB channels with either soft- or hard-decision detection outputs are calculated. Besides the type of output, the number of interfering users, level of IFI and characteristics of the channel affect the rates achieved by impulse radio. The results indicate that compared to the AWGN channel, the frequency-selectivity of the UWB channel limits information rates at medium and large values of SNR. The interference from the other users restricts the rates further at high values of SNR, where the MAI dominates system performance. On the other hand, the mutual information achieved by soft-output systems in the limit of zero SNR are equivalent for all channel models with the same received signal energy. Soft outputs are observed to offer a much better performance than hard outputs in the region of low SNR. While increasing the constellation size is always advantageous for soft-output systems, high  $M$  is preferred for hard-output systems only when SNR is sufficiently large.

In the second part, by assuming the possibility of TDD operation, the maximum SINR values achievable by a transmitter-receiver pair that employs rake combining both at the transmitter and the receiver with a limited total number of rake fingers,  $F$ , is investigated in a search for the optimum transceiver design. Although the design with the post-rake structure that combines the first arriving paths has a sufficient performance at larger values of  $F$ , simulations suggest that there might be better choices for the paths to be combined when  $F$  is lower. The complexity of the calculation of the pre- and post-rake vectors for systems that have ISI requires an iterative algorithm as opposed to the ISI-free case which admits closed form expressions. However, it is

shown that the optimum distribution of the rake fingers between the transmitter and the receiver does not change significantly when ISI is present. Thus, as can be done in a future work, optimization of the finger selection process for the post-rake structure of systems without ISI may provide valuable insight for how the systems with ISI should be designed.

The effects of non-Gaussian noise on the rake receiver design are presented in the third part, where the robust rake receiver proposed for the TH-PPM UWB system using MRC is shown to perform better for the extreme NLOS CM4 UWB channel by over an order of magnitude at practical SNR values (4-12 dB) and number of fingers in impulsive noise compared to the conventional rake receiver with linear matched filters and MRC. Succeeding the matched filter at each rake finger, a robust nonlinearity is required. The performance of the robust receiver is very much dependent on the trimming parameter,  $d$ , the choice of which becomes difficult in the case of a frequency-selective multiple access channel. The accurate estimation of the MAI and  $d$  before the choice and application of the nonlinearity is expected to improve the performance of the robust receiver. As a future work, when the number of users is large and MAI becomes one of the performance limiting factors as well, the outputs of the nonlinearities following the rake finger outputs may be combined according to the MMSE criterion.

The last part of the thesis is devoted to multiuser detection techniques for non-Gaussian UWB channels. A well-known approach to eliminate MAI, multiuser detection, requires that the transmitting UWB users are synchronized. The robust  $mD$  detector developed in the last part of the thesis for TH-BPSK systems propagating over frequency-selective UWB channels and embedded in impulsive noise sustains a performance improvement over its linear version and the alternative structures even when the channel information is incomplete or inaccurate. The  $dM$  detector, which decorrelates paths before multipath combining, suffers substantially from the decorrelation loss. With unknown channel gains it is only applicable for transmissions through frequency-selective channels that have only a few paths. Even when channel information is used to optimize the performance of the  $dM$  detector as in this work, it is worse than that of the proposed robust  $mD$  detector. For UWB communications, multipath-

combining by using channel information and subsequently decorrelating the users has lead us to the  $mD$  detector. In the absence of decorrelation, which corresponds to rake reception, the induction of error floors cannot be prevented and low BER values cannot be obtained.

## APPENDIX A: DERIVATION OF THE MINIMUM SOFT-OUTPUT $E_b/N_0$

By defining a new random vector  $\tilde{\mathbf{y}}' = \tilde{\mathbf{y}}/\sqrt{E_s N_s} = [\tilde{y}'_0 \dots \tilde{y}'_{M-1}]^T$ , whose elements are jointly Gaussian with the mean vector  $\mathbf{m}_{\tilde{\mathbf{y}}'}^i = \mathbf{A}^T \check{\mathbf{m}}_{\mathbf{y}}^i$ , given the  $i$ th symbol is transmitted, and the covariance matrix  $\Sigma_{\tilde{\mathbf{y}}'} = \mathbf{A}^T \check{\mathbf{M}}_{\mathbf{y}} \mathbf{A} \times N_0/2E_s$ ,  $\mathcal{C}_s$  may be expressed as a function of  $E_s/N_0$ :

$$\begin{aligned} \mathcal{C}_s(E_s/N_0) &= -\frac{1}{\ln 2} \sum_{i=0}^{M-1} p(\mathbf{x}_i) E_{\tilde{\mathbf{y}}'/\mathbf{x}_i} \ln \left\{ \sum_{j=0}^{M-1} p(\mathbf{x}_j) \right. \\ &\quad \left. \times \exp \left( \sum_{m=0}^{M-1} \frac{2E_s \tilde{y}'_m}{N_0 \sigma_{\tilde{y}',m}^2} (m_{\tilde{y}',m}^j - m_{\tilde{y}',m}^i) + \frac{(m_{\tilde{y}',m}^i)^2 - (m_{\tilde{y}',m}^j)^2}{2\sigma_{\tilde{y}',m}^2} \frac{E_s}{N_0} \right) \right\} d\tilde{\mathbf{y}}', \end{aligned} \quad (\text{A.1})$$

where  $\mathbf{m}_{\tilde{\mathbf{y}}'}^i = [m_{\tilde{y}',0}^i \dots m_{\tilde{y}',M-1}^i]^T$ ,  $\Sigma_{\tilde{\mathbf{y}}'} = \mathbf{A}^T \check{\mathbf{M}}_{\mathbf{y}} \mathbf{A} = \text{diag}\{\sigma_{\tilde{y}',0}^2, \dots, \sigma_{\tilde{y}',M-1}^2\}$  and  $p(\mathbf{x}_i)$  are obtained using the soft-output Arimoto-Blahut algorithm. Taking the derivative of  $\mathcal{C}_s$  with respect to  $E_s/N_0$  and evaluating it for  $E_s/N_0 \rightarrow 0$  results in

$$\begin{aligned} \dot{\mathcal{C}}_s(0) &= -\frac{1}{2 \ln 2} \sum_{i=0}^{M-1} p(\mathbf{x}_i) E_{\tilde{\mathbf{y}}'/\mathbf{x}_i} \left\{ \sum_{j=0}^{M-1} p(\mathbf{x}_j) \right. \\ &\quad \left. \times \sum_{m=0}^{M-1} \frac{2\tilde{y}'_m (m_{\tilde{y}',m}^j - m_{\tilde{y}',m}^i)}{\sigma_{\tilde{y}',m}^2} + \frac{(m_{\tilde{y}',m}^i)^2 - (m_{\tilde{y}',m}^j)^2}{\sigma_{\tilde{y}',m}^2} \right\}. \end{aligned} \quad (\text{A.2})$$

Equation (3.62) follows from (A.3), which is the vector representation for (A.2)

$$\begin{aligned} \dot{\mathcal{C}}_s(0) &= \frac{1}{2 \ln 2} \sum_{i=0}^{M-1} p(\mathbf{x}_i) \sum_{j=0}^{M-1} p(\mathbf{x}_j) \\ &\quad \times [(\mathbf{m}_{\tilde{\mathbf{y}}'}^i)^T (\Sigma_{\tilde{\mathbf{y}}'}')^{-1} \mathbf{m}_{\tilde{\mathbf{y}}'}^i + (\mathbf{m}_{\tilde{\mathbf{y}}'}^j)^T (\Sigma_{\tilde{\mathbf{y}}'}')^{-1} \mathbf{m}_{\tilde{\mathbf{y}}'}^j - 2(\mathbf{m}_{\tilde{\mathbf{y}}'}^i)^T (\Sigma_{\tilde{\mathbf{y}}'}')^{-1} \mathbf{m}_{\tilde{\mathbf{y}}'}^j] \\ &= \frac{1}{2 \ln 2} \sum_{i=0}^{M-1} p(\mathbf{x}_i) \sum_{j=0}^{M-1} p(\mathbf{x}_j) \\ &\quad \times [(\check{\mathbf{m}}_{\mathbf{y}}^i)^T \check{\mathbf{M}}_{\mathbf{y}}^{-1} \check{\mathbf{m}}_{\mathbf{y}}^i + (\check{\mathbf{m}}_{\mathbf{y}}^j)^T \check{\mathbf{M}}_{\mathbf{y}}^{-1} \check{\mathbf{m}}_{\mathbf{y}}^j - 2(\check{\mathbf{m}}_{\mathbf{y}}^i)^T \check{\mathbf{M}}_{\mathbf{y}}^{-1} \check{\mathbf{m}}_{\mathbf{y}}^j]. \end{aligned} \quad (\text{A.3})$$

## REFERENCES

1. Win, M. Z. and R. A. Scholtz, “Impulse Radio: How It Works”, *IEEE Communication Letters*, Vol. 2, pp. 36–38, February 1998.
2. Win, M. Z. and R. A. Scholtz, “Ultra-Wide Bandwidth Time-Hopping Spread-Spectrum Impulse Radio for Wireless Multiple-Access Communications”, *IEEE Transactions on Communications*, Vol. 48, pp. 679–691, April 2000.
3. Park, C. and T. S. Rappaport, “Short-Range Wireless Communications for Next-Generation Networks: UWB, 60 GHz Millimeter-Wave WPAN, and ZigBee”, *IEEE Wireless Communications*, Vol. 14, pp. 70–78, August 2007.
4. “First Report and Order, Revision of Part 15 of the Commission’s Rules Regarding Ultra-Wideband Transmission Systems”, Federal Communications Commission, Washington, DC, ET Docket 98-153, April 2002.
5. Hirt, W., “Ultra-Wideband Radio Technology: Overview and Future Research”, *Computer Communications*, Vol. 26, pp. 46–52, January 2003.
6. Porcino, D. and W. Hirt, “Ultra-Wideband Radio Technology: Potential and Challenges Ahead”, *IEEE Communications Magazine*, Vol. 41, pp. 66–74, July 2003.
7. Roy, S., J. R. Foerster, V. S. Somayuzulu and D. G. Leeper, “Ultrawideband Radio Design: The Promise of High-Speed, Short Range Wireless Connectivity”, *Proceedings of the IEEE*, Vol. 92, pp. 295–311, February 2004.
8. Yang, L. and G. B. Giannakis, “Ultra-Wideband Communications: An Idea Whose Time Has Come”, *IEEE Signal Processing Magazine*, Vol. 21, pp. 26–54, November 2004.
9. Win, M. Z. and R. A. Scholtz, “On the Robustness of Ultra-Wide Bandwidth

- Signals in Dense Multipath Environments”, *IEEE Communication Letters*, Vol. 2, pp. 51–53, February 1998.
10. Welborn, M. L., “System Considerations for Ultra-Wideband Wireless Networks”, *Proceeding of IEEE Radio and Wireless Conference*, pp. 5–8, May 2001.
  11. Fiorina, J. and W. Hachem, “On the Asymptotic Distribution of the Correlation Receiver Output for Time-Hopped UWB Signals”, *IEEE Transactions on Signal Processing*, Vol. 54, pp. 2529–2545, July 2006.
  12. Zhuang, W., X. Shen and Q. Bi, “Ultra-Wideband Wireless Communications”, *Wireless Communications and Mobile Computing*, Vol. 3, pp. 663–685, September 2003.
  13. Gursoy, M. C., H. V. Poor and S. Verdu, “On-off Frequency-Shift Keying for Wideband Fading Channels”, *Eurasip Journal on Wireless Communications and Networking*, Vol. 2006, Article ID 98564, 15 pages, 2006. doi:10.1155/WCN/2006/98564.
  14. Esmailzadeh, R., E. Sourour and M. Nakagawa, “Prerake Diversity Combining in Time-Division Duplex CDMA Mobile Communications”, *IEEE Transactions on Vehicular Technology*, Vol. 48, pp. 795–801, May 1999.
  15. Blackard, K. L., T. S. Rappaport and C. W. Bostian, “Measurements and Models of Radio Frequency Impulsive Noise for Indoor Wireless Communications”, *IEEE Journal on Selected Areas in Communications*, Vol. 11, pp. 991–1001, September 1993.
  16. Rappaport, T. S., *Wireless Communications: Principles and Practice*, Prentice Hall, Upper Saddle River, NJ, 2nd edn., 2002.
  17. Molisch, A. F., J. R. Foerster and M. Pendergrass, “Channel Models for Ultra-wideband Personal Area Networks”, *IEEE Wireless Communications*, pp. 14–21,

December 2003.

18. Foerster, J. R., “Channel Modeling Sub-Committee Report (Final), Tech. Rep. P802.15-02/368r5-SG3a”, IEEE P802.15 Working Group for Wireless Personal Area Networks (WPANs), December 2002.
19. Saleh, A. and R. Valenzuela, “A Statistical Model for Indoor Multipath Propagation”, *IEEE Journal on Selected Areas in Communications*, Vol. SAC-05, pp. 128–137, February 1987.
20. Rajeswaran, A., V. S. Somayuzulu and J. R. Foerster, “Rake Performance of a Pulse Based UWB System in a Realistic UWB Indoor Channel”, *Proceedings of IEEE International Conference on Communications*, pp. 2879–2883, May 2003.
21. Foerster, J. R., “The Effects of Multipath Interference on the Performance of UWB Systems in an Indoor Wireless Channel”, *Proceedings of IEEE Vehicular Technology Conference*, pp. 1176–1180, May 2001.
22. Shannon, C. E., “A Mathematical Theory of Communication”, *Bell Systems Technical Journal*, Vol. 27, pp. 379–423, 623–656, July-October 1948.
23. Cover, T. M. and J. A. Thomas, *Elements of Information Theory*, John Wiley & Sons, 1991.
24. Zhao, S. and A. M. Haimovich, “Capacity of M-ary PPM Ultra-Wideband Communications over AWGN Channels”, *Proceedings of IEEE 54. Vehicular Technology Conference*, Vol. 2, pp. 1191–1195, 7-11 October 2001.
25. Zhao, S. and A. M. Haimovich, “The Capacity of an UWB Multiple-Access Communications System”, *Proceedings of IEEE International Conference on Communications*, Vol. 3, pp. 1964–1968, 28 April -2 May 2002.
26. Zhao, S. and A. M. Haimovich, “Multi-User Capacity of M-ary PPM Ultra-Wideband Communications”, *Proceedings of IEEE Conference on Ultra Wideband*

- Systems and Technologies*, pp. 175–179, 21-23 May 2002.
27. Pasand, R., S. Khalesehosseni, J. Nielsen and A. Sesay, “Exact Evaluation of M-ary PPM TH-PPM UWB Systems in AWGN Channels for Indoor Multiple-Access Communications”, *IEE Proceedings in Communications*, Vol. 153, pp. 83–92, February 2006.
  28. Ramírez-Mireles, F., “On the Capacity of UWB Over Multipath Channels”, *IEEE Communications Letters*, Vol. 9, pp. 523–525, June 2005.
  29. Zhang, H. and T. A. Gulliver, “Capacity of Time-Hopping PPM and PAM UWB Multiple Access Communications Over Indoor Fading Channels”, *EURASIP Journal on Wireless Communications and Networking*, Vol. 2008, Article ID 273018, 9 pages, 2008. doi:10.1155/2008/273018.
  30. Erseghe, T., “Capacity of UWB Impulse Radio with Single-User Reception in Gaussian Noise and Dense Multipath”, *IEEE Transactions on Communications*, Vol. 53, pp. 1257–1262, August 2005.
  31. Arimoto, S., “An Algorithm for Computing the Capacity of Arbitrary Discrete Memoryless Channels”, *IEEE Transactions on Information Theory*, Vol. IT-18, pp. 14–20, January 1972.
  32. Blahut, R. E., “Computation of Channel Capacity and Rate-Distortion Functions”, *IEEE Transactions on Information Theory*, Vol. IT-18, pp. 460–473, July 1972.
  33. Blahut, R. E., *Computation of Information Measures*, Ph.D. thesis, Cornell University, Ithaca, New York, 1972.
  34. Qui, R. C. and I.-T. Lu, “Multipath Resolving with Frequency Dependence for Wide-Band Wireless Channel Modeling”, *IEEE Transactions on Vehicular Technology*, Vol. 48, pp. 273–285, January 1999.
  35. Ramírez-Mireles, F., “Signal Design for Ultra-wide-band Communications in Dense

- Multipath”, *IEEE Transactions on Vehicular Technology*, Vol. 51, pp. 1517–1521, November 2002.
36. Proakis, J. G., *Digital Communications*, McGraw-Hill, Singapore, 4th edn., 2001.
  37. Gezici, S., H. Kobayashi, H. V. Poor and A. F. Molisch, “Optimal and Suboptimal Linear Receivers for Time-Hopping Impulse Radio Systems”, *Proceedings of IEEE Conference on Ultra Wideband Systems and Technologies*, pp. 11–15, May 2004.
  38. Pinsker, M. S., V. V. Prelov and S. Verdu, “Sensitivity of Gaussian Channel Capacity and Rate-Distortion Function to NonGaussian Contamination”, *Proceedings of IEEE International Symposium on Information Theory*, p. 10, 17-22 September 1995.
  39. Chao, Y.-L. and R. A. Scholtz, “Multiple Access Performance of Ultra-Wideband Transmitted Reference Systems in Multipath Environments”, *Proceedings of IEEE Wireless Communications and Networking*, pp. 1788–1793, March 2004.
  40. Taha, A. and K. M. Chugg, “Multipath Diversity Reception of Wireless Multiple Access Time-Hopping Digital Impulse Radio”, *Proceedings of IEEE Ultra Wideband Systems and Technologies Conference*, pp. 283–287, May 2002.
  41. Dolinar, S., D. Divsalar, J. Hamkins and F. Pollara, “Capacity of Pulse-Position Modulation (PPM) on Gaussian and Webb Channels”, *LPL TMO Progress Report 42-142*, 2000.
  42. Shanmugan, K. S. and A. M. Breipohl, *Random Signals: Detection, Estimation and Data Analysis*, John Wiley & Sons, 1988.
  43. Stark, W. E., “Capacity and Cutoff Rate of Noncoherent FSK with Nonselective Rician Fading”, *IEEE Transactions on Communications*, Vol. COM-33, pp. 1153–1159, November 1985.
  44. Porrat, D., “Information Theory of Wideband Communications”, *IEEE Commu-*

*nications Surveys & Tutorials*, Vol. 9, pp. 2–16, 2nd Quarter 2007.

45. Krusevac, S., P. Rapajic and R. A. Kennedy, “Channel Capacity Estimation for MIMO Systems with Correlated Noise”, *Proceedings of IEEE Global Telecommunications Conference*, Vol. 5, pp. 2816–2820, December 2005.
46. Wilson, S. G., *Digital Modulation and Coding*, Prentice-Hall, Upper Saddle River, NJ, 1996.
47. Gursoy, M. C., “On the Energy Efficiency of Orthogonal Signaling”, *Proceedings of IEEE International Symposium on Information Theory*, pp. 599–603, 6-11 July 2008.
48. Shannon, C. E., “Communication in the Presence of Noise”, *Proceedings of IRE*, Vol. 37, pp. 10–21, January 1949.
49. Usuda, K., H. Zhang and M. Nakagawa, “Pre-Rake Performance for Pulse Based UWB System in a Standardized UWB Short-Range Channel”, *Proceedings of IEEE Wireless Communications and Networking Conference*, Vol. 2, pp. 920–925, March 2004.
50. Jun, M. and T. Oh, “Performance of Pre-Rake Combining Time Hopping UWB System”, *IEEE Transactions on Consumer Electronics*, Vol. 50, pp. 1033–1037, November 2004.
51. Barreto, A. N. and G. P. Fettweis, “Performance Improvement in DS-Spread Spectrum CDMA Systems Using a Pre- and a Post-RAKE”, *Proceedings of International Zurich Seminar on Broadband Communications*, pp. 39–46, February 2000.
52. Irmer, R., A. N. Barreto and G. P. Fettweis, “Transmitter Precoding for Spread-Spectrum Signals in Frequency-Selective Fading Channels”, *Proceedings of IEEE 3G Wireless*, pp. 939–944, May 2001.
53. Han, J.-K., M.-W. Lee and H.-K. Park, “Principal Ratio Combining for Pre/Post-

- RAKE Diversity”, *IEEE Communications Letters*, Vol. 6, pp. 234–236, June 2002.
54. Gezici, S., M. Chiang, H. V. Poor and H. Kobayashi, “Optimal and Suboptimal Finger Selection Algorithms for MMSE Rake Receivers in Impulse Radio Ultra-Wideband Systems”, *EURASIP Journal on Wireless Communications and Networking*, Vol. 2006, DOI 10.1155/WCN/2006/84249.
  55. Strang, G., *Introduction to Linear Algebra*, Wellesley-Cambridge Press, 2003.
  56. Choi, R. L., R. D. Murch and K. B. Letaief, “MIMO CDMA Antenna System for SINR Enhancement”, *IEEE Transactions on Wireless Communications*, Vol. 2, pp. 240–249, March 2003.
  57. Imada, S. and T. Ohtsuki, “Pre-Rake Diversity Combining for UWB Systems in IEEE 802.15 UWB Multipath Channel”, *Proceedings of International Workshop on Ultra Wideband Systems. Joint with Conference on Ultrawideband Systems and Technologies*, pp. 236–240, May 2004.
  58. Bellorado, J., S. S. Ghassemzadeh, L. J. Greenstein, T. Sveinsson and V. Tarokh, “Coexistence of Ultra-wideband Systems with IEEE-802.11a Wireless LANs”, *Proceedings of IEEE GLOBECOM*, Vol. 1, pp. 410–414, December 2003.
  59. Aazhang, B. and H. V. Poor, “Performance of DS/SSMA Communications in Impulsive Channels-Part I: Linear Correlation Receivers”, *IEEE Transactions on Communications*, Vol. COM-35, No. 11, pp. 1179–1188, November 1987.
  60. Middleton, D., “Statistical-Physical Models of Electromagnetic Interference”, *IEEE Transactions on Electromagnetic Compatibility*, Vol. EC-19, pp. 106–127, August 1977.
  61. Vastola, K. S., “Threshold Detection in Narrow-Band Non-Gaussian Noise”, *IEEE Transactions on Communications*, Vol. COM-32, pp. 134–139, February 1984.
  62. Delic, H. and A. Hocanin, “Robust Detection in DS-CDMA”, *IEEE Transactions*

*on Vehicular Technology*, Vol. 51, pp. 155–170, January 2002. For corrections: Vol. 54, pp. 1223, May 2005.

63. Huber, P. J., *Robust Statistics*, New York: Wiley, 1981.
64. Poor, H. V. and M. Tanda, “Robust Multiuser Detection in Frequency Selective Non-Gaussian Channels”, *European Transactions on Telecommunications*, Vol. 14, pp. 255–263, May/June 2003.
65. Wang, X. and H. V. Poor, “Robust Multiuser Detection in Non-Gaussian Channels”, *IEEE Transactions on Signal Processing*, Vol. 47, pp. 289–305, February 1999.
66. Fishler, E. and H. V. Poor, “Low-Complexity Multiuser Detectors for Time-Hopping Impulse-Radio Systems”, *IEEE Transactions on Signal Processing*, Vol. 52, pp. 2561–2571, September 2004.
67. Yang, L. and G. B. Giannakis, “Multistage Block-Spreading for Impulse Radio Multiple Access Through ISI Channels”, *IEEE Journal on Selected Areas in Communications*, Vol. 20, pp. 1767–1777, December 2002.
68. Spaulding, A. D. and D. Middleton, “Optimum Reception in an Impulsive Interference Environment-Part I: Coherent Detection”, *IEEE Transactions on Communications*, Vol. COM-25, pp. 910–923, September 1977.
69. Lupas, R. and S. Verdú, “Linear Multiuser Detectors for Synchronous Code-Division Multiple-Access Channels”, *IEEE Transactions on Information Theory*, Vol. 35, pp. 123–136, January 1989.
70. Verdú, S., *Multiuser Detection*, Cambridge University Press, 1998.
71. Poor, H. V. and M. Tanda, “Multi-User Detection in Flat Fading Non-Gaussian Channels”, *IEEE Transactions on Communications*, Vol. 50, pp. 1769–1777, November 2002.

72. Huang, H. C. and S. Verdu, “Linear Differentially Coherent Multiuser Detection for Multipath Channels”, *Wireless Personal Communications*, Vol. 6, pp. 113–136, January 1998.
73. Cassioli, D., M. Z. Win, F. Vatalaro and A. F. Molisch, “Performance of Low-Complexity Rake Reception in a Realistic UWB Channel”, *Proceedings of ICC*, Vol. 2, pp. 763–767, April/May 2002.
74. Molisch, A. F., “Time Variance for UWB Wireless Channels”, IEEE P802.15 Working Group Document, November 2002.